Hochschule für Angewandte Wissenschaften Hamburg
Hamburg University of Applied Sciences

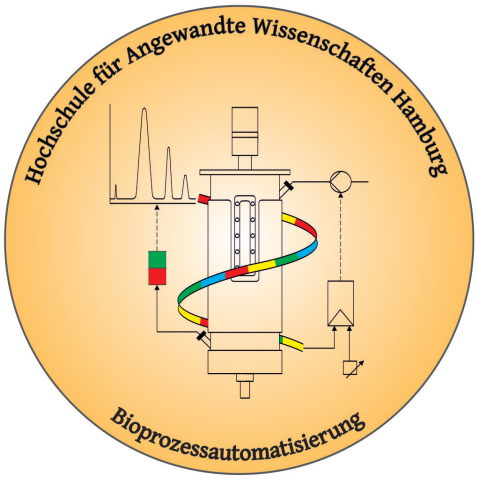

Developement of a biotechnological process suitable for the large-scale production of antimicrobial peptides

Master Thesis

Garry Schulze
Matrikelnummer: [redacted]

May 22, 2020

first referee: Prof. Dr. Gesine Cornelissen
second referee: Prof. Dr. Jörg Andrä

Abstract

The drug pollution of aquatic enviroments including surface water, groundwater and even drinking water is a growing concern. Antibiotics, which belong to the most useful family of pharmaceuticals, pose another threat aside from drug pollution, since their misuse and overuse can lead to the emergence of drug-resistant microbes. The ultimate goal of the interdisclipinary project called PharmCycle is the reduction of the drug pollution of aquatic environments. One approach for achieving this goal is the development of sustainable drugs. Antimicrobial peptides (AMPs) are regarded as a promising candidate for the developement of sustainable antimicrobial/antibacterial agents, since it is harder for microbes to develope resistance against them. AMPs mainly exert their antimicrobial effect by disrupting the cell envelope of the target cell. In order to establish AMPs as an alternative to antibiotics, it has to be produced in a sufficient quantity. Developing a biotechnological process aided by recombinant DNA technology has the potential of producing high yields of AMPs.

This study, which is part of PharmCycle, focuses on developing a biotechnological process, that can be scaled up in order to enable production of greater amounts of the AMP NK2-ALK, which is derived from the porcine NK-Lysin. In the upstream segment of the process, a high cell density culture (HCDC) was performed using *E. coli* BL21 (DE3). NK2-ALK is linked to a carrier protein called Onconase, which leads to the expression of the fusion protein in an insoluble state (formation of inclusion bodies). Thus, the first step of downstream process was the disruption of the cells via high pressure homogenization followed by the solubilization of the inclusion bodies. The fusion protein had a relatively high purity ($\geq$ 80 %) after just one Immobilized metal ion affinity chromatography (IMAC) step. Due to the linker containing an acid susceptible motif, acetic acid was sufficient to seperate NK2-ALK from its fusion partner. The recombinant NK2-ALK retained its antimicrobial activity as verified by radial diffusion assay. The yield was determined to be up to 2.6 mg of fusion protein per 1 g of wet biomass. Thus, the theoretical maximum amount of AMPs, which can be released from the fusion protein, is 0.51 mg per 1 g of wet biomass

Eidestattliche Erklärung

Ich versichere, dass ich die vorliegende Masterarbeit "Development of a biotechnological process suitable for the large-scale production of antimicrobial peptides" ohne fremde Hilfe selbständig verfasst und nur die angegebenen Quellen und Hilfsmittel benutzt habe. Wörtlich oder dem Sinn nach aus anderen Werken entnommene Stellen sind unter Angabe der Quelle kenntlich gemacht.

Statutory Declaration

I hereby formally declare, that the master thesis with the title "Development of a biotechnological process suitable for the large-scale production of antimicrobial peptides" was written independently by myself. I did not use any outside support except for the quoted literature and other sources mentioned in the thesis. Passages and ideas originating from external sources are marked clearly, either literally or analogously.

Ort, Datum

Unterschrift

Danksagung

Zuallererst gilt mein Dank Frau Prof. Dr. Gesine Cornelissen und Herr Prof. Dr. Jörg Andrä, die es mir ermöglicht haben, meine Abschlussarbeit im Rahmen des spannenden und zukunftsweisenden PharmCycle-Projektes zu erstellen. An nächster Stelle bedanke ich mich bei Herr Scheffler und Herr Bertelsen, welche mir mit Rat und Tat zur Seite standen. Weiterhin bedanke ich mich bei Frau Derr für die Nutzung diverser Labormaterialien aus dem BVT-Labor. Mein Dank gilt auch Herr Müller für die Bereitstellung von Daten und für das Korrekturlesen. Zum Schluss möchte ich mich beim gesamten BPA-Teams bedanken für die sehr schöne und spannende Zeit.

Table of Contents

List of Figures

List of Tables

Abbreviations

E. coli	*Escherichia coli*
AMP	Antimicrobial peptide
BSA	Bovine serum albumin
CDW	Cell dry weight
CFU	Colony-forming unit
CV	Column volume
DCU	Digital control unit
DNA	Deoxyribonucleic acid
EBA	Expanded bed adsorption
HCDC	High cell density cultivation
IB	Inclusion bodies
IDA	Iminoacetic acid
IMAC	Immobilized metal ion affinity chromatography
IPTG	Isopropyl β-D-1-thiogalactopyranoside
LPS	Lipopolysaccharide
MIC	Minimal inhibitory concentration
mRNA	messenger RNA
MWCO	Molecular weight cut-off
NTA	Nitrilotriacetic acid
P&ID	Piping and instrumentation diagram
RBS	Ribosome binding site
RNA	Ribonucleic acid
RP-HPLC	Reversed-phase high performance liquid chromatography
rpm	Revolutions per minute
RT	Room temperature
SCADA	Supervisory control and data acquisition
SDS-PAGE	Sodium dodecyl sulfate-polyacrylamide gel electrophoresis
SEC	Size exclusion chromatography
SOP	Standard operating procedure

STP	Sewage treatment plant

1 Introduction

The presence of drugs and drug metabolites in the environment has just recently became a topic of great relevance, even though few paper had been released in the 1970's and 1980's which focused on the drug pollutant in the environment (Bedding *et al.*, 1982; Hignite and Azarnoff, 1977; Richardson and Bowron, 1985). Drugs are developed with the sole purpose of exerting a biological effect. And in order to achieve this goal, different pharmaceuticals share similiar physico-chemical traits like being liphophilic to pass biomembranes and possessing a certain degree of stability/persistance in order to reach the target without being inactivated beforehand. These traits are also the ones, which promote bioaccumulation and exert effects in terrestrial and aquatic environments (Halling-Sørensen *et al.*, 1998).

1.1 Sources of environmental drug pollution

Several pathways exist for pharmaceuticals to enter the environment (Santos *et al.*, 2010). One Pathway is the excretion of drugs via urine and feces. In this pathway, the drug is excreted as a mixture of its metabolized and unaltered form (Halling-Sørensen *et al.*, 1998). The drugs and metabolites then reaches Sewage Treatment Plants (STP's), where it is partially eliminated. Incomplete elimination means, that STP effluents will carry pharmaceutical products and release them into the aquatic environment (Kümmerer and Henninger, 2003; Kümmerer, 2009). Improper Disposal of unused or expired drugs (e.g. via sink or toilet) also create a pathway for drugs to enter aquatic environments (Braund *et al.*, 2009; Persson *et al.*, 2009). Hospital effluents also contain a substantial amount of pharmaceuticals. But contrary to popular belief, hospital effluents do not cause the major part of drug pollution present in municipal sewage (Kümmerer, 2009; Wise, 2002). Furthermore, it has been reported, that substantial amounts of pharmaceuticals have been detected in effluents originating from drug manufactories (Larsson *et al.*, 2007).

In animal husbandry it is common practice to use antibiotics as feed additives in order to treat or prevent diseases. Additionally, antibiotics may serve as growth promoting agents. Like with humans, the antibiotics, unaltered and metabolized forms, are excreted

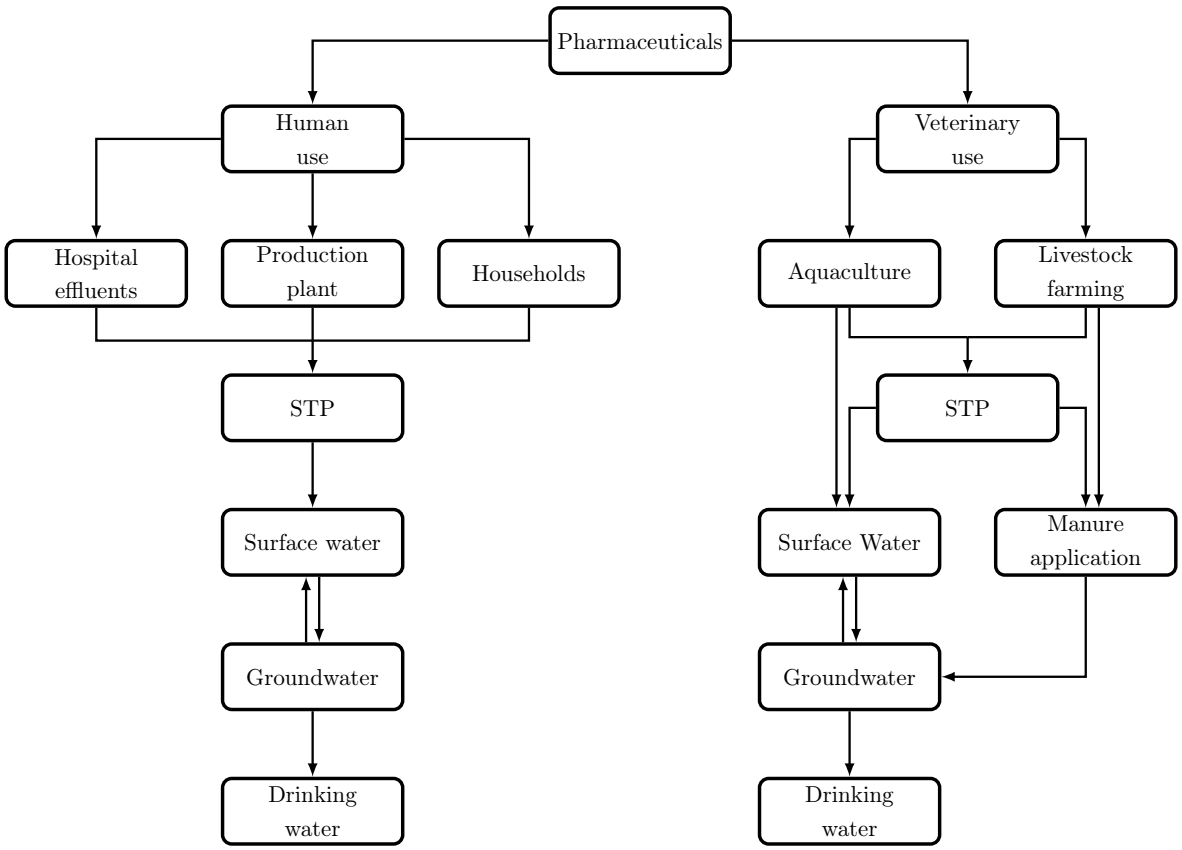

Figure 1: Sources and pathways of pharmaceuticals in the environment

with urine and feces. This creates antibiotic-carrying manure and biosolids, which are in turn used as fertilizer (Du and Liu, 2011). For one, the surrounding soil is immediately contaminated after manure application. Secondly, antibiotics may reach groundwater and surface water through run-off (Kemper, 2008; Santos *et al.*, 2010). Contamination of groundwater and surface water can eventually lead to drug pollution of drinking water (Khetan and Collins, 2007). Antibiotics may also directly enter aquatic environments through the application of antibiotics in fish farms/aquacultures (Gaw *et al.*, 2014). The simplest form of application is carried out by just mixing the antiobiotics into the food, which the fish are receiving. The animals however, are unable to take up all of the medicated feed and thus a significant amount of the feed sinks to the sea bed and accumulates there (Jacobsen and Berglind, 1988). After ingestion of the medicated feed, unaltered forms of the antibiotic are released directly into the surrounding environment via renal or gill excretion, while its metabolites are released together with feces and urine

(Gaw *et al.*, 2014). Aquaculture is predominantly carried out in asian countries as they account for 94 % of the total global production (Sapkota *et al.*, 2008).

There are three ways on how pharmaceuticals may exert their toxic effects on living organisms. Either they kill cells, alter their genetic information and thereby increasing the risk of cancer formation, or disrupt chemical signaling mechanism relevant for developement of an organism. The last named mechanism is the least understood out of the three and termed as endocrine disruption (Khetan and Collins, 2007).

1.2 Problem of antibacterial resistance

Antibiotics have been one of the most useful family of drugs developed to date, but its overuse/misuse has given rise to another concern other than the ecotoxicological one. This concern stems from the growing emergence of bacterial pathogens, which are resistant towards antibacterial agents. Antibacterial resistance is a serious problem, which has to be tackled, as it can render treatment of infections unsuccesful and therefore increase the risk of a lethal outcome (Levy, 1998; Levy and Marshall, 2004; Martinez, 2009). There is a dire need of new antimicrobial agents, in order to escape a crisis, where even a simple infection can lead to a prolonged treatment or even a precarious situation (Michael *et al.*, 2014). But despite the urgent need for new antibiotics, big drug manufacturers less and less develop new antibacterial agents. The reason is due to the unique traits of this class of pharmaceuticals, which lead to less incentive in developing new agents. For one, antibiotics are consumed in short period of time in contrast to other drugs. Also the prescription is deliberately kept low in order to prevent the emergence of drug-resistant pathogens (Brogan and Mossialos, 2013).
Antimicrobial peptides (AMP's) are a promising alternative to antibiotics and may be valuable assets in combating the rise of (multi) drug-resistant pathogens (Galdiero *et al.*, 2015; Lazarev and Govorun, 2010). AMPs are an integral part of the innate immune system/defense system of animal, plants and humans alike (Andrä and Leippe, 1999; Li, 2009).

Some advantages, which may prefer the use AMPs over antibiotics include: broader spectrum of antimicrobial activity, local application, dosage in nanomolar range and greater obstacle in the formation of resistance mechanism (Lazarev and Govorun, 2010). Unlike antibiotics, data regarding the ecotoxicity of AMP's is scarce as of yet (Galdiero *et al.*, 2015).

1.3 Goal of this study

The study is part of the interdisclipinary research project called PharmCycle, whose ultimate is goal is to reduce the drug pollution, especially that caused by antibiotics, of aquatic environments. One measure in order to achieve this goal is the biotechnological production of AMPs, which are regarded as a sustainable alternative for antibiotics (Floeter, 2017). The particular aim of this study is to develop a strategy, which enables the scale-up of the biotechnological process in order to increase the AMP yield.

2 Theoretical background

2.1 Antimicrobial peptides

AMPs are part of the innate immune system of nearly all organism. Classification of AMPs is complicated by their diversity regarding the structure (Zasloff, 2002). Different classification methods are available. For instance, classification on the basis of the source is possible as AMPs may be of bacterial, fungal, plant or animal origin. Classification on the basis of their secondary structure is also often applied (Deng *et al.*, 2017; Zasloff, 2002). Predominant structures of AMPs include disulphate bridged β-sheet peptides, linear α-helical peptides, extended peptide and peptides with a loop structure (Deng *et al.*, 2017; Sahl *et al.*, 2004). But despite their diversity, all of them interact with the cellular envelope of microbes. This interaction is the result of the amphipathic character of the AMP (Zasloff, 2002).

AMPs are composed of hydrobphobic and positively charged residues (arginine and lysine), which are responsible for its amphiphatic character (Rai *et al.*, 2016). The hydrophobic residues interact with the fatty acids of the membrane, while the cationic residues are responsible for the selectivity of AMPs towards the bacterial cell envelope due to their negative netto charge (Nguyen *et al.*, 2011). It is interesting to note, that linear AMPs are unstructured in a hydrophilic/aqueous environment. Only in a hydrobphobic or membrane-like environment they adopt an amphipathic, α-helical structure (Hwang and Vogel, 1998). The cell membrane of microbes are permeabilized upon contact with AMPs, leading to a lethal outcome (Andrä, Monreal, *et al.*, 2007). But not all AMPs exert a membrane disruptive action, since some AMPs pass the membrane and target intracellular structures like DNA and cytoplasmic proteins (Brogden, 2005).

2.1.1 Mode of actions

There are several models, which explain how AMPs permeabilize the membrane of cells. The most promoinent models are the barrel stave model, the carpet model and the toroidal pore model. In the barrel stave model, linear, α-helical AMP monomers

oligomerize to form a pore, which spans the membrane. The AMP monomers are the 'staves' of the 'barrel' (pore). The hydrophilic regions of the amphipathic AMP monomers are orientated towards the pore lumen, while the hydrophobic regions faces the lipids of the bilipid layer (Brogden, 2005).

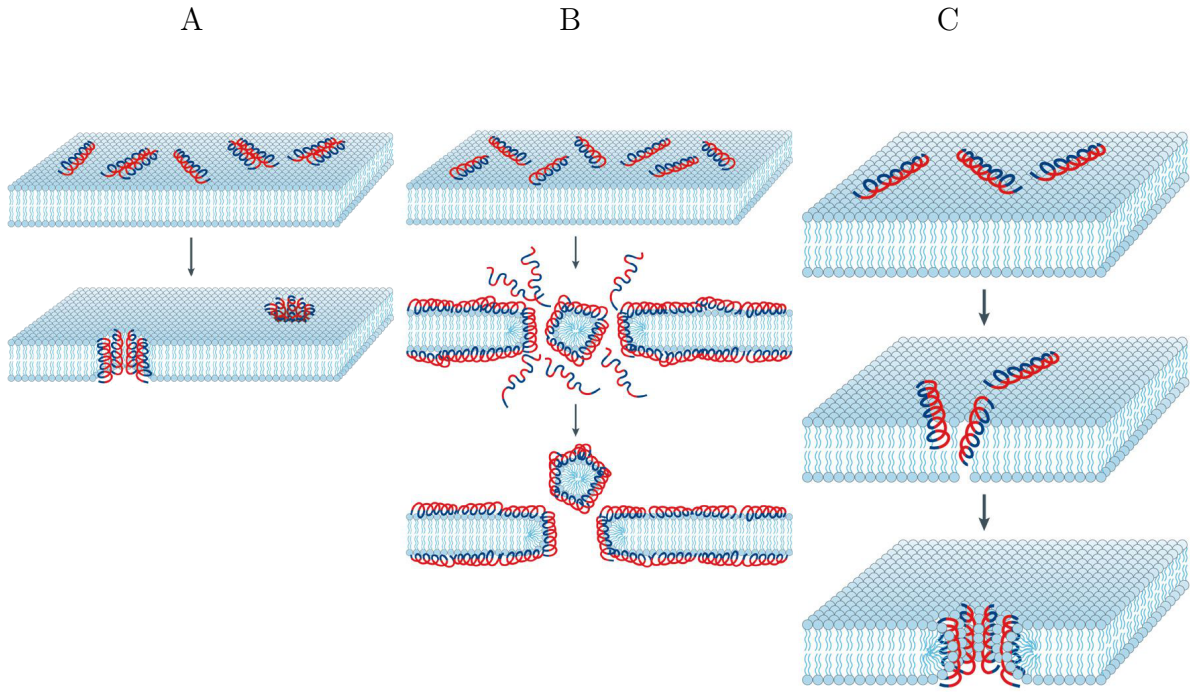

Figure 2: In this figure three major models regarding the membrane permeabilization action of AMPs are depicted. In the barrel stave model (A), monomeric AMP aggregate to form a pore in the cell envelope. Hydrophobic regions (blue) are orientated towards the lipids within the bilipid layer, while the hydrophilic regions encompass the pore lumen. (B) is a visual representation of the carpet mode model. In this model, AMP align on the surface of the biomembrane after being electrostatically attracted. After a threshold concentration has been surpassed, micelles are formed, which cause desintegration of the cell membrane. The toroidal model (C) is similar to the barrel stave model, as the AMP monomers perpendiculary insert to the membrane to form a pore. But unlike the barrel stave model, the headgroups of the phospholipid are constantly connected to each other. This results in a continous bend of the phospholipid monolayer from top to bottom (Brogden, 2005).

The carpet model describes the disruption of the membrane in a detergent-like manner (Nguyen *et al.*, 2011). First the cationic AMPs are attracted electrostatically by the negatively charged suface of the membrane. The AMPs then align on the surface of the membrane in a carpet-like manner. The positiv regions of the AMPs are in contact with the negatively charged phospholipid head groups. After a threshold concentration has been reached, AMPs start to permeate the membrane, which causes the membrane to disintegrate as micelles are formed (Brogden, 2005; Shai and Oren, 2001). According to

the toroidal model, AMPs are inserted perpendiculary into the membrane. But unlike the barrel stave model, the headgroups of the phospholipids are constantly bound to the AMPs and thus a torus-like structure is formed. This means, that the lipid monolayer is continously bend from top to bottom. A pore is formed, whose lumen is lined by AMPs and headgroups of the phospholipids (Yang *et al.*, 2001).

2.1.2 NK-lysin

NK-lysin is an antimicrobial peptide produced in porcine cytotoxic T and NK cells (Andersson *et al.*, 1995; Andrä and Leippe, 1999). It shares structural and functional similarities with amoebapores, which are produced in amoeba. Like amoebapores, it contains four amphipathic α-helical regions and three intrachain disulfide bonds. Helix 3 in amoebapores was determined to be the most bioactive region. As NK-lysin shares structural and functional similarities with amoebaphores, it contains a region, which correpsonds to helix 3 of amoebaphores. This highly cationic region, served as blueprint for the creation of synthetic peptides. The first two synthetic peptides derived from NK-lysin were NK1(40-63) and NK2(39-65), with the letter being the more potent peptide in terms of antimicrobial activity. The number in the brackets specify positions of the amino acid within the parent peptide. The higher potency of NK2(39-65) is probably due to its higher positive net charge compared to NK1(40-63) (Andrä and Leippe, 1999).

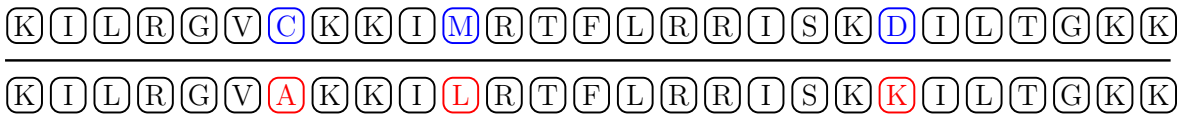

Figure 3: Depiction of the amino acid sequence of NK2 (top) and NK2-ALK (bottom). The positions of the substitions are colored.

In order to increase the activity and stability of NK2(39-65), the sequence of the peptide was altered at three positions (see figure 3). Cysteine, methionine and aspartic acid were replaced by alanine, leucine and lysine respectively. The substitution of aspartic acid with lysine led to an increased positive net charge.

2.2 Expression of recombinant antimicrobial peptides

Highly bioactive AMPs may be extracted from living organism, but this procedure has its disadvantages. These drawbacks include low yield and presence of impurities in the isolates. Then there is also the possbility to synthesize AMPs. Although the chemical synthesis leads to peptides with high purity, this procedure is expensive. In addition, the synthesis of longer peptides is not feasible. The heterologous production of AMPs on the other hand has it fair share of advantages like reduced costs, high yields, simplified isolation, alteration of the peptide via site-directed mutagenesis and feasibility of scale-up (Deng *et al.*, 2017; Piers *et al.*, 1993). Expression of AMPs are mostly carried out in *E. coli* and yeast. Especially *E. coli* is an attractive host due to low cost and its high growth rate. Additionally, post-translational modification is not needed for the proper expression of bioactive AMPs (Li, 2009).

Direct expression of AMPs in a bacterial expression system may be hard to accomplish. One reason is the toxicity towards the bacterial host due to the intrinsic antimicrobial properties of AMPs. Also, the small size and the high positive net charge make AMPs more susceptible for degradation. To overcome these obstacles, AMPs are mostly linked to a fusion partner via recombinant DNA techniques (Piers *et al.*, 1993). The linker connecting the AMP with the fusion partner contains a motif, which can be cleaved in a chemical or enzymatic manner (Li, 2009). Depending on the fusion partner the AMP is linked to, the expressed fusion protein will be in a soluble or insoluble state . In the latter case, formation of inclusion bodies (IBs) will be induced (LaVallie *et al.*, 2000; Lee *et al.*, 2000).

2.2.1 Onconase as Carrierprotein/fusion partner

The denatured form of onconase (ONC) has been rationally designed as a carrier protein for the production of recombinant proteins. ONC-DCless-H6 is the result of these efforts as its amino acid sequence has been altered, in order to achieve chemical cleavage with high specifity. Together with its fusion partner, it is expressed at high levels in an insoluble state (formation of IBs) and therefore the toxicity of the AMP towards the host is reduced. Also, the high purity of the fusion protein within the inclusion body facilitates

purification. The denatured form of ONC-DCless-His6 is soluble at a pH beolw 4, while it is insoluble at a neutral pH range. Thus, the pH-dependet solubility of this protein can be utilized for efficient separation of AMP from ONC-DCless (Pane *et al.*, 2016). The amino acid sequence with the modified/substituted amino acids is depicted in figure 4.

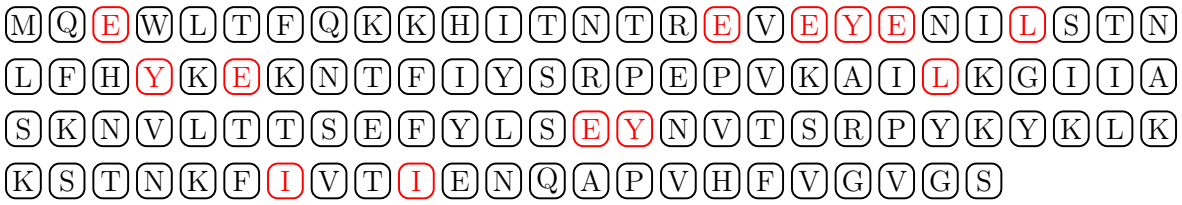

Figure 4: Amino acid sequence of the carrier protein ONC-DCless. The colored amino acids indicate the positions, where modifications were executed.

2.2.2 Fusion protein ONC-DCless-H6-(P)-NK2-ALK

The AMP NK2-ALK is linked to ONC-DCless-H6 in order to mask its toxicity. The linker with the sequence GTGDP is identical to the sequence used by Pane *et al.* (2016). This sequence allows cleavage in an acidic environment due to hydrolysis of the Asp-Pro (DP) dipeptide. The (P) in ONC-DCless-H6-(P)-NK2-ALK indicates, that one additional proline is present at the N-terminus of the peptide after separation from its fusion partner via acid cleavage (Pane *et al.*, 2016). The schemaitc illustration of the fusion construct is shown in figure 5.

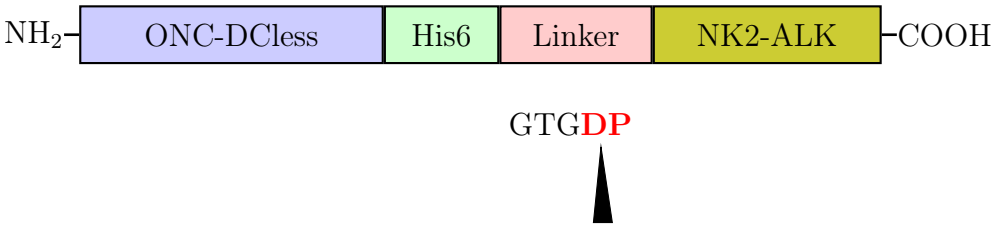

Figure 5: Schematic illustration of the fusion construct ONC-DCless-H6-(P)-NK2-ALK. The cleavage site within the linker sequence is highlighted (red). Cleavage is accomplished in an acidic environment.

2.3 Expression system and vector

The selection of the proper expression system for the expression of a recombinant protein is dependent on different factors such as extracellular and intracellular expression, posttranslational modification of the protein of interest, growth kinetic of the host and regulations regarding the expression of proteins intended for therapeutic use (Makrides, 1996). *E. coli* is the most frequently used host for the production recombinant protein. Major advantages for the use of bacterial expression systems include high cell growth rates, capability of reaching high cell densities and availability of many expression vectors. Also the growth on inexpensive minimal media is a great advantage. But like other expressions systems, bacterial systems including *E. coli* do have some drawbacks. For one, posttranslational modification is not feasible in in these systems and for another, the pyrogenic endotoxins (lipopolysaccharides) on the outer membrane of *E. coli* and other gram negative bacteria is a big concern regarding the expression of proteins for therapeutic use (Terpe, 2006).

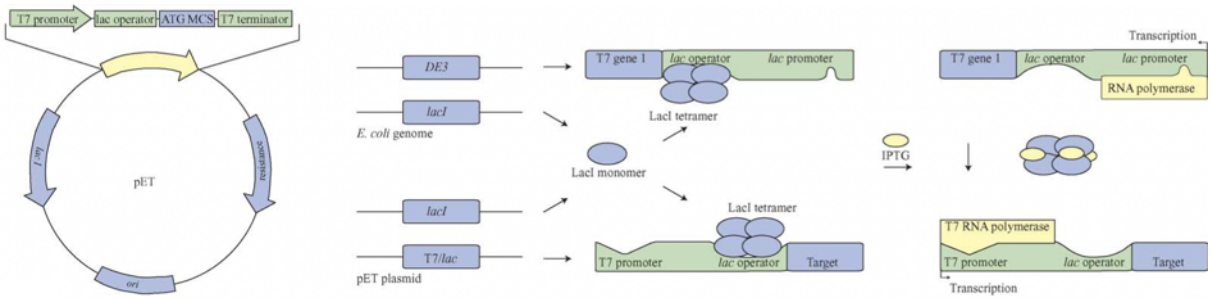

Figure 6: General assembly of the pET vector is depicted on the left side of the illustration. The right side of the illustation shows the repression of the lac operator by the tetrameric LacI and the displacement of the repressor upon induction with IPTG. Induction with IPTG enables the expression of the RNA and T7 polymerase (modified from Sørensen and Mortensen (2005)).

E. coli BL21 (DE3) is a strain commonly used for the production of recombinant protein. It lacks *ompT*, an outer membrane protease, whose absence is beneficial for the production of heterologous proteins (Jeong *et al.*, 2009). A lambda phage derivative called DE3 is inserted into the genome of this strain. The prophage contains the gene for the T7 RNA polymerase, which is under control of the inducible *lacUV5* promotor (Studier and

Moffatt, 1986). Thus, this strain is used as host in the pET expression system. The pET vector contains the hybrid T7/lac promotor. LacI is responsible for the repression of *lacUV5* and T7/lac hybrid promotor in the absence of an inducer (IPTG) (Sørensen and Mortensen, 2005).

2.4 Biotechnological production of recombinant protein

For the successul production of a protein or other biomolecules at production scale, a high cell number per culture volume is needed (Riesenberg, 1991). Three major modes of operations regarding cultivation exist. These three modes are batch, fed-batch and continous fermentation. Each of these modes have their advantage and drawbacks, but only the ones for batch and fed-batch fermentation will be explained.

Out of the three major modes of operation, the batch mode is the simplest form, as all the ingedrients needed are added into the reactor at the beginning of the fermentation. No substrate is added to the system during cultivation (Cinar, 2003). Only gases (e.g.O_2) as well as base and acid for control of the pH are added during cultivation (Yee and Blanch, 1992). Operating in a batch mode provides flexibility in comparison to operation in a continous mode, since the production plant can be used for production of different products. But a great disadvantage for running a cultivation in batch mode as well as fed-batch mode is the dead time between the runs. The unproductive time stems from the time needed for preparing, cleaning and sterilizing the bioreactor (Cinar, 2003).

Fed-batch process is distinguished from batch process by the addition of fresh substrate into the culture broth (Longobardi, 1994). Theoretical description of fed-batch fermentation were first conducted by Yoshida *et al.* (1973). Fed-batch fermentation first starts off as a batch cultivation, as the medium containing the nutrient is inoculated with cells. The microorganisms grow exponentially at their maximum growth rate. After the substrate is depleted, fresh substrate is fed into the reactor (Yee and Blanch, 1992). There are different feeding strategies available. Feeding may be achieved with a predetermined feeding profile (linear or exponential). Then, there is also the possibility of a feedback

controlled feeding strategy (Yamanè and Shimizu, 1984). High substrate concentration can lead to the formation of by-product, which in turn can inhibit cell growth. For instance, excessive glucose lead to the formation of growth-inhibiting acetate even under aerobic condition. This effect is similiar to the crabtree effect observed in yeast, as they can produce ethanol under aerobic conditions if excessive glucose is available (Luli and Strohl, 1990; Yee and Blanch, 1992). Therefore, the accumulation of acetic acid has to be prevented in order to achieve a high cell density (Riesenberg, 1991). The obstacle caused by acetate inhibition can be overcome by adjusting the concentration of the substrate in the feed and by controlling the growth rate via a substrate limiting feeding rate (Riesenberg, 1991; Yee and Blanch, 1992). The specific growth rate has to be set low enough ($\mu < \mu_{crit}$) via the feeding rate in order to successfully minimize acetate accumulation (Korz *et al.*, 1995). The reduction of the growth rate is also beneficial for reducing the oxygen demand, since the oxygen consumption is proportional to the cell density and the growth rate (Yee and Blanch, 1992). The suppression of acetate accumulation allows high cell densities to be reached at the end of a fed-batch cultivation. Cell dry weight well above $100\,\mathrm{g\,l^{-1}}$ can be reached (Korz *et al.*, 1995; Riesenberg, 1991). The cell density obtained through fed-batch cultivation are higher compared to batch cultivation, and thus a higher productivity can be achieved with a fed-batch fermentation (Longobardi, 1994; Yee and Blanch, 1992).

3 Material and Methods

This Chapter will contain all the media/solutions and methods used in this work. All other lists are found in the appendix.

3.1 Materials

List of chemicals, equipment, consumables and kits are found in Appendix A. Only media, buffers and vectors used for this work are described in this section.

3.1.1 Media and buffers

Table 2: Stock solutions used for pre-culture and batch medium

Stock solution	Component	Concentration (g/l)
Glucose stock		
	Glucose monohydrate	695.00
$MgSO_4$ stock		
	$MgSO_4 \cdot 7\,H_2O$	240.00
Trace metal stock		
	Iron(III)citrate	6.00
	$CoCl_2 \cdot 6\,H_2O$	0.25
	$MnCl_2 \cdot 2\,H_2O$	1.80
	$CuCl_2 \cdot 2\,H_2O$	0.15
	H_3BO_3	0.30
	$Na_2MoO_4 \cdot 2\,H_2O$	0.25
	$Zn(CH_3COO)_2 \cdot 2\,H_2O$	0.80
	EDTA	0.84

Table 3: Recipe for pre-culture medium, pH is set to 6.5 with NaOH/HCl

Component	Concentration
KH_2PO_4	$13.30\,g\,l^{-1}$
$(NH_4)_2HPO_4$	$4.00\,g\,l^{-1}$
Citric acid	$1.7\,g\,l^{-1}$
Trace metal stock	$10\,ml\,l^{-1}$
Glucose stock	$7.9\,ml\,l^{-1}$
$MgSO_4$ stock	$2.4\,ml\,l^{-1}$

Table 4: Recipe for batch medium, pH is set to 6.5 with NaOH/HCl

Component	Concentration
KH_2PO_4	$13.30\,g\,l^{-1}$
$(NH_4)_2HPO_4$	$4.00\,g\,l^{-1}$
Citric acid	$1.7\,g\,l^{-1}$
Trace metal stock	$10\,ml\,l^{-1}$
Glucose stock	$25\,ml\,l^{-1}$
$MgSO_4$ stock	$2.4\,ml\,l^{-1}$

Table 5: Feeding solution 1&2

Feeding solution	Component	Concentration (ml/l)
Feed 1		
	Glucose stock	432.65
	$MgSO_4$ stock	40.00
	Trace metal stock	10.00
Feed 2		
	Glucose stock	863.31
	$MgSO_4$ stock	40.00
	Trace metal stock	10.00

Table 6: Buffer for resuspension of frozen cell pellet, pH is set to 7.4 withNaOH/HCl

Component	Final concentration
Tris, pH 7.4	20 mM

Table 7: Recipe for solubilization buffer, pH is set to 7.4 withNaOH/HCl

Component	Final concentration
Tris, pH 7.4	20 mM
Guanidine-HCl	6 M
DTT	3 mM

Table 8: Recipe for equilibration buffer 1, pH is set to 7.4 withNaOH/HCl

Component	Final concentration
Tris, pH 7.4	20 mM
Guanidine-HCl	6 M

Table 9: Recipe for equilibration buffer 2, pH is set to 7.4 withNaOH/HCl

Component	Final concentration
Tris, pH 7.4	20 mM
Guanidine-HCl	4 M
Imidazole	10 mM

Table 10: Recipe for elution buffer 1, pH is set to 7.4 withNaOH/HCl

Component	Final concentration
Tris, pH 7.4	20 mM
Guanidine-HCl	6 M
Imidazole	100 mM

Table 11: Recipe for elution buffer 1, pH is set to 7.4 withNaOH/HCl

Component	Final concentration
Tris, pH 7.4	20 mM
Guanidine-HCl	4 M
Imidazole	500 mM

Table 12: Lysis buffer

Component	Final concentration
NaCl	150 mM
Tris, pH 7.4	50 mM
Sodium Deoxycholate	0.5 % (w/v)
DTT	0.5 % (w/v)

Table 13: Sample buffer for Tris-glycine gels

Component	Final concentration
Roti®-Load2 (4x)	500 µl ml^{-1}
demineralized H_2O	490 µl ml^{-1}
DTT (1 M)	10 µl ml^{-1}

Table 14: Running buffer for Tris-glycine gels

Component	Amount
10x Tris/Glycine/SDS	100 ml
Deionized H_2O	ad 1 l

Table 15: Staining solution for polyacryalmide gels

Component	Amount
Roti-Blue®5x	200 ml
Ethanol($\geq$ 99.8 %))	200 ml
Deionized H_2O	ad 1 l

Table 16: Destaining solution for polyacryalmide gels

Component	Amount
Ethanol($\geq$ 99.8 %))	250 ml
Deionized H_2O	ad 1 l

Table 17: Anode buffer (10x) for tris-tricine SDS-PAGE, pH is set to 8.9 withNaOH/HCl

Component	Amount
Tris (2 M)	24.23 g
Deionized H_2O	ad 0.1 l

Table 18: Cathode buffer (10x) for tris-tricine SDS-PAGE, pH is set to 8.25 withNaOH/HCl

Component	Amount
Tris (1 M)	6.06 g
Tricine (1 M)	8.96 g
SDS (1 %)	0.50 g
Deionized H_2O	ad 0.05 l

Table 19: Gel buffer (3x) for tris-tricine SDS-PAGE, pH is set to 8.44 withNaOH/HCl

Component	Amount
Tris	36.34 g
SDS	8.96 g
Sodium azide	1 ml from 1 % solution
Deionized H_2O	ad 0.1 l

Table 20: Buffer S for tris-tricine SDS-PAGE, pH is set to 6.8 withNaOH/HCl

Component	Amount
Tris	6.1 g
SDS	0.424 g
Sodium azide	1 ml from 1 % solution
Deionized H_2O	ad 0.1 l

Table 21: Sample buffer for tris-tricine SDS-PAGE

Component	Amount
Buffer S	2.5 ml
SDS	2 g
Orange G	40 mg
Glycerol (87 %)	20 mg
Deionized H_2O	ad 0.1 l

Table 22: Fixation solution for tris-tricine SDS-PAGE, pH is set to 8.5 withNaOH/HCl

Component	Amount
Boric acid	12.37 g
Glutardialdehyde (25 %)	100 ml
Deionized H_2O	ad 0.5 l

Table 23: TSB mixture

Component	Amount
Tryptone	8.50 g
Peptone	1.50 g
Glucose	1.25 g
NaCl	2.50 g
Na_2HPO_4	1.25 g

Table 24: Sodium phosphate buffer

Component	Amount
Na_2HPO_4	0.71 g
Demi. H_2O	ad 500 ml

Table 25: TSB medium for shake flask

Component	Amount
TSB mixture	3.6 g
Demi.H_2O	ad 120 ml

Table 26: Bottom layer agarose

Component	Amount
TSB mixture	0.03 g
Agarose	1 g
Tween20	20 µl
Sodium phosphate buffer, ph 7.4	ad 100 ml

Table 27: Top layer agarose

Component	Amount
TSB mixture	6 g
Agarose	1 g
Sodium phosphate buffer, ph 7.4	ad 100 ml

3.1.2 Used plasmid

The plasmid map of pET30a ONC-DCless-H6(P) NK2-ALK is depicted in figure 7. The vector contains the genetic information necessary for the expression of the fusion protein fusion protein ONC-DCless-H6(P) NK2-ALK. The fusion protein is under control of the T7 promoter, as it is located upstream of the sequence coding for it. Downstream of the T7 promoter and upstream of the fusion protein, a ribosome binding site is present (RBS). As the name implies, a ribosome binds at this site on the mRNA transcript so that the sequence can be translated into an amino acid sequence.

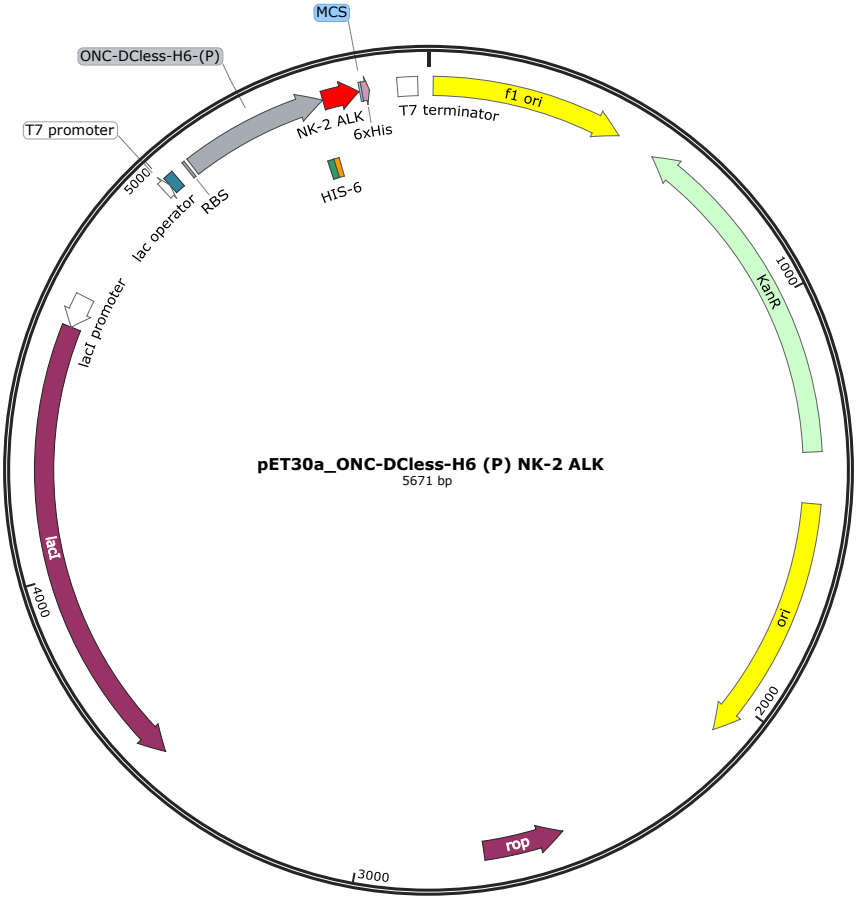

Figure 7: Plasmid map of pET30a ONC-DCless-H6(P) NK2-ALK

The plasmid also contains the gene coding for the LacI repressor, which prevents the expression of the fusion protein. After induction with Isopropyl β-D-1-thiogalactopyranoside (IPTG), the repressor proteins are displaced from the lac operon on the genome of *E.*

coli BL21 (DE3) and from the lac operon on the plasmid. This allows the T7 polymerase, whose sequence is present on the genome (prophage) of *E. coli* BL21 (DE3), to be expressed. The T7 polymerase can now bind to the T7 promoter and enable the transcription of the gene coding for ONC-DCless-H6(P) NK2-ALK. Downstream of the gene coding for the fusion protein, a T7 terminator is present. The plasmid contains a kanamycin resistance gene, which is used as selection marker.

3.2 Upsream processing

For the cultivation of cells a bioreactor from B. Braun Biotech International is used. The fermentation starts with a batch phase and is followed by a fed-batch phase, where a feeding solution containing glucose as limiting substrate is fed from a reservoir into the reactor. The production of the target protein is initiated in the last phase of the cultivation. *E. coli* BL21 (DE3) is used as expression system in this work. It is transformed with the aforementioned plasmid (see figure 7) carrying the genetic information for NK2-ALK. The fed-batch fermentation is detailed in section 3.2.1.

3.2.1 Fed-Batch fermentation

The process is subdivided into four phases. These four phases are: Batch, Fed-Batch 1, Fed-Batch 2 and Production. The batch phase itself is also subdivided into two phases. In the first phase of the batch phase pO_2 is not controlled. The second phase of the batch phase starts, when pO_2 drops to 25 %. After that, the pO_2 is controlled via pO_2/agitation control. In the batch phase, the cells take up the substrate present in the media and achieve their maximum growth rate μ_{max}. This means, that the increase of c_{XL},

$$c_{XL}(t) = c_{XL0} \cdot e^{\mu_{max} \cdot t} \tag{1}$$

with:

c_{XL}	=	Cell density at t	$[\mathrm{g\,l^{-1}}]$
c_{XL0}	=	Cell density at the start of the cultivation	$[\mathrm{g\,l^{-1}}]$
μ_{max}	=	Maximum growth rate	$[\mathrm{h^{-1}}]$
t	=	Time	[h],

is the strongest during this phase. After depletion of the substrate, batch-end detection will be activated and the next phase will be initiated. The selected batch-end detection parameters are pO_2 and stirrer speed (N_{St}). pO_2 has to be greater than 30 %, while N_{St} has to drop by 40 rpm within 60 s (four consecutive cycles with one cycle equaling 15 s). The reason for this cascade is, that absence of substrate inhibits growth of the cells. Thus, the oxygen demand is decreased. This in turn leads to the rise of pO_2. If pO_2 rises above the set point, then N_{St} decreases. If the batch end detection has been carried out succesfully, then substrate (glucose) is fed from the first reservoir (R1) into the reactor. An exponential feeding profile is selected in order to maintain exponential growth of the cells. The growth rate (μ_{set}) is controlled in an open-loop manner via the feeding rate. For the calculation of the feeding rate (F_R),

$$F_{Rj} = \frac{\left(\mu_{set} + q_{S/Xm} \cdot y_{X/Sgr}\right) \cdot V_{Lj} \cdot c_{XLj}}{y_{X/Sgr} \cdot c_{SR}} \tag{2}$$

with:

F_{Rj}	=	Feeding rate at t_j	$[\mathrm{ml\,min^{-1}}]$
μ_{set}	=	Set growth rate	$[\mathrm{h^{-1}}]$
$q_{S/Xm}$	=	Maintenance term/mortality rate	$[\mathrm{h^{-1}}]$
$y_{X/Sgr}$	=	Yield coefficient for cell growth	$[\mathrm{g\,g^{-1}}]$
V_{Lj}	=	Volume of the liquid phase at t_j	[l]
c_{XLj}	=	Cell concentration at t_j	$[\mathrm{g\,l^{-1}}]$
c_{SR}	=	Substrate concentration of feeding reservoir	$[\mathrm{g\,l^{-1}}]$,

the constant parameters $q_{S/Xm}$ and $y_{X/Sgr}$ are assumed to be $0.01\,\mathrm{h^{-1}}$ and $0.48\,\mathrm{g\,g^{-1}}$ respectively. The growth rate μ_{set} is lowered after certain amount of time has passed. The decrease of μ_{set} is necessary in order to postpone the onset of oxygen limitation. The cultivation are executed with or without aid of pure oxygen. Aeration with oxygen starts when the stirrer is about to reach its maximum level and the risk of oxygen limitation is growing. The oxygen gas flow rate is raised stepwise everytime N_{St} reaches a certain value. The total aeration rate is kept constant, meaning that an increase of the oxygen gas flow rate F_{nO2} leads to the decrease of the air gas flow rate F_{nAir} by the same value.

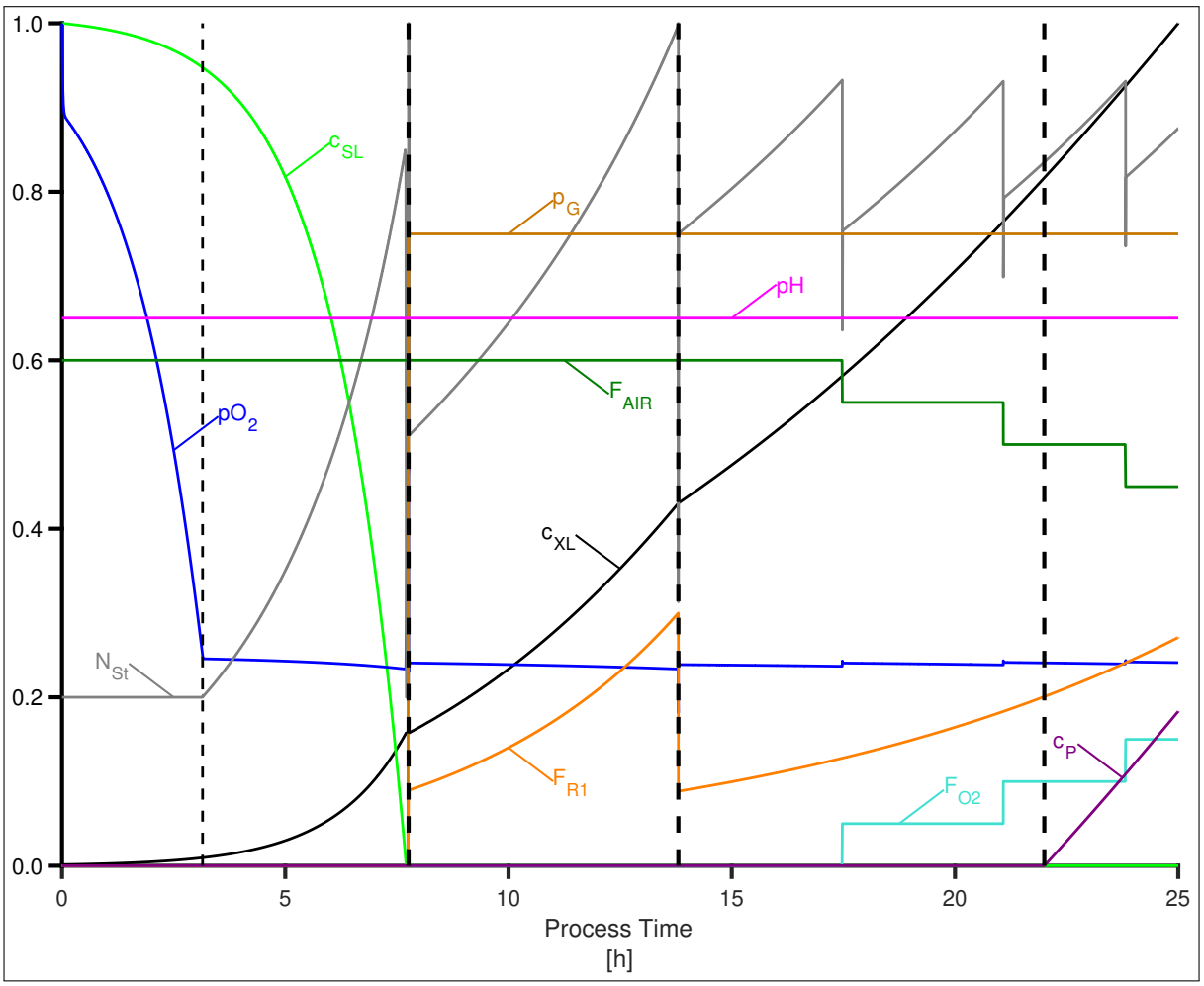

Figure 8: The theoretical course of the bioprocess is depicted here. The bioprocess is subdivided into four phases: batch, fed-batch 1, fed-batch 2 and production phase. The batch phase itself consists of two phases. In the first phase of the batch phase, pO_2 is uncontrolled. The second phase starts when pO_2 drops to 25 %. Data for the simulation were provided by Müller (Unpublished)

For the purpose of automatizing the process, some fermentations are executed with two pumps instead of one pump. This means, that the feeds are not connected to each other, but each of the reservoir is connected to a different pump. The p&I diagram for this two pump strategy is found in Appendix B.

For the preperation of the preculture, buffers and stock solutions (see 3.1.1) have to be autoclaved. The completion of the preculture media takes place under a sterile workbench. The preculture media is divided among three 1 l shake flask, with each flask containing 100 ml of preculture media. After that, each of the preculture media within the shake flasks is inoculated with 200 µl of *E. coli* glycerol stock. The incubation of the preculture

takes place in an incubator with the temperature being set at 28 °C. The duration of the incubation is around 17-18 h and was determined via a preliminary experiment. After this time period, the optical density at a wavelength of 600 nm (OD_{600}) should be around 4. At this value, the cells are still within the exponential growth phase, which is crucial for the inoculation of the batch media.

The batch phase is initiated after inoculation. The batch process is carried out until the subtsrate is depleted. After succesful batch end detection or the manually induced transition, the feeding pump F_{R1} starts working and the fed-batch starts. The fed-batch is subdivided into two phases. In the first phase μ_{set} is set to $0.2\,h^{-1}$. In the second phase of the fed-batch phase, μ_{set} is decreased to $0.1\,h^{-1}$. This is done in order to decrease the oxygen uptake rate (OUR), which is proportional to the growth rate, and thus early oxygen limitation is prevented. Expression of the target protein is induced by Isopropyl β-D-1-thiogalactopyranoside. The final concentration of IPTG within the culture broth should be 1 mM after addition. If pure oxygen was used to support the oxygen supply during fed-batch, then expression is induced at approx. $OD_{600} = 100$. Otherwise protein expression is induced at around $OD_{600} = 80$.
Samples are taken during cultivations, with the sample taking frequency being dependent on the phase of the process. During batch phase, the frequency for sample taking is between 30 and 60 min. During fed-batch fermentation with the growth rate being set to $0.2\,h^{-1}$ and after induction, samples are taken approximately every 60 min. After decrease of μ_{set} to $0.1\,h^{-1}$, sample taking is carried out approx. every 2 h. The sampling valve is sterilized with steam for 10 min after every sampling step.
Measurement of optical density at a wavelength of 600 nm provides a fast and simple method to keep track of the cell growth, as the optical density is proportional to the amount of cells in the suspension. Measurement is carried out with a photometer. To ensure, that measurement takes place within the linear range, the OD_{600} should not exceed 0.6. If OD_{600} is greater than 0.6, then dilution of the sample is necessary. H_2O is used as a blank. c_{XL} can be estimated through,

$$c_{XL} = (OD_{600,Sus} - OD_{600,H_2O}) \cdot f_D \cdot f_{X/OD} = \Delta OD_{600} \cdot f_D \cdot f_{X/OD} \tag{3}$$

with:

c_{XL}	=	Cell density	$[\mathrm{g\,l^{-1}}]$
ΔOD_{600}	=	Optical Density of the suspension after blank substraction	[AU]
$OD_{600,Sus}$	=	Optical Density of the suspension	[AU]
OD_{600,H_2O}	=	Optical Density of H_2O	[AU]
f_D	=	Dilution factor	[-]
$f_{X/OD}$	=	Factor describing the correlation between c_{XL} and OD_{600} $[\mathrm{g\,l^{-1}\,AU^{-1}}]$,	

ΔOD_{600}, since the latter is directly proportional to the cell density. A gravimetric method is applied for the measurement of the cell dry weight (CDW). For this approach, empty 1.5 ml reaction tubes have to be weighed. Before weighing, the reaction tubes are placed in a drying cabinet overnight with the temperature being set at 105 °C. 1 ml from the sample/cell suspension is transferred to a weighed tube. Samples are obtained from the fermentation at different points in time. The tube is then centrifuged (14 000 rpm;5 min). Next, the supernatant is discarded and the tube is placed again in the drying cabinet at 105 °C. The drying takes places overnight and the caps of the tubes are opened during this process. The tubes with the dryed content are then weighed. The cell density $c_{XL,CDW}$ can be calculated,

$$c_{XL,CDW} = \frac{(m_{tot} - m_{empty})}{V_S} = \frac{m_P}{V_S} \tag{4}$$

with:

$c_{XL,CDW}$	=	Cell concentration calculated via CDW	[g l^{-1}]
m_{tot}	=	Mass of the reaction tube + pellet	[g]
m_P	=	Mass of the dry cell pellet /CDW	[g]
m_{empty}	=	Mass of empty reaction tube	[g]
V_S	=	Sample volume	[l],

after CDW has been determined. The growth curve is obtained by plotting $c_{XL,CDW}$ values against their corresponding time points.
If protein expression is induced, then the termination of the cultivation is followed by a partial harvest of the cell suspension. The cell suspension is filled in 500 ml centrifugation bottles. About 300 ml of suspension is filled in each bottle. At least four of the centrifugation bottles are used for harvesting. The filling of the centrifugation bottles with cell suspension is followed up by a centrifugation step (9600 $\times g$;40 min; 4 °C). After the centrifugation is finished, the supernatant is discared and the cell pellets are transferred to a freezer bag with a spatula. The freezer bag containing the cell pellet is then stored at −20 °C.

3.2.2 Bioreactor ED5 and its instrumentation

The vessel used for the fermentation process is called ED5 and was produced by B. Braun Biotech International (now Sartorius Stedim Systems). The maximum volume inside the vessel is 7.1 l, while the maximum operational volume is 5 l. The vessel contains a sight-glass, through which the level of the liquid inside the reactor can be visually observed. Several ports are present, which enable the connection of various probes (pH, pO_2, temperature, pressure, turbidity and high foam).

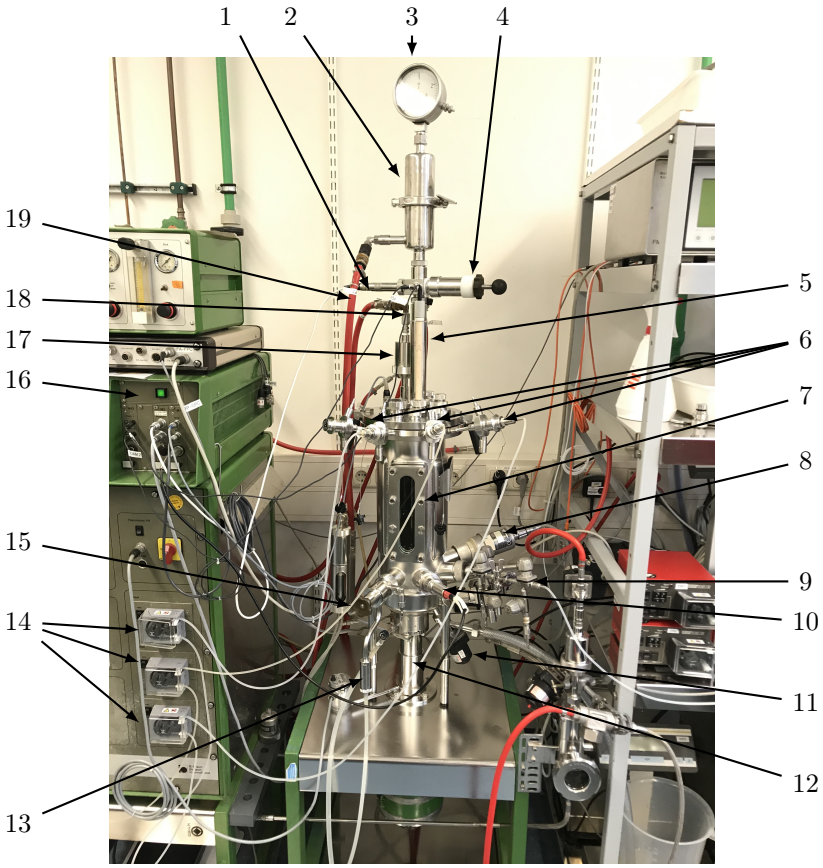

Figure 9: On this picture the ED5 prepared for fermentation is depicted. Legend: 1. Pressure sensor, 2. Filter housing, 3. Pressure gauge, 4. Safety valve, 5. Foam probe, 6. Ports with sterile connection mechanism for acid, base and antifoam, 7. Sight glass, 8. Turbidity probe, 9. Valve for feeding, 10. pH probe, 11. Drain valve, 12. Stirrer, 13. Sterile sleeve , 14. Pumps for acid, base and antifoam 15. Sampling valve, 16. Digital control unit (DCU), 17. Filter housing, 18. Gas inlet, 19. Exhaust. It should be noted, that the air cooler of the exhaust is not visible due to it being obstructed by the foam probe and the filter housing for the gas inlet.

The signals detected by the pH, pO_2 and temperature probe have to be increased by an operational amplifier in order to obtain adequate measurement signals. To achieve homogenously mixing of the reactor content, three sets of 6-bladed impellers are attached on the agitation shaft. The agitation shaft is connected to a motor located on the bottom of the vessel. The piping and instrumentation diagram (P& ID) of the vessel and its periphery are depicted in figure 10.

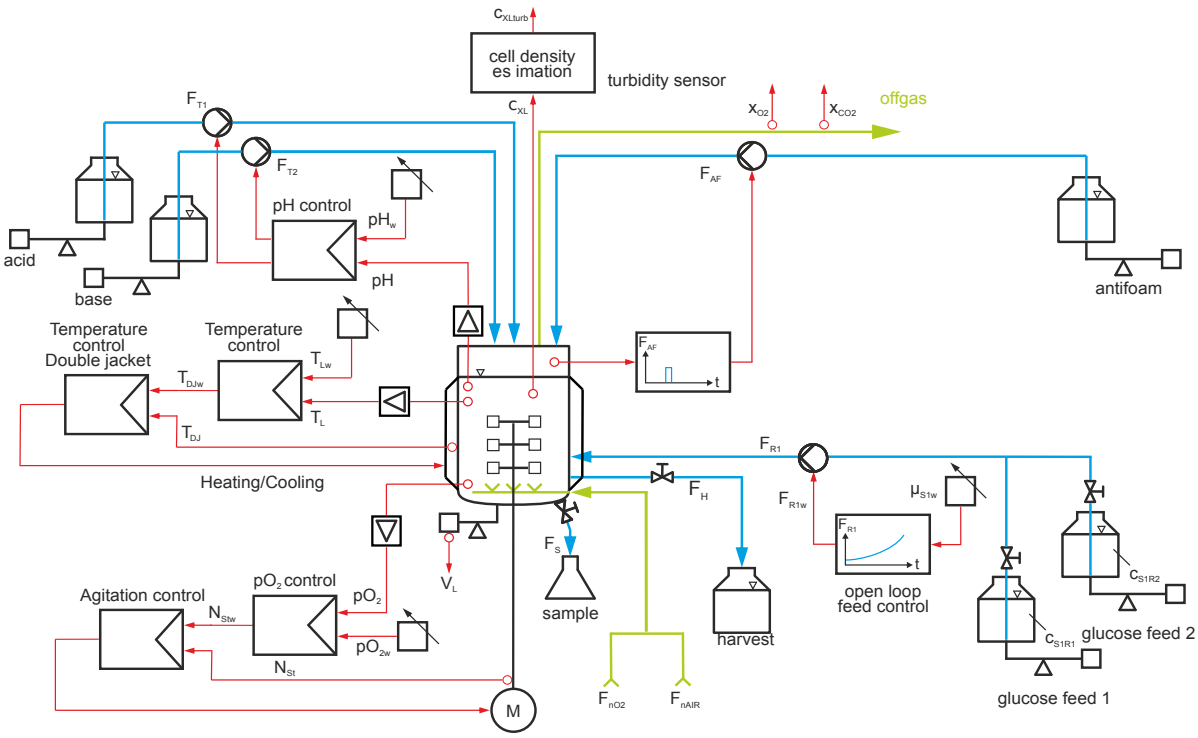

Figure 10: P& ID of the ED5 bioreactor system

The reservoirs of the titrants (acid and base) and the feed are placed on scales in order to track the consumption of their content during fermentation. The reactor itself is placed on a scale, which enable estimation of the volume inside the vessel. The flow of gases into the reactor is controlled via mass flow controller (not depicted on the piping and instrumentation diagramm). The mole fraction of O_2 and CO_2 are estimated via off gas analysis.

Feeding of substrate into the reactor is carried out by a peristaltic pump. Pump calibration is executed with glucose solutions containing the same concentrations as the two feeding solutions ($300\,\mathrm{g\,l^{-1}}$ and $600\,\mathrm{g\,l^{-1}}$). A gravimetrical method is applied for the pump calibration as the resrvoirs/bottles are placed on a scale and solution is pumped out of them. F_{R1max} is then calculated,

$$F_{R1max} = \dot{V} = \frac{\Delta m}{\Delta t \cdot \rho_R} \tag{5}$$

with:

F_{R1max}	=	Maximum pump rate	$[\mathrm{l\,h^{-1}}]$
$\dot{V}$	=	Change of volume per time unit	$[\mathrm{l\,h^{-1}}]$
Δm	=	Mass difference	[g]
Δt	=	Time difference	[h]
ρ_R	=	Density of the feeding/glucose solution	$[\mathrm{g\,l^{-1}}]$,

via the change of mass per time unit. If each of the feeding solution is transported by a separate pump, then F_{R2max} has to be determined just like F_{R1max}. For ρ_R, values from external literature are taken (see Appendix B). The rotational speed of the pump head has to be above the critical value of 5 % or otherwise the substrate is fed inaccurately into the bioreactor. Inaccuracy in regards to the feeding rate may result in problems concerning pO_2 control, as low feeding rates lead to pulsation, and thus short phases of substrate depletion can emerge, which in turn results in the rise of pO_2. The transition from fed-batch 1 to fed-batch 2 requires the switch of the reservoirs. A delay time t_D during this transition is considered,

$$t_D = \frac{\pi \cdot d_i^2 \cdot l}{4 \cdot F_{R1}\left(t_{sw}\right)} \tag{6}$$

with:

t_D	=	Delay time	[min]
d_i	=	Inner diameter of tube	[cm]
l	=	Length of tube behind y tube connector	[cm]
$F_{R1}\left(t_{sw}\right)$	=	Feeding rate at the time of the reservoir switch	$[\mathrm{ml\,min^{-1}}]$,

since the substrate from reservoir 1 in the tube has to be replaced with the feeding

solution from reservoir 2. The feeding rate F_{R1},

$$F_R = \frac{\dot{m}_R}{\rho_R \cdot 1000} = \frac{m_R\,(t_j) - m_R\,(t_{j+n})}{t_{j+n} - t_j} \cdot \frac{1}{\rho_R \cdot 1000} \tag{7}$$

with:

F_R	=	Feeding rate	$[\mathrm{l\,h^{-1}}]$
m_R	=	Mass reservoir	[g]
$\dot{m}_R$	=	Change of mass per time unit	$[\mathrm{g\,h^{-1}}]$
t	=	Time	[h]
ρ_R	=	Density of feeding solution	$[\mathrm{g\,ml^{-1}}]$,

is determined numerically by using scale signals. Next, it is possible to calculate the volumetric substrate transfer rate Q_{SR},

$$Q_{SR} = \frac{F_R \cdot c_{SR}}{V_L} = \frac{\dot{m}_S}{V_L} \tag{8}$$

with:

Q_{SR}	=	Volumetric substrate transfer rate	$[\mathrm{g\,l^{-1}\,h^{-1}}]$
$\dot{m}_S$	=	Mass flow subtrate	$[\mathrm{g\,h^{-1}}]$
F_R	=	Feeding rate	$[\mathrm{l\,h^{-1}}]]$
c_{SR}	=	Substrate concentration of feeding reservoir	$[\mathrm{g\,l^{-1}}]$
V_L	=	Volume of liquid phase in the bioreactor	[l],

through F_R and V_L. For simplicity, the mass of the liquid phase is treated as V_L. The

weight of the bioreactor is increased periodically due to sampling and the subsequent attachement of a metal hose on the sample valve for sterilization via steam. These spikes are noises and filtering them out of V_L leads to $V_{L,MA}$,

$$V_{L,MA} = \frac{1}{n} \cdot \left(V_{L,j} + V_{L,j-1} + \ldots + V_{L,j-(n-1)}\right) \tag{9}$$

with:

V_L	=	Volume of liquid phase within bioreactor	[l]
$V_{L,MA}$	=	Average of volume within window	[l]
n	=	Windowsize	[-],

by using the moving average method. The filter capacity can be adjusted via the windowsize.

3.2.3 MFCS

The SCADA (**S**upervisory **c**ontrol **a**nd **d**ata **a**cquisition) software MFCS/win is developed and distributed by Sartorius. It enables the control as well as monitoring of bioprocesses and data acquisition. Figure 11 depicts the connections between the digital control unit (DCU), MFCS/win and the expanded bed adsorption (EBA) system. The pc with MFCS/win installed on it is the supervisory computer, and thus it is the central component of the control system. All data is gathered by MFCS/win and commands are given out in order to succesfully control the process.

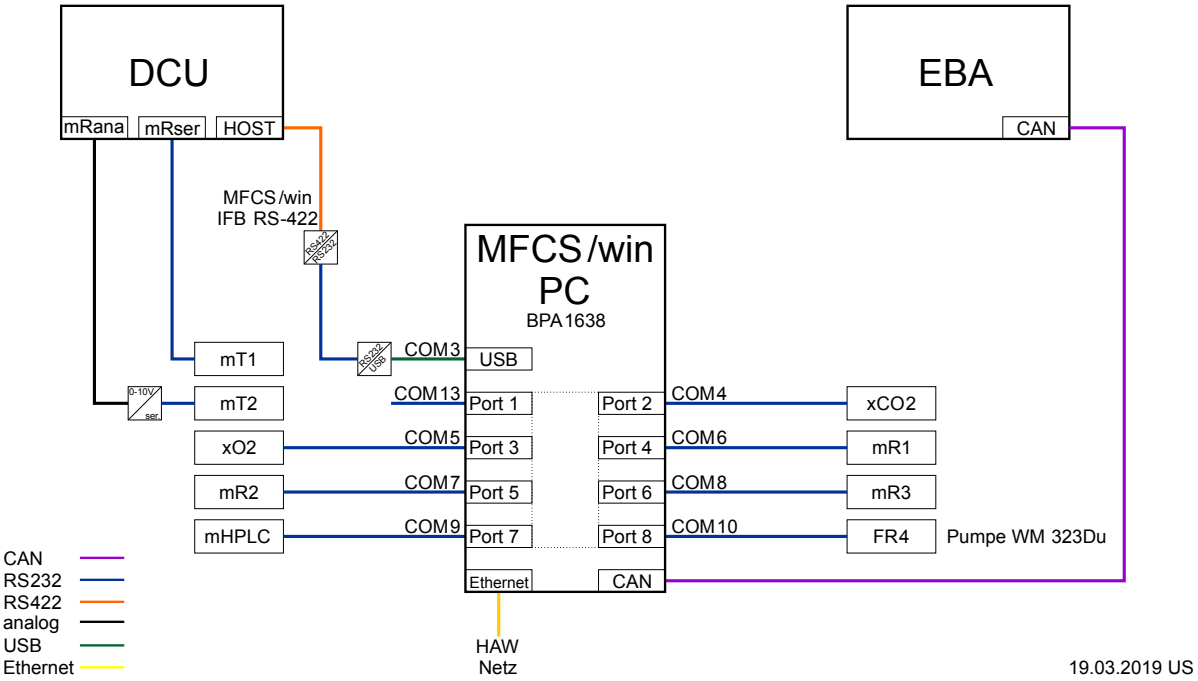

Figure 11: The digital interfaces of the ED5 system is depicted on this illustration. The pc with the SCADA software MFCS/win installed on it is the supervisory computer and it communicates with the DCU and the EBA system (US, 2019).

With the recipe function of MFCS/win, it is possible to automatically control single phases of a bioprocess. The recipe used for this work consist of five phases. These five phases are: initial phase, inoculation, batch phase, fed-batch phase, fed-batch 2 phase and end phase.

The first phase is the initial phase. In the first block of this phase the starting conditions variables and set points are set. For instance, the determined maximum pump rate F_{R1max} is listed here. In the next block (Set_DCU_Controller) the control status, control mode and set points of the controlled variables are set. The setpoint of the pump rate F_{R1} is set at 0 (Set_Pump_Controller), since no feeding occurs at the beginning of the process. The block Set_Calculations enables the recording of process variables, which are calculated with the help of measured variables. At last a query block is present in this phase, which asks if the control mode of the pumps for the tritants and antifoam have been set to auto.

In the second phase of the recipe inoculation takes place. First the aeration is turned off

and a query block follows (Init_Inoculation). If the query is answered with yes, then the aeration is switched on again and the next phase begins.

The batch phase starts with time syncronisation (Initialize_Batch), which sets the time to 0. The next block of this phase is only activitated as soon as pO_2 drops to 30 %. If this condition is met, then the pO_2 /agitation control is activated. At the same time, a timer is started, which automatically activates the batch end detection after 2 h (switch variable sw_BE is switched from -1 to 0) . The batch end detection is executed if the switch variable sw_BE is set to 1. This is either carried out by an external program called Toolbox for MFCS/win(V3.1.1) or manually.

Execution of batch end initiates the first fed-batch phase. The pump rate is calculated on the basis of equation (2) by Toolbox for MFCS/win(V3.1.1). A query starts as soon as exponential feeding is initiated. This query ask if the reservoir has been switched to reservoir 2. As long as the query is ignored, feeding with reservoir 1 takes place. If the query is answered with yes, then a timer is activated. The duration of the timer equals the the time, which is necessary for replacing the first feeding solution with the second feeding solution in the tube (see equation (6)). After the time is up, the fed-batch phase 1 is terminated and the second fed-batch phase is initiated.

For the second fed-batch phase, the starting feeding rate is calculated again (see equation (2)). This is necessary, since some parameters are changed. These parameters inlcude μ_{set} (from $0.2\,\mathrm{h}^{-1}$ to $0.1\,\mathrm{h}^{-1}$), c_{SR} (from $300\,\mathrm{g\,l}^{-1}$ to $600\,\mathrm{g\,l}^{-1}$), V_L and c_{XL}. Every time the average stirrer speed reaches 1200 rpm, a timer with a duration of 15 min is activated. After the 15 min have been completed, F_{nO2} is increased by $0.5\,\mathrm{l\,min}^{-1}$ while F_{nAIR} is decreased by the same value. In total, 6 increases and decreases are allowed for F_{nO2} and F_{nAIR} respectively. A Timer is activated after the last increase of F_{nO2}. The duration is set to 20 h. After that, the fed-batch phase 2 is terminated. The duration of the timer is intentionally chosen too be this relatively long, since a transition to the end phase can be executed manually.

In the last phase the control mode of all controlled variables are set to off.

3.3 Downstream processing

Downstream processing encompasses the thawing and resuspension of the frozen cell pellets, disruption of the cells, solubilization and purification of the target protein. The outline of the downstream processing is depicted in figure 12.

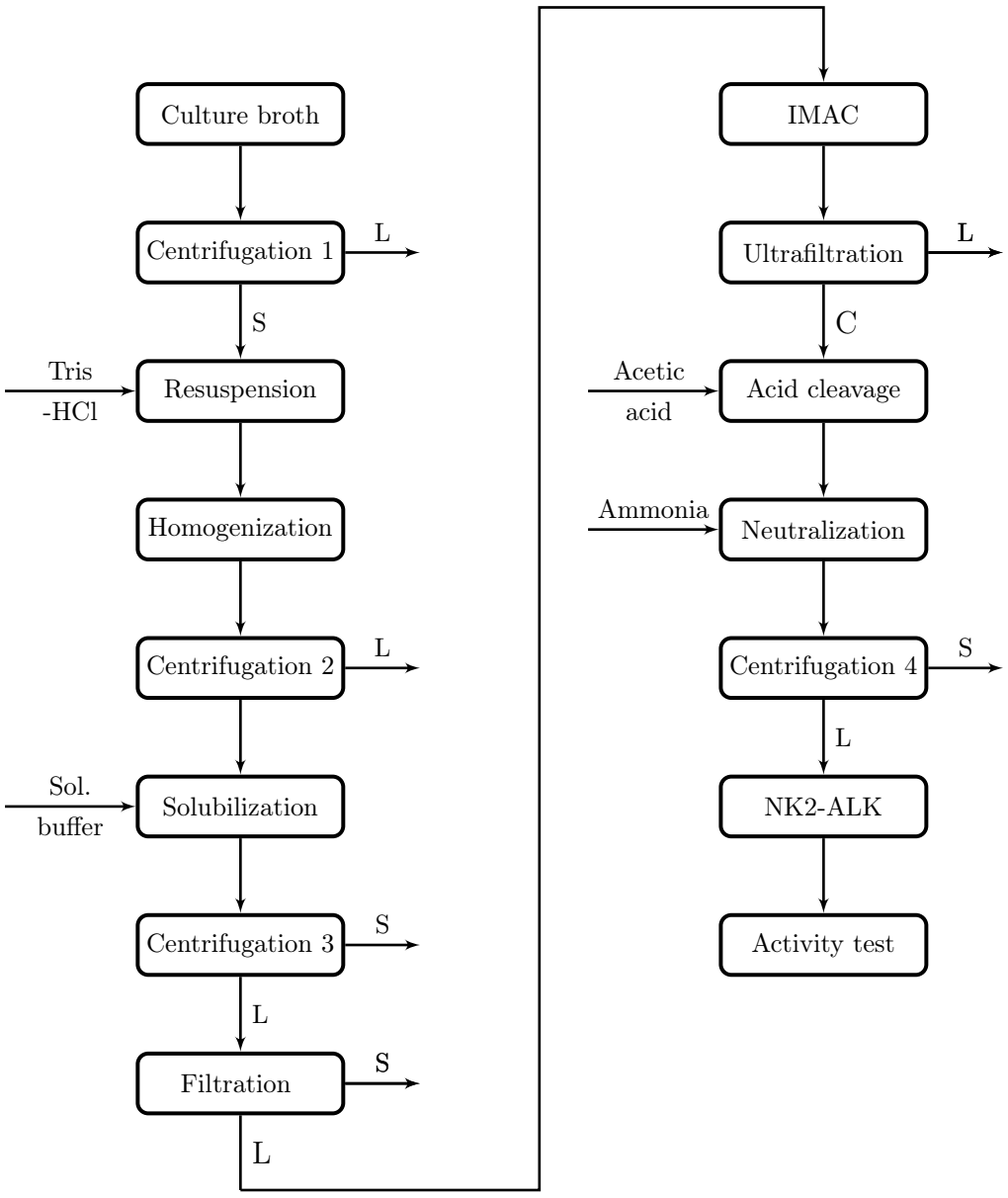

Figure 12: Outline of the downstream process for the purification of ONC-DCless-H6-(P)NK2-ALK. L: Liquid phase, S: Solid phase, C: Concentrated protein.

Purification is primarily achieved by Immobilized metal ion affinity chromatography (IMAC). After the purification step is completed, the protein is precipitated and the onconase is seperated from the AMP by the use of acid. The onconase is then removed via centrifugation.

3.3.1 Cell disruption via homogenization

One common method for the disruption of cells includes the use of a high pressure homogenizer. Its continous operation mode is suited for large scale cell disruption (Harrison, 1991). A positive displacement pushes the suspension through an orifice and it leaves the center of a valve seat. The pressurized suspension is radially discharged across a narrow, adjustable gap of the valve unit and subsequently collides with an impact ring (Harrison, 1991; Middelberg, 1995). It is assumed that the primary cause for the disruption of the cells are due to shearing stress, cavitation resulting from the strong pressure drop and impingement on the impact ring (Middelberg, 1995).

At first 50 g of frozen cell pellet is resuspended in 1 l of 50 mM Tris-HCl ph 7.4. The high pressure homogenizer used for the disruption is Panda Plus 2000, which is manufactured by GEA Niro Soavi. After turning on the system and setting the pressure to around 1000 bar (precise adjustment not possible due to fluctuation).

Figure 13: High pressure homogenisator Panda Plus 2000. Legend: 1. Compression block, 2. Product inlet, 3. Control panel, 4. Homogenization valve 1. stage, 5. Homogenization valve 2. stage, 6. Outlet

The suspension is poured into the product inlet and homogenization is initiated. The homogenate is collected in a 1 l bottle, which is placed within a bucket with cold water.

After the homogenization is completed, the homogenate is again poured in the product inlet and thereby starting the next passage. 3 to 6 passages are carried out. After each passage, sample is taken from the homogenate for OD measurement and other analytic purposes.

3.3.2 Solubilization of the inclusion bodies

Solubilization of the inclusion bodies is realized by using a chaotropic agent, in this case guanidine-HCl. Stored pellet from 3.3.1 is resuspended in 20 ml solubilization buffer (see table 7). The Suspension is incubated at 50 °C for at least 1 h. The solution is centrifuged (20 000 × *g*; 30 min; 4 °C) after the incubation is completed. The supernatant is transferred to a new tube.

3.3.3 Purification via Immobilized metal ion affinity chromatography

Immobilized Metal ion Affinity Chromatography can be applied to proteins, whose histidine residues are exposed on the surface. Alternatively, a polyhistdine tag can be added to the protein of interest via recombinant DNA techniques (Gaberc-Porekar and Menart, 2001). A chelating agent/compound is covalently linked to an insoluble chromatographic support. Common used chelating compounds include iminodiacetic acid (IDA) and nitrilotriacetic acid (NTA). IDA forms tridentate metal chelate, while NTA leads to the formation of tetradentate metal chelate. The most common transitions metal used in IMAC are Ni^{2+}, Cu^{2+}, Co^{2+} and Zn^{2+}. The side chain of histidine is capable of binding to the immobilized metal ion resulting in the capturing of protein, which possess exposed histidine residue on the surface (Arnold, 1991). In the case of his-tagged proteins, IMAC has a very high affinity and specifity (Block *et al.*, 2009). One purification step can suffice to yield recombinant protein high purity (> 90 %) (Block *et al.*, 2009; Gaberc-Porekar and Menart, 2001). Another major advanatge of IMAC is the robustness, since operation under denaturing conditions (6 M guanidine-HCl and 8 M urea) is possible.

Figure 14: IMAC columns for the purification of the target protein. For the small scale purification, a prepacked column with a volume of 1 ml is used (right). Larger sample volumes are purified with a packed column (left). The bed volume of the packed column is approx. 25 ml. The chelated metal ion for both columns is Ni^{2+}.

Sample preperation. The supernatant from 3.3.2 is filtrated by a cellulase acetate filter with a pore size of 0.22 µm. For larger volumes of solubilized inclusion bodies, two filtering steps with different pore size are used. First step is carried out with a grade 597 1/2 filter paper. In the second step, a vacuum filtration using nitrate cellulose membrane with a pore size of 0.22 µm is executed.

Equilibration. The column is flushed with 5 CV of equilibration buffer before the sample is applied. For a packed column, 2 CV to 5 CV of equilibration buffer are sufficient.

Sample Amplication. A defined volume is transferred to a new falcon tube (e.g. 15 ml) and the complete sample is injected on to the column via the sample pump (direct sample injection). A bottle is used instead of a falcon if a larger sample volume has to be applied on the column.

Column Washing. After the sample has been injected onto the column, the washing step is initiated and 5 CV to 10 CV of equilibration buffer is run through the column.

Elution. Isocratic elution is applied for the purification of the target protein. The fractions containing the target proteins are collected for further purification steps.

Figure 15: Operation parameters for different IMAC columns

Parameter	HisTrap crude FF 1 ml	Packed column
Flow rate	1 ml min^{-1}	5 ml min^{-1}
Max. pre column pressure	0.5 MPa	2 MPa
Max. delta column pressure	0.3 MPa	0.1 MPa

3.3.4 Concentration via ultrafiltration

For the concentration of the pooled fractions, 500 µl of the solution was transferred to a spin filter column with a MWCO of 3 kDa. The spin filter is subsequently centrifuged at 14 000 $\times g$ and 4 °C for 10 min. The supernatant gained after centrifugation is transferred to a fresh 1.5 ml reaction tube for the acidic cleavage of the fusion protein (see 3.3.6 for description).

For a scale up, a 20 ml spin filter with the same MWCO as the samller spin filter is used. If a fixed angle rotor is used, then the maximum capacity is 14 ml. The spin filter is centrifuged at 6000 $\times g$ and 20 °C for 2 h.

3.3.5 Ethanol precipitation

For the successful SDS-PAGE-analysis of samples, high concentrations of guanidine-HCl should not be present in order to prevent the precipitation of SDS. Therefore the fusion protein is precipitated by cold ethanol. 5 µl of sample is mixed with 1 ml of ice cold ethanol. The mixture is then incubated for 1 h at −20 °C. After incubation is completed, the mixture is centrifuged at 20 000 × g and 4 °C for 10 min. The supernatant is carefully discarded and the pellet is washed with ice cold ethanol. The mixture is again centrifuged (20 000 × g;4 °C;10 h). The supernatant is again discarded and the pellet is dried by not closing the lids of the reaction tubes. Duration for the drying process is at least 1 h. After drying is completed, the pellet are resuspended in 25 µl PBS buffer. The samples are now ready to be prepared for SDS-PAGE (see **??**).

3.3.6 Acid cleavage of ONC-DCless-H6-(P)NK2-ALK

In a 1.5 ml reaction tube containing the concentrated fusion protein solution, 1 ml of acetic acid (0.1 M) is added to the tube. The solution is then incubated at 60 °C for 24 h. For the neutralisation, an equimolar amount of NH_3 (based on acetic acid) is added to the solution. Therefore, 75 µl of 2.5 % NH_3 is added to the solution. The pH is checked, by pipetting a small volume of the mixture (approx. 5 µl) on a pH indicator paper stripe. An additional incubation step follows at 28 °C for at least 16 h. After incubation is completed, the mixure is centrifuged at 20 000 × g for 1 h. The pellet is discarded, while the supernatant is transferred to a fresh reaction tube.

3.3.7 Radial diffusion assay

The radial diffusion assay is carried out in order to verify if the purified NK2-ALK is biologically active. The test is carried out according to the SOP 'Agardiffusionstest zur Wirksamkeitsprüfung von toxischen Substanzen; speziell antimikrobielle Peptiden' written by Brandt and Demmer (2016). The SOP is based on the assay developed by *Lehrer* et al. (1991). The assay utilizes two thin layers, which contain agarose as gelling agent, to achieve a very high sensitivity. Cells, which are in the exponential growing phase, are casted in the underlayer. The AMP as well as other samples (e.g. controls) are

pipetted in punched out wells. The solutes diffuse radially thereafter. After incubation is completed, the upper layer is casted on top of the bottom layer. The upper layer contains a higher concentration of nutrients compared to the bottom layer. The assay will not be described here in detail. Only the steps, which differ from the SOP will be highlighted in this segment.

The testing strain used for the assay is *E. coli* WBB01 instead of *E. coli* K12 M15. The strain WBB01 is a deep rough mutant and therefore has a higher sensitivity than K12 M15, since the former possesses a minimal lipopolysaccharide structure known as ReLPS (Brandenburg *et al.*, 2002; Koch *et al.*, 1999). WBB01 has a lower growth rate than K12 M15, and thus the inoculation volume and duration of incubation are readjusted. The inoculation volume for the first shake flask is 100 µl instead of 50 µl. The inoculation of the second flask on the next day is carried out with 300 µl instead of 200 µl. The length of the subsequent incubation is prolonged from 2.5 h to 3.5 h. The media for upper layer and bottom layer are kept at 42 °C and not 48 °C as described in the SOP. This is necessary to keep the cells alive for the assay, as a temperature above 42 °C may in result in their premature death.The seeding of the bottom layer is executed with a CFU of $4 \cdot 10^6$. After the top layer has been casted, an incubation with a duration of 40 h follows.

3.4 Analysis via SDS-PAGE and Bradford

In this section, the analytic methods needed for visualization and estimation of the target protein is described.

3.4.1 SDS-PAGE

SDS-PAGE is an established method, which allows the electrophorical seperation of proteins. This method was first described by Laemmli (1970). PAGE stands for Polyacrylamide gel electrophoresis. And as the name suggests, proteins move thorugh a polyacrylamid gel, which function as a sieve. The proteins are treated with SDS, a detergent, which results in their denaturation. SDS molecules are negatively charged and thus the netto charge of the SDS-protein complexes are negative. Since the intrinsic

netto charges of the proteins are masked by the negative charge of SDS, the migration rates of the proteins within the polyacrylamid gel are primarily determined by their molecular weights. Smaller proteins move faster towards the anode than their bigger counterparts. A discontinous gel system is commonly applied, since the gels consist of a stacking gel on top of a resolving gel (Brunelle and Green, 2014).

The 'TGX™FastCast™Acrylamide Kit' from Bio-Rad is used for the casting of 10 % tris-glycine polyacrylamide gel. In table 28 the amount of the components needed for the casting of two gels is listed.

Table 28: Casting of two 10 % acrylamide gel using fastcast system

	Component	Amount	Cast volume/gel
Resolver	Resolver A	4 ml	3.5 ml
	Resolver B	4 ml	
	TEMED	8 µl	
	APS(10 %)	40 µl	
Stacker	Stacker A	2 ml	1.5 ml
	Stacker B	2 ml	
	TEMED	8 µl	
	APS(10 %)	20 µl	

The recipe for the sample buffer and the running buffer are listed in table 13 and 14 respectively. An equal volume of sample buffer and sample are mixed together. After that, the sample is heated at 95 °C for 5 min. 20 µl of each sample is loaded onto one well of the gel, while 10 µl of the marker is applied on the gel. The marker in use for the standar tris-glycin SDS-PAGE is 'Precision Plus Protein™Unstained Standards' from Bio-Rad. The gel is run at 200 V for approx. 45 min. After the run is terminated, the gel is directly placed in a box, which contains the staining solution (see table 15 for recipe). The staining takes place overnight, while the box is placed on a rocker. When staining is completed, the gel is placed in a box containing approx. 100 ml destaining

buffer (see table 16 for recipe). The box is then placed on a rocker for at least 5 min. After 5 min are over, the destaining solution is discarded and replaced with the same amount of fresh destaining solution. The destaining process is carried out three times in total. After destaining is completed, the gels are visualized by using GelDoc™EZ Imager.

During cultivation, samples are taken specifically for SDS-PAGE analysis according SOP 'PAGE Probenvolumen für Minigele' by Ernst Sanders. These samples are centrifuged at 16 000 $\times g$ for 5 min. The supernatants are discarded and the pelleted cells are either stored at −20 °C or directly prepared for SDS-PAGE. Before the samples can be applied on an acryalmide gel, the cells have to be lysed. The cells are chemically lysed by adding 50 µl of freshly prepared lysis buffer to the pellets (see table 12 for recipe). The suspension is incubated for 15 min. After incubation is finished, the samples are prepared as usual (addition of sample buffer and subsequent heating at 95 °C for 5 min.

3.4.2 Tris-tricine SDS-PAGE

The Laemmli SDS-PAGE system (tris-glycine system) is not suited for the seperation of protein, whose molecular weights fall below 10 kDa. For the seperation of small proteins and peptides, the tris-tricine SDS-PAGE system is suited for this task as the range for seperation is 1 kDa to 100 kDa (Schägger and Jagow, 1987).
First the resolving gel is casted, then the spacer gel follows and at last the stacking gel is casted. It is imprtant to note, that the different gels are casted directly after each other before start of polymerization.

Sample preparation is similiar to the sample preparation executed for tris-glycine SDS-PAGE (see 3.4.1). Sample buffer for tris-tricin SDS-PAGE (see 21) is used for sample preparation. If reducing conditions are desired, then DTT is added to the sample buffer to a final concentration of 100 mM.
For the electrophoresis, 20 µl of each sample and 10 µl of the marker is loaded on to the wells of the gel. The marker used for tris-tricin SDS-PAGE is 'Polypeptide SDS-PAGE Molecular Weight Standards' from Bio-Rad. The current is set to 20 mA/gel for the

Table 29: Composition of polyacrylamide gels for SDS-PAGE using tris-tricine system. The listed amounts are calculated for the casting of two gels.

Component	Resolving gel	Spacer gel	Stacking gel
Acrylamid mix (40 %)	3.75 ml	2.25 ml	1 ml
Gel buffer (3x)	3.30 ml	3.30 ml	3.30 ml
Glycerol (87 %)	2 ml	1 ml	-
APS (10 %)	48 µl	36 µl	9 µl
TEMED	18 µl	10 µl	10 µl
Demi. H_2O	18 µl	10 µl	10 µl
Casting volume per gel	3 ml	0.5 ml	1 ml

electrophoretic seperation of the polypeptides. The run is stopped after 3.0 h to 3.5 h. After electrophoresis is finished, the gel is placed in a box containing fixation solution (see 22 for recipe). The incubation within the fixation solution lasts 30 min. After the 30 min are completed, the fixation solution is poured off and demineralized water is poured into the box. The box including the gel is then put on a rocker for 5 min. The water is replaced with fresh water 5 min and the washing procedure is repeated. Washing is executed three times. After the last washing step is performed, the water is poured off and staining solution (see table 15 for recipe) is poured into the box. Staining lasts for at least 3 h. Staining is followed by destaining. Destaining is performed like described in 3.4.1.

3.4.3 SDS-PAGE densitometry

Protein concentrations can be estimated through laser densitometry of stained SDS-PAGE gels since the intensity of the stained bands is proportional to the amount of protein present within the band. The limit of detection for coomassie stained proteins within polyacrylamide gels is in the range of 40 ng to 50 ng (Knight and Chambers, 2003).

In order to estimate the protein concentration of the target protein, different concentra-

tions of BSA are also loaded onto the same gel for SDS-PAGE. The stained bands of BSA are used to create a calibration curve by plotting the bands intensity against the corresponding amount. The creation of the calibration curve is automatically carried out by Image Lab Software (Bio-Rad) after stating the mass of each protein standard. For the determination of the protein concentration c_P,

$$c_P = \frac{m_{SDS}}{V_{SDS}} \cdot f \tag{10}$$

with:

c_P	=	Protein concentration of sample	[µg µl^{-1}]
m_{SDS}	=	Mass of protein applied on gel	[µg]
V_{SDS}	=	Volume of sample applied on gel	[µl]
f	=	Dilution factor	[-],

steps leading to dilution have to be considered (e.g. mixing sample with sample buffer).

3.4.4 Bradford assay

Bradford assay provides a rapid and sensitive method for the quantification of proteins . The underlying mechanism is the binding of Commassie Blue Brilliant G-250 to the protein resulting in a protein-dye complex. Comassie Blue Brilliant G-250 exists in two color forms.If unbound, it is present in the red form. Upon binding to a protein, it switches to the blue form (Bradford, 1976). The absorption maximum of the dye-protein complex then is 595 nm. The dye binds to basic amino acids, especially arginine (Compton and Jones, 1985). Thus, the amount of dye molecules binding to the protein is dependent on the amount of basic amino acid residues within the protein. Ideally, the protein used as standard and the protein of interest should contain a similar amount of basic amino acid residues (Knight and Chambers, 2003).

For the creation of the calibration curve, BSA is chosen as protein standard as stated in the instruction supplied with Roti®Quant. The BSA protein standards, the dilution of Roti®Quant and the samples are prepared according to the instruction. Aside from the 1:20 and 1:40 dilutions of the samples, an additional 1:80 dilution of the samples is prepared if necessary. 200 µl of the diluted reagent is pipetted into the wells according to a schedule (designed by the operator). Next, the samples and standards are added to the reagent according to the schedule. The samples are incubated for 5 min at RT. After incubation is completed, the absoprtion of the samples are messed at a wavelength of 595 nm. The absorbance of the standards are plotted against their corresponding protein concentrations. The calibration curve is then obtained via linear regression. The measured absorbance of the samples are compared to the calibration curve in order to determine the corresponding protein concentration.

4 Results and Discussion

4.1 Upstream

The results obtained from the upstream processing will be described and discussed in this section.

4.1.1 Preliminary experiment

Shake flask experiment were carried out in order to determine the optimal duration of the preculture so that midlogarithmic cells can be obtainded for the inoculation of the batch medium. Four precultures were prepared for the experiment. Each of the shake flask was inoculated with a different volume of the *E. coli* gylerol stock (200 µl, 300 µl, 400 µl and 500 µl). In figure 16 the course of the four cultures are depicted.

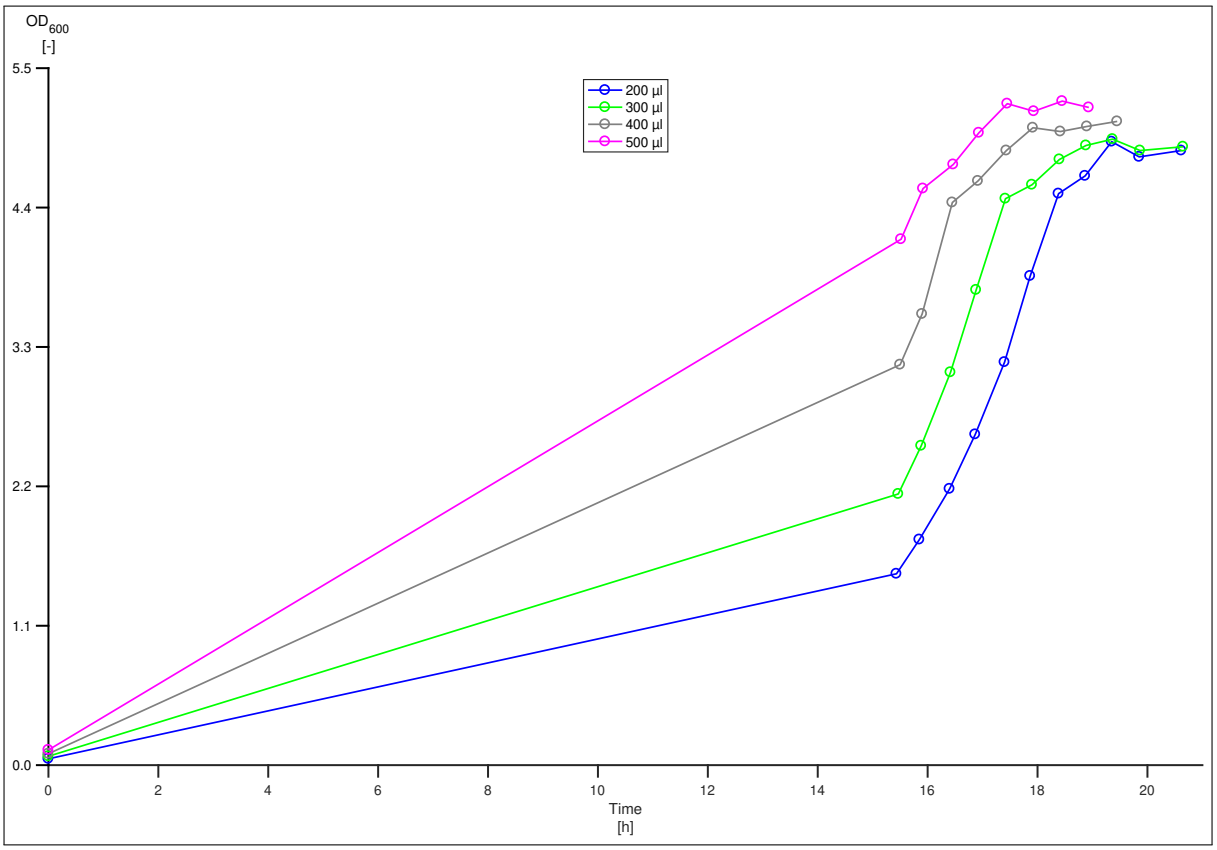

Figure 16: Time course of precultures. Each of the cultures were inoculated with a different volume of the *E. coli* BL21 (DE3) glycerol stock used for expression of the target protein.

As expected, the culture reaches stationary phase faster the higher the applied inoculation volume is. This due to the fact, that the amount of cells at the start of the culture is proportional to the inoculation volume. It seems also, that a higher concentration at the start offsets the final OD_{600} values upwardly. For the main experiments, 200 µl of *E. coli* glycerol stock was chosen for inoculation, since the preferred duration of the preculture was 17 h to 18 h and the cells are within the exponential growth phase in this time range.

4.1.2 Fermentations

The first Fed-Batch cultivation is not described, since it was treated as a preliminary exercise. The batch-end of all fermentations were executed manually, since the automatic batch-end detection was not working. In table 30, relevant data of all cultivations are summarized. These data include the duration of the cultivations, number of pumps used, determined values of μ_{max}, maximum achieved cell density, type of aeration and information regarding the induction status. The plots of fed-batch fermentation 5,6 and 7 are found in Appendix B.

Table 30: This table provides an overview of all cultivations. Listed are the duration of each cultivation, the maximum growth rate during the batch phase(μ_{max}), maximum achieved cell density of each cultivation (c_{XLmax}), type of aeration, number of pumps and information regarding the induction status.

Cultivation	Duration [h]	μ_{max} [h^{-1}]	c_{XLmax} [$g\,l^{-1}$]	Aeration	No. Pumps	Induced?
2	29.52	0.71	46.8	Air	1	No
3	22.71	0.72	49.2	Air	1	Yes
4	25.53	0.77	56.6	Air, Air + O_2	1	Yes
5	29.23	0.68	39.8	Air, Air + O_2	2	No
6	26.51	0.70	38.8	Air, Air + O_2	2	No
7	29.18	0.82	34.0	Air, Air + O_2	2	No
8	26.84	0.66	60.6	Air, Air + O_2	1	Yes
9	24.35	0.60	70.5	Air, Air + O_2	1	Yes

Fed-batch fermentation 2. In the batch phase of the second fed-batch fermentation, the cells grew exponentially with μ_{max} at $0.71\,h^{-1}$ as seen in figure 17. The pO_2 dropped from 100 % to around 20 % due to the increasing cell density. At the same time the stirrer rose exponentially. The pO_2 should be kept at 25 %, but the pO_2 sharply rose at approx. 2.5 h until it reached around 40 %. From there on the pO_2 steadily descends in a oscillating manner until its value was 10 %. The pO_2 rose again and fluctuated around 20 % until the substrate was depleted. Depletion of the substrate led to an immediate rise of the pO_2, while N_{St} sharply decreased. x_{CO2} rises exponentially during the complete batch phase. Its rise also indicates the growth of the cells, since the produced amount of CO_2 is proportional to c_{XL}. After the fed-batch phase 1 was initiated, the pO_2 decreased again. pO_2 strongly oscillated aorund 20 %. An instable control system was present, because the amplitudes were steadily increasing. The control parameters were changed in order to make the controller more robust (by increasing x_P). The system indeed became more stable, but keeping pO_2 was still not possible due to its steady downward drift. The pO_2 then suddenly dropped to 0 % at around 12.6 h. This was probably due to the addition of antifoam. x_{CO2} and N_{St} rose exponentially since start of the first fed-batch phase. N_{St} was also strongly oscillating until the control parameters were changed. But the pO_2/agitation control was too inert, since the drop of pO_2 to 0 % did not cause a strong increase of the stirrer speed. Due to the first reservoir (R1) not being changed to the second reservoir (R2) before next day, it run empty and thus Q_{S1R} dropped to $0\,g\,l^{-1}\,h^{-1}$.

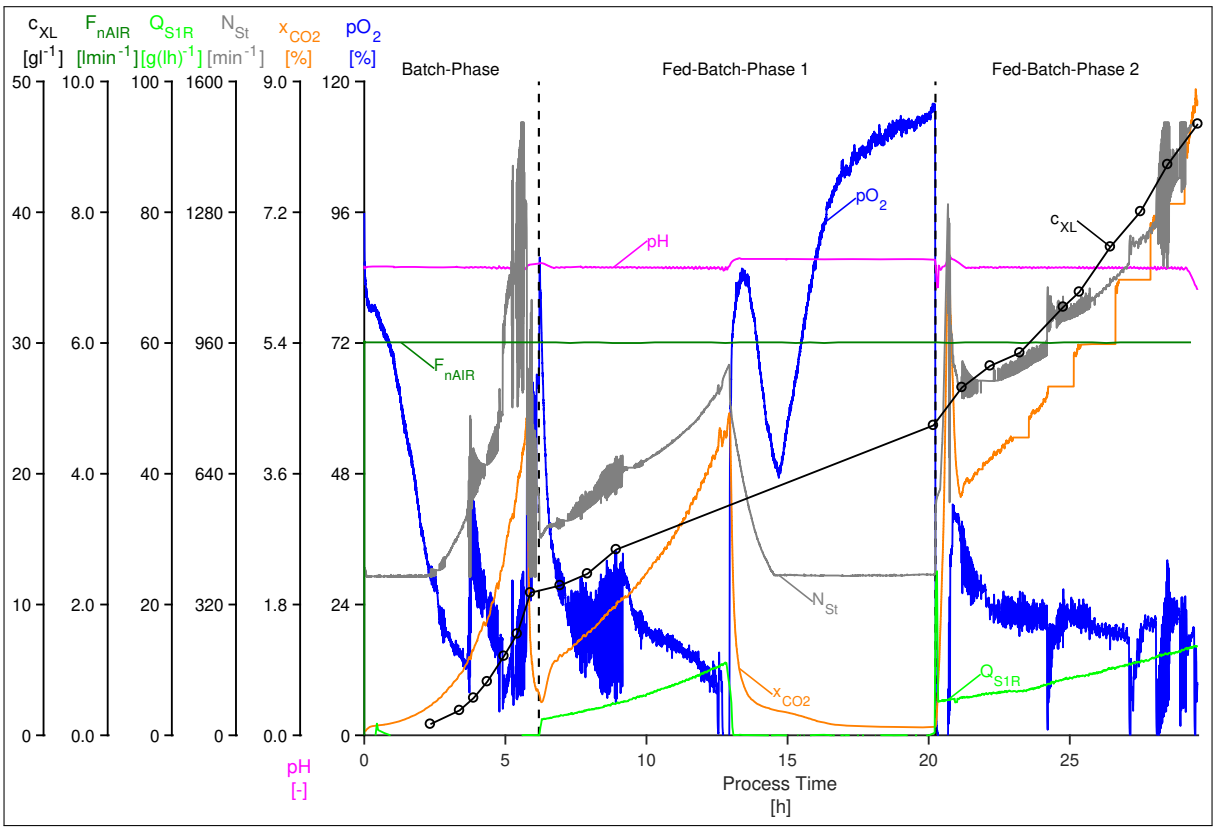

Figure 17: The course of fed-batch fermentation no. 2 is depicted in this figure. The online values, which are shown here, include N_{St}, pO_2, pH, F_{nAIR} and x_{CO2}. The offline value c_{XL} was determined gravimetrically. Q_{S1R} was determined via the online measured weight signals of the feeding reservoirs.

This led to the decrease of N_{St} and x_{CO2}, while pO_2 rose to approx. 85 %, since no substrate was fed into the medium. After reaching 85 %, pO_2 began to drop again. This is probably due to the consumption of acetate, which was produced by the cells itself. x_{CO2} just increased slightly during the consumption, which supports the assumption, that acetate is being metabolized by the cells. After the consumption of the accumulated acetate was completed, the pO_2 rose again until it reached almost 120 %. The rise of pO_2 above 100 % was due to to the overpressure being set to 500 mbar at the start of fed-batch phase 1. The stirrer did not react to the drop and the subsequent rise of pO_2 due to it still being above the set point during this period. On the next day the second fed-batch phase was initiated by switching from R1 to R2. Since substrate was now again available for the cells, pO_2 dropped to 0 % while N_{St} and x_{CO2} sharply rose to 1300 rpm and 7 % respectively. Both began to drop after reaching their respective maximum. N_{St} decreased to approx. 830 rpm and from there on rose exponentionally until the end of

the process due to the rising demand of oxygen for the growing cells. Even though a clear trend of the stirrer speed was visible, it was still oscillating, meaning that the control parameters were still not properly adjusted. The behavior of x_{CO2} resembled that of N_{St}, since it also spiked shortly after fed-batch phase 2 was started and subsequently began to decrease until its value reached approx. 3.3 %. And like N_{St}, x_{CO2} began to rose exponentially. But as it rose, it displayed a "stair"-like behavior. This problaby meant that the communication between the off-gas sensor and MFCS was lagging. The spike exhibited by N_{St} and x_{CO2} and their subsequent decrease shortly after initiation of fed-batch phase 2 indicates that cells had to adapt their metabolism due to the relatively long duration of "starvation". The offline value c_{XL} also began to rose exponentially after start of fed-batch phase 2. Thus, it could be assumed, that no metabolic shift occured, which could have a negative effect on the growth of the cells. The pO_2 remained at 0 % shortly after start of fed-batch phase 2 until it rose to around 40 %. This spike was succeeded by a subsequent drop. After pO_2 dropped to approx 25 %, the decrease started to slow down. But the controller was still not capable of maintaining pO_2 at 25 % as a downward trend was visible. The oscillation of pO_2 increased towards the end of the cultivation. The fluctuation of N_{St} in turn als increased towards the end of the cultivation with the amplitudes reaching 1500 rpm, the maximum agitation speed.

Fed-batch fermentation 3. After inoculation of the medium with cells, pO_2 immediately dropped to around 80 % (see figure 18). From there, it rose slightly then fell to around 20 %. pO_2 oscillated around 20 % until a sudden drop occured at approx.4.5 h. After falling below 5 %, pO_2 began to rise to 20 % again and stayed there until the end of the batch phase. Activation of the pO_2/agitation control led to the rise of N_{St}. The sudden drop of pO_2 at 4.5 h led to the sharp rise of N_{St}. After that strong rise, N_{St} continued to increase until it reached a maximum value of approx. 1270 rpm. x_{CO2} rose exponentially throughtout the whole batch phase and thereby indicating that the cells are growing exponentially. The offline determined values of c_{XL} confirmed the exponential growth of the cells. Depletion of the substrate led to the instant increase of pO_2, while N_{St} and x_{CO2} simultanously decreased. After transition to fed-batch phase 1 was manually executed, feeding solution was fed into the reactor and pO_2 decreased again

until started to heavily fluctuate around 20 %. This strong fluctuation caused N_{St} to fluctuate too, as it tried to keep pO_2 at around the setpoint. Adjustment of the control parameters decreased the fluctuation of N_{St} and pO_2. The rise of N_{St}, x_{CO2} and c_{XL} during the fed-batch phase 1 was shallower compared to their increase in the batch phase due to the μ_{set1} being $0.2\,h^{-1}$, and thus smaller than μ_{max}. At 11.686 h the second phase of fed-batch 2 was initiated. This led to the spike of pO_2 and the sudden drop of N_{St} as well as x_{CO2}. The cause for these sudden changes were due to the cells adapting to the decreased feeding rate. μ_{set2} was set to be lower than μ_{set1} and this led to the more shallow exponential increase of N_{St} and x_{CO2}.

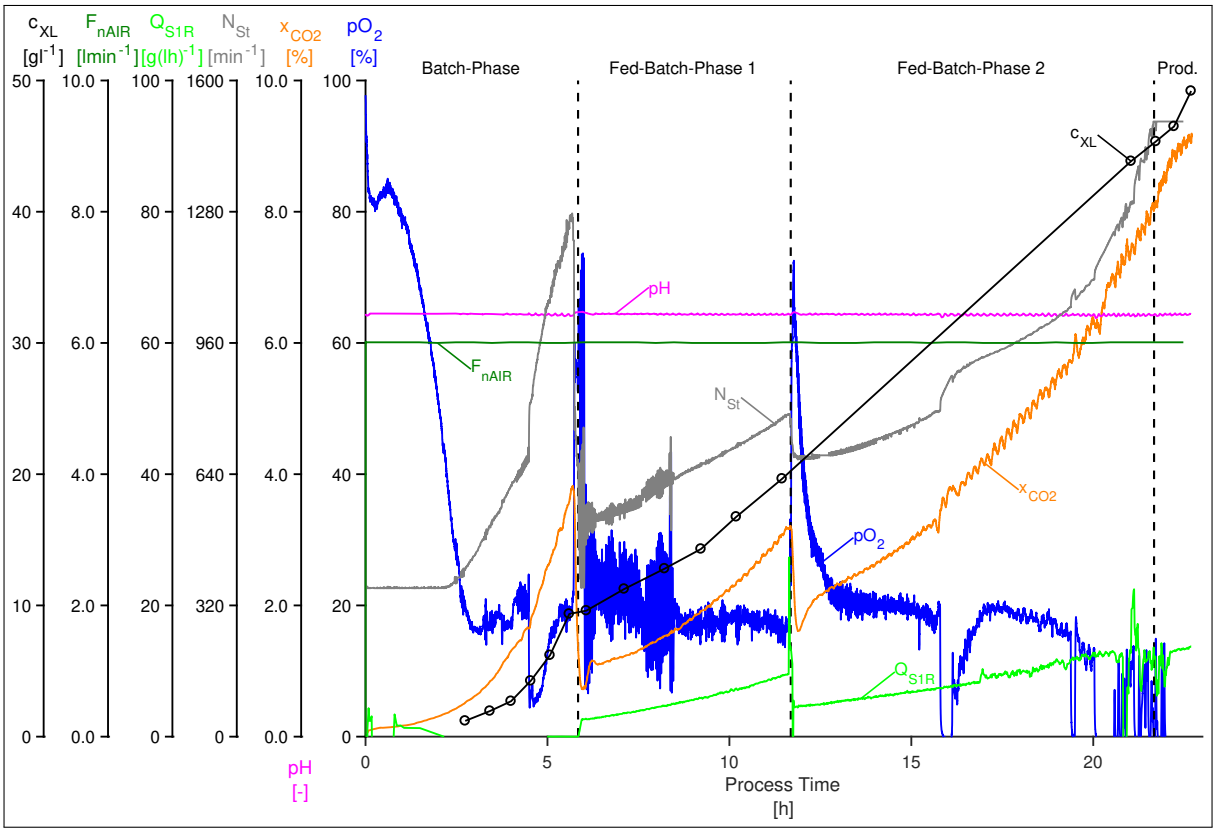

Figure 18: The course of fed-batch fermentation no. 3 is depicted in this figure. The online values, which are shown here, include N_{St}, pO_2, pH, F_{nAIR} and x_{CO2}. The offline value c_{XL} was determined gravimetrically. Q_{S1R} was determined via the online measured weight signals of the feeding reservoirs.

After reaching a maximum value of approx. 70 %, the pO_2 decreased until 20 %. From there, it slowly decreased, since the controller was apparently too inert to prevent the growing deviation. At around 15.8 h, the pO_2 promptly dropped to 0 %. Antifoam was

pumped in to the media after foamin occured. pO_2 remained at 0 % for about 10 min. After that, it strongly rose to 10 % and from there on it slowly approached 20 %. Again, pO_2 began to drift downwards after reaching 20 % until a second sudden drop to 0 % at 19.4 h occured. After a short while pO_2 increased again until it was just under 20 % only for it to start decrease again slowly. pO_2 strongly oscillated towards the end of the cultivation, while droping to 0 % severly times. This is for one caused by limitation of the oxygen transfer due to the stirrer reaching its maximum value, and for another caused by the inability of the controller to maintain pO_2 at the setpoint. Finally, pO_2 remained at 0 % after around 22 h. Q_{S1R} rose exponentially without greater disturbance until around 20.8 h, where it started to fluctuate. It may be due to insufficient filtering of the spikes of the bioreactor weight (see 3.2.2 for explanation of the spikes/noises). x_{CO2} increased exponentially until the end of fermentation. IPTG was injected into the culture broth at 21.67 h and thus production was initiated. c_{XL} rose exponentionally throughout fed-batch phase 2. Induction did not seem to have an negative impact on the growth of the cells.

Fed-batch fermentation 4. As with previous cultivations, the controller was unable to keep pO_2 stable near the setpoint. After inoculation, it dropped until it stabilized around 10 %. It then rose to approx. 15 % and remained there until end of the batch phase. x_{CO2} and N_{St} rose exponentially and thereby indirectly indicating the exponential growth of the cell density. The offline measured c_{XL} also confirmed that, exponential growth occured during the batch phase. The determined μ_{max} value was 0.70 h^{-1}. Depletion of the substrate at 4.87 h led to the characteristic sudden rise of pO_2, while x_{CO2} and N_{St} dropped. Transition to fed-batch phase 1 was then manually initiated. Shortly after begin of the fed-batch phase 1, pO_2 and N_{St} were heavily oscillating, due to the control parameters not being properly set. The controller was adjusted to be more inert (increasing x_P) ,and thus pO_2 as well as N_{St} stopped oscillating. For the rest of fed-batch phase 1, pO_2 gradually decreased from 30 % to 15 %. N_{St} and x_{CO2} increased exponentially, but with a shallower course than in the batch phase due to the reduced growth rate. c_{XL} displayed the same behavior.

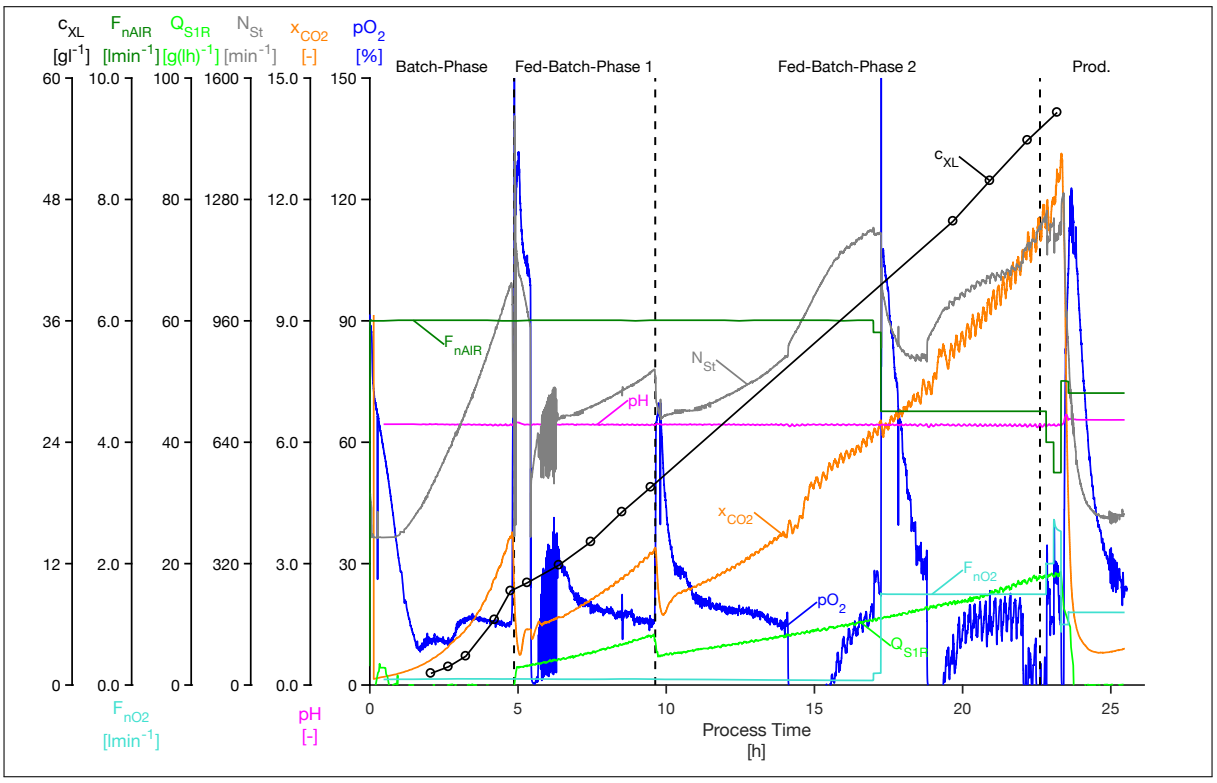

Figure 19: The course of fed-batch fermentation no. 4 is depicted in this figure. The online values, which are shown here, include N_{St}, pO_2, pH, F_{nO2}, F_{nAIR} and x_{CO2}. The offline value c_{XL} was determined gravimetrically. Q_{S1R} was determined via the weight signals of the feeding reservoirs..

Fed-batch phase 2 was initiated at 9.63 h. This led again to the spike and subsequent descend of pO_2. After reaching approx. 30 %, pO_2 slowly decreased until it suddenly dropped immediatley to 0 % at around 14 h. It remained there relatively long and then began to rise gradually after 15.5 h. N_{St} rose exponentially throughout fed-batch phase 2 with the course getting steeper after the drop of the pO_2 to 0 %. But the stronger increase of N_{St} was still unable to reduce the control deviation. The rapid drop of pO_2 was probably induced by addition of antifoam into the reactor as a result of a preceded foam build up. x_{CO2} grew exponentially, while the noise of its signal also increased. The sudden rise of N_{St} at 14 h also led to a sudden increase of x_{CO2}. N_{St} triggered the increase of F_{n02} after reaching 1200 rpm at 16.97 h. F_{n02} increased to 0.2 l min^{-1}. But since the N_{St} did not react to the now increased oxygen transfer, the next increase of F_{n02} was initiated. F_{n02} increased from 0.2 l min^{-1} to 1.5 l min^{-1}. This was a mistake, as it was intended for F_{n02} to rise by 0.2 l min^{-1} after each step. N_{St} dropped this time and

therefore could not immediately initiate the next increase of F_{n02}. It dropped to approx. 850 rpm and gradually increased from there until the next increase of F_{n02} was triggered. N_{St} was again left more or less unfazed and therefore triggered the next increase of F_{n02} from $2\,\mathrm{l\,min^{-1}}$ to $2.5\,\mathrm{l\,min^{-1}}$. A last change of F_{n02} was induced by N_{St}, but this time F_{n02} decreased to $1\,\mathrm{l\,min^{-1}}$ due to the MFCS recipe not being properly set up. Since the controller was still too inert, the stirrer fluctuated around 1200 rpm and thus induced the next change of F_{n02}. F_{n02} increased from $1\,\mathrm{l\,min^{-1}}$ to $1.2\,\mathrm{l\,min^{-1}}$ and remained there until the end of the process. F_{nAIR} decreased everytime F_{n02} increased so that the total gas flow always remained at $6\,\mathrm{l\,min^{-1}}$. After reservoir R2 was depleted as indicated by the drop of Q_{S1R} to $0\,\mathrm{g\,l^{-1}}$ at 23.74 h, it rapidly decreased due to the strong increase of pO_2. pO_2 was heavily oscillating after the second half of the fed-batch phase 2, especially after the oxygen transfer was increased due to F_{n02}. The controller was inable of keeping pO_2 around the setpoint, as it even dropped to 0 % on multiple occasions throughout the later part of fed-batch phase 2. c_{XL} as well as x_{C02} increased throughout fed-batch phase 2 until the end of the process. IPTG was injected into the reactor at 22.61 h. After the process was terminated, about 1.2 l of the cell broth was harvested for downstream processing.

Fed-batch fermentation 8. Like in the previous cultivations, the batch phase of Fed-Batch 8 lasted for around 5 hours. The pO_2 dropped immediately from 100 % to approx. 60 % after inoculation . From there on the pO_2 decreased until ist was below 30 %. This led to the activation of the pO_2/agitation control. Even though pO_{2w} was set at 25 %, the controller did not manage to keep the pO_2 at this value, as there was permanent control deviation. Instead, pO_2 was more or less stable at around 10 %. Thus, a control deviation of 15 % was present. But this did not seem to affect the growth of the cells like in previous cultivations. N_{St} and x_{CO2} rose exponentially until the depletion of the substrate. Depletion of the substrate was indicated by the strong rise of pO_2 at 5.6 h. The immediate drop of x_{CO2} also confirmed that glucose was depleted, and thus the production of CO_2 decreased.

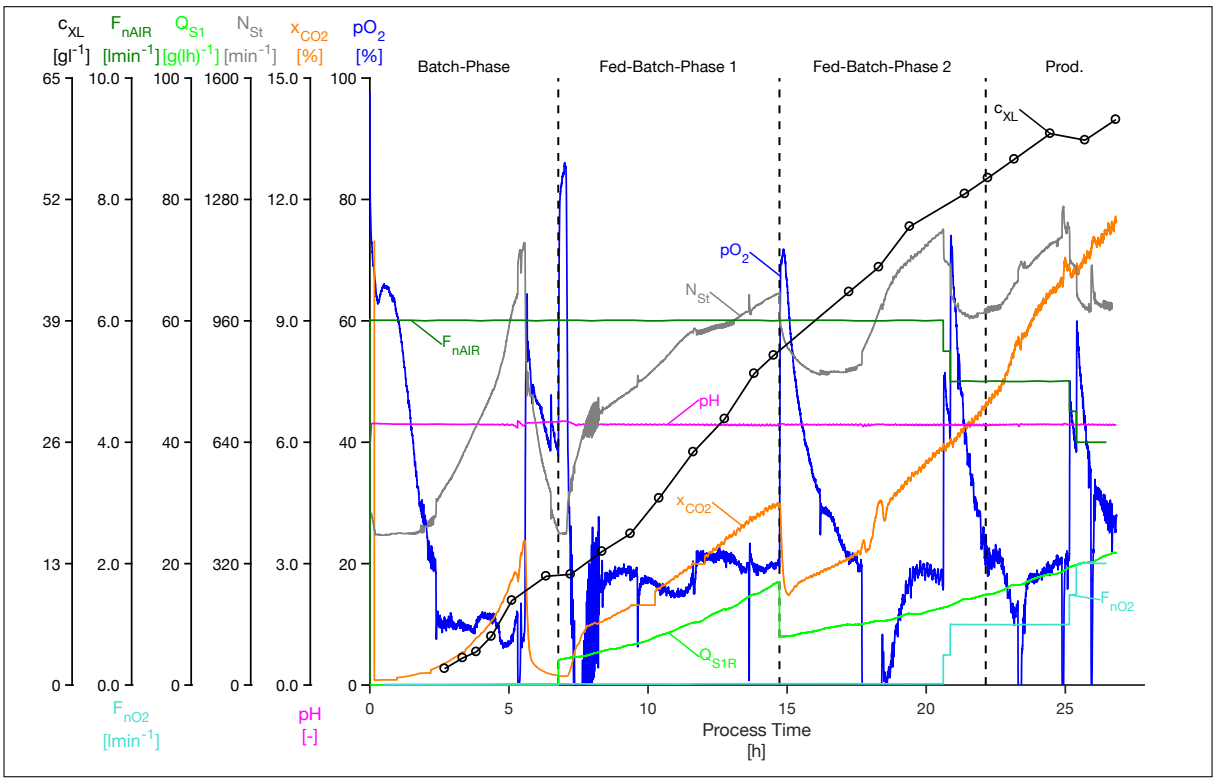

Figure 20: The course of fed-batch fermentation no. 8 is depicted in this figure. The online values, which are shown here, include N_{St}, pO_2, pH, F_{nO2}, F_{nAIR} and x_{CO2}. The offline value c_{XL} was determined gravimetrically. Q_{S1R} was determined via the online measured weight signals of the feeding reservoirs.

The fed-batch did not start immediately after depletion of the substrate, since the batch-end detection did not start automatically even though the batch-end detection conditions were altered (time frame for drop of N_{St} was decreased from 45 s to 30 s). Thus, the start of the fed-batch phase was initiated manually as with the previous cultivations. At the start of the fed-batch phase 1, the controller was again incapable of stabilizing pO_2, which is indicated by the oscillating behaviour of pO_2 . After changing the control parameters at 8.22 h, the pO_2 could be stabilized at just below 20 %. A small upward shift of pO_2 occured at around 11.8 h, which led to pO_2 fluctuating around 20 % until the remaining time of fed-batch phase 1. c_{XL} rose exponentially during fed-batch phase 1, but the increase was shallower than in the batch phase. Increase of the cell density also meant that x_{CO2} as well as N_{St} were increasing throughout fed-batch phase 1. Fed-batch phase 2 started at 14.76 h. This again led to the sudden rise of pO_2, while N_{St} and x_{CO2} decreased. pO_2 peaked at approx. 75 % and then began to drop over a relatively long

period until it finally reached 0 % at around 18 h. The slow drop was probably due to the controller being too inert. N_{St} did not respond to the decrease of pO_2. 15 min after N_{St} reached 1200 rpm, F_{nO2} rose from 0 l min^{-1} to 0.5 l min^{-1}. At the same time F_{nAIR} was decreased by 0.5 l min^{-1}. The increase of oxygen transfer was accompanied by the strong increase of pO_2. But since the controller was still too inert to react fast to the change of the pO_2, N_{St} remained at 1200 rpm, and thus triggered the next increase of F_{nO2}. Consequently, F_{nO2} rose from 0.5 l min^{-1} to 1 l min^{-1}. pO_2 was still falling when the second increase of F_{nO2} occured, and thus it rose again until it peaked at approx. 75 %. pO_2 then began to decrease until it reached 20 %. But pO_2 did remain there for only for a short period before descending further. Then antifoam was pumped into the reactor at around 23 h leading to the immediate drop of pO_2 until it reached 0 %. pO_2 remained there for about 6 min until it began to rise again. After reaching 20 %, pO_2 slowly increased until the next increase of F_{nO2} occured, and thus lead to another sharp increase of pO_2. Due to the controller still being too inert, the next increase of F_{nO2} was triggered. The spike was followed by a drop, but pO_2 did not reach 20 % before the end of the cultivation. c_{XL} increased throughout fed-batch phase 2, but it did not rise as fast as in fed-batch phase 1 due to μ_{set} being decreased. Even after injecting IPTG into the culture broth at 22.14 h in order to initate the production of the target protein, c_{XL} was still increasing. A higher cell density could be achieved, since c_{XL} and especially x_{CO2} did not show signs of a flattening curve. Lampert (2019) achieved a maximal cell density of 94.2 g l^{-1} by also increasing the oxygen transfer rate with the help of pure oxygen. after the cultivation was finished, about 1.2 l of the culture broth was harvested.

Fed-batch fermentation 9. During the whole batch phase a rather big control deviation was present, since pO_2 was more or less stable at around 5 %. But despite that fact, microbial growth was seemingly not negatively impacted. The determined μ_{max} was 0.60 h^{-1} and thus the lowest μ_{max} of all cultivations. μ_{max} of fed-batch fermentation 8 was the second lowest. It should be noted that, for the fermentation 8 and 9 a new working cell bank (WCB) was prepared out of the previous WCB. Therefore, it may be possible, that the growth characteristics were slightly altered. N_{St} and x_{CO2} rose exponentially without any disturbance (see figure21) . Fed-batch phase 1 was started

after sudden rise of pO_2 indicated the depletion of the substrate at 5.82 h.

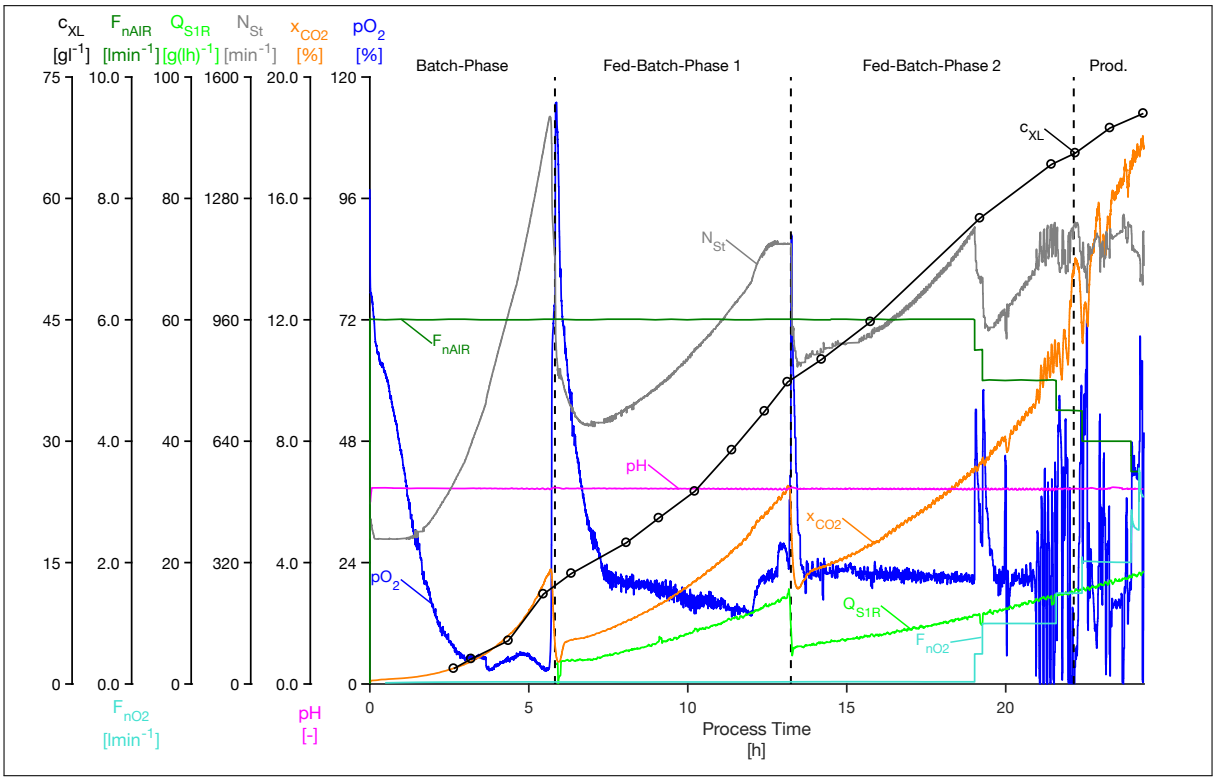

Figure 21: The course of fed-batch fermentation no. 9 is depicted in this figure. The online values, which are shown here, include N_{St}, pO_2, pH, F_{nO2}, F_{nAIR} and x_{CO2}. The offline value c_{XL} was determined gravimetrically. Q_{S1R} was determined via the online measured weight signals of the feeding reservoirs.

The control paramters were adjusted at the start of the fed-batch phase, by making the controller more inert, since previous fermentations showed that oscillation of pO_2 and N_{St} are more likely at the start of a new phase. pO_2 dropped from around 115 % to approx. 25 %. From there, a downward drift occured until around 12 h. pO_2 jumped to approx. 25 % due to further adjustment of the control parameters (T_I was decreased). pO_2 jumped up again slightly before it immediately rose up to just under 90 %, because of of the transition from fed-batch phase 1 to fed-batch phase 2 which is accompanied by the reduction of μ_{set} . c_{XL} rose exponentially throughout fed-batch phase 1, but with a shallower course than in the batch phase. The same can be applied to N_{St} as well as x_{CO2}. In fed-batch pahse 2, pO_2 was stable at approx. 20 % for about 5 h. As soon as F_{nO2} was increased from 0 l min^{-1} to 0.5 l min^{-1}, the controller as not possible to keep the pO_2 as it was heavily fluctuating. Even adjustment of the control parameters had no

effect and so the fluctuation of pO_2 and N_{St} continued until the end of the cultivation. The cells were growing throughout fed-batch phase 2 and the production phase, though c_{XL} appeared to increase linearly rather than exponentially. x_{CO2} on the other side grew exponentially until the end of the cultivation, but it seemed as if the strong fluctuation of the stirrer als inrease the fluctuation of x_{CO2}. Induction by IPTG was executed at 22.14 h. Approx. 3.6 l of the culture broth were harvested after cultivation was ended.

4.1.3 Numerical determination of the feeding rate

For the determination of F_R and Q_{S1R} an numerical method, which uses the weight signals of the reservoirs (m_R), was used (see equation 7). MFCS also receives signals directly from the pump, which could be used for used for plotting and calculations. In figure 22, the volumetric substrate transfer rate determined via the indirect method (Q_{S1R}) and via the pump signal (Q_{S1Rp}) are plotted against the process time. The data from fed-batch fermentation 2 are used. The depletion of reservoir R1 in fed-batch fermentation 2 shows why the indirect method has an advantage against the feeding rate determined by the pump signal. The letter method can not discriminate between an empty and a filled reservoir, since the voltage signal just keeps increasing. The indirect method on the other hand uses the weight signals of the feed reservoir and therefore depletion of the reservoir will be visible on the plot.

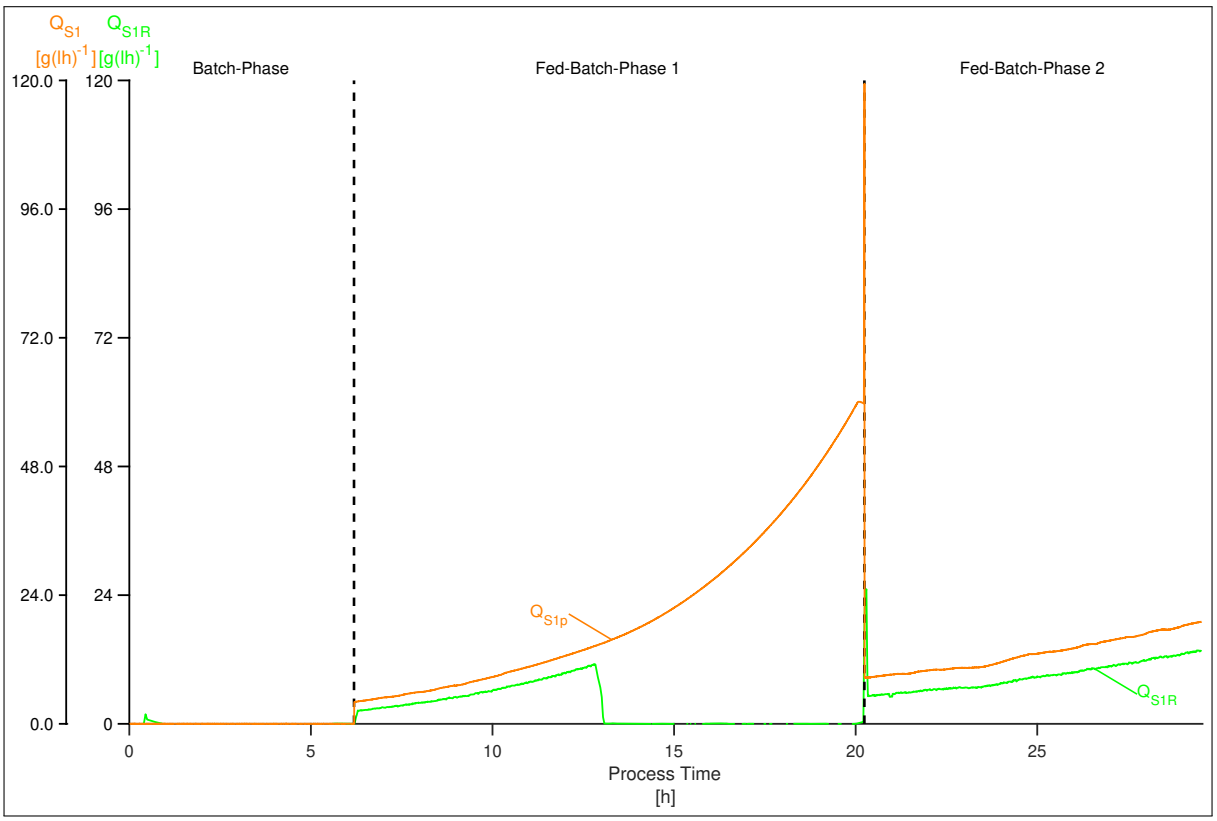

Figure 22: Comparison of the volumetric substrate transfer rate determined by weight signals (Q_{S1R}) of the reservoir and by the signals obtained from the pump (Q_{S1p}).

4.1.4 Correlation of cell density and optical density

For each cultivation, c_{XL} and ΔOD_{600} were determined at various time points throughout the process. The correlation factor $f_{X/OD}$ was then determined via linear regression for each cultivations. The plot depicting the correlation between c_{XL} and ΔOD_{600} is depicted in figure 23.

All curves indicate, that a strong linear correlation between c_{XL} and ΔOD_{600} is present, as all R^2 values are at least 0.991. Thus, the optical density can be used for estimating the cell density. It is important to note, that for the fed-batch fermentations 2, 3 and 4 a systematic error regarding the calculation of c_{XL} was present. Double determination was carried out for the estimation of c_{XL}. In fed-batch fermentation 2, 3 and 4, the same pipette tip was used for transferring the cell suspension into the reaction tubes for the first and second determination. This caused the second tube to contain more of the cell suspension. Thus, the cell dry weight in the second tube was in most cases higher than the

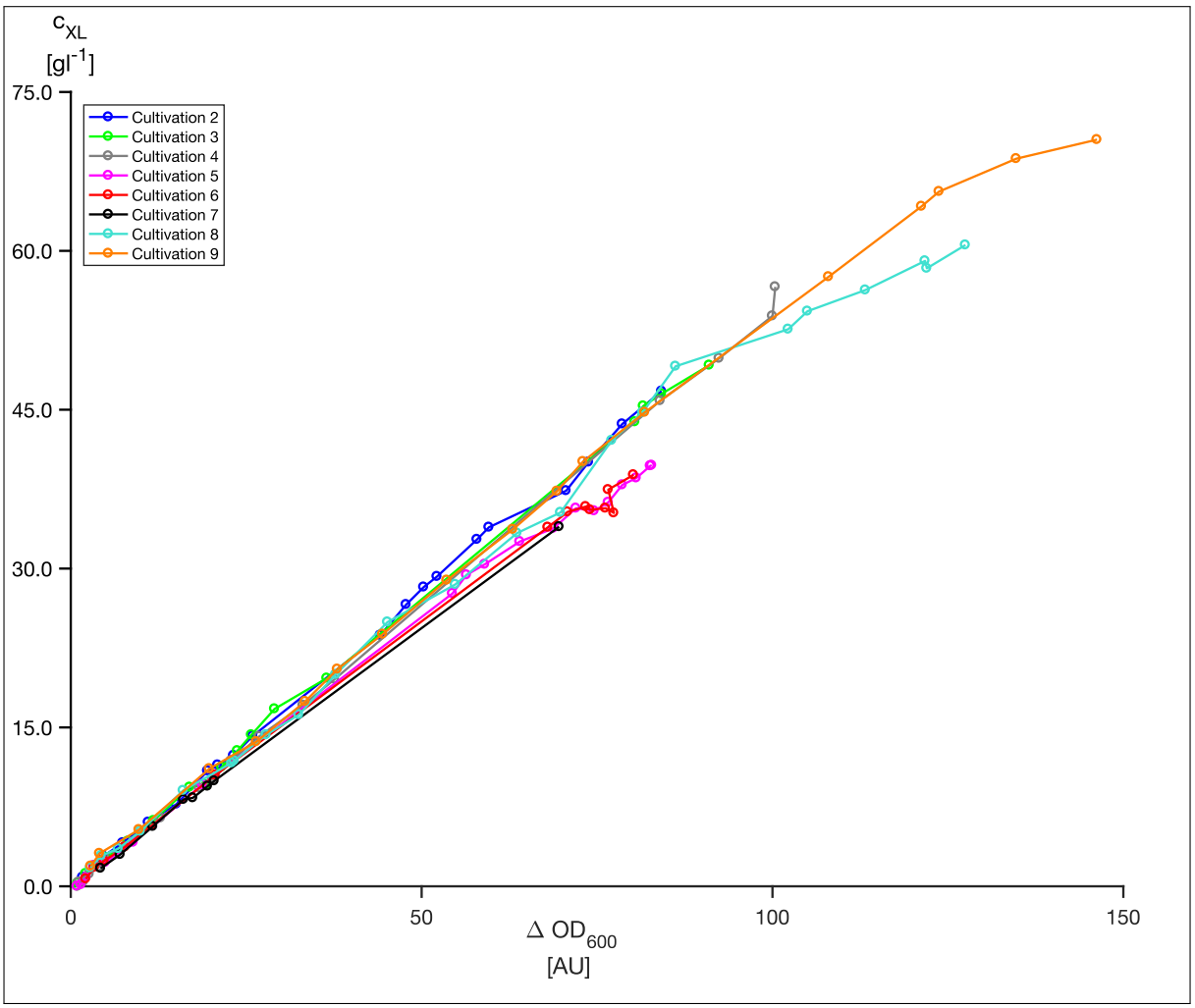

Figure 23: The correlation between c_{XL} and ΔOD_{600} for all cultivations is depicted in this plot. c_{XL} was determined gravimetrically.

first tube. In order to compensate this error, the pipette tip was changed for the second tube. Indeed, the systematic error was no longer present in the succeeding cultivations. This systematic error is visible in the $f_{X/OD}$ values of the fed-batch fermentations 2, 3 and 4, as their values are significantly higher than the correlation factors determined for the other cultivations. If these three values are excluded from the calculation of the average, then the mean value is $0.49\,\mathrm{g\,l^{-1}\,AU^{-1}}$. If they are regarded for the calculation of the average, then a value of $0.51\,\mathrm{g\,AU^{-1}}$ is determined. The values are all listed in table 31

Table 31: $f_{X/OD}$ and R^2 values for all cultivations.

Cultivation	R^2 [-]	$f_{X/OD}$ [$g\,l^{-1}$]
2	0.9985	0.55
3	0.9994	0.55
4	0.9992	0.55
5	0.9971	0.49
6	0.9975	0.48
7	0.9995	0.49
8	0.9910	0.49
9	0.9954	0.51

4.1.5 Control paramater settings

The control paramters of the pO_2/agitation controller were altered in every fermentation in order to keep pO_2 stable around the set point (25 %). The plot of fed-batch fermentation 9 serves as representative (see figure 24) for describing the impact of the parameter changes. The changes of the control paramters are represented by the red vertical lines in the plot. Table 32 contains the detailed information regarding the parameter changes. During batch phase, a strong control deviation was present. Therefore, x_P was decreased to make the controller more responsive. Decreasing T_I also had no impact. After fed-batch phase 1 was initiated, x_P was increased in order to make the controller more inert. This prevented a strong control deviation like in batch phase 1. pO_2 could still not be kept at 25 %, since it gradually decreased. Only after T_I was decreased from 750 s to 200 s, the controller was able to keep pO_2 stable at around 24 %. pO_2 started to oscillate heavily towards the end of fed-batch phase 2. Despite increasing the T_I two times, pO_2 was not able to stabilize.

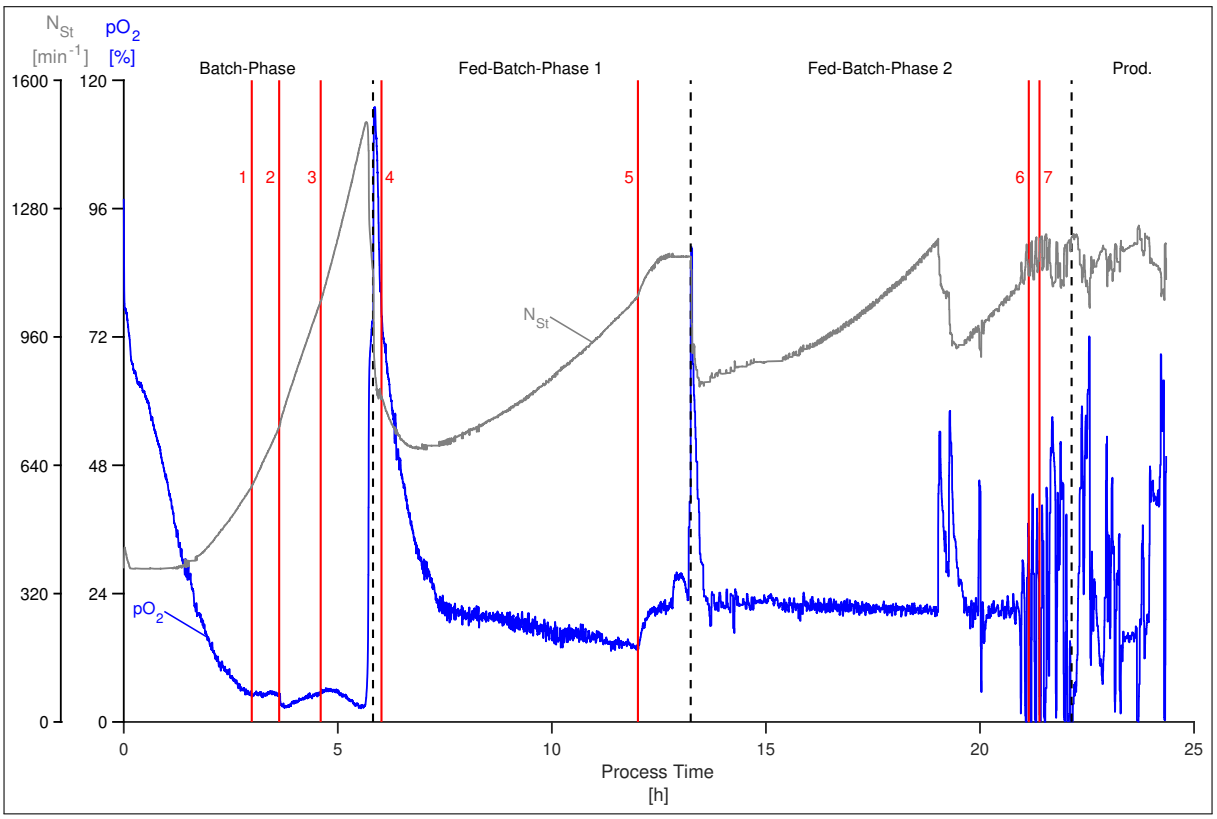

Figure 24: The control paramters of the pO_2/agitation controller were changed during of fed-batch fermentation 9. The time of the changes are indicated by the red vertical lines. In table 32 the control paramter changes are listed.

Table 32: Overview of all executed changes of the control parameters during fed-batch fermentation 9.

No.	Time [h]	Changes	x_P [-]	T_I [s]	Reason for change
1	2.99	x_P: 750 → 500	500	1000	Control deviation
2	3.63	T_I: 1000 → 750	500	750	Control deviation
3	4.60	x_P: 500 → 375	375	750	Control deviation
4	6.02	x_P: 500 → 375	750	750	Start of new phase
5	12.01	T_I: 750 → 200	750	200	Gradually increasing control deviation
6	21.14	T_I: 200 → 500	750	200	Strong oscillation of pO_2
7	21.39	T_I: 500 → 1000	750	200	Strong oscillation of pO_2

4.2 Downstream

In this section, the results of the downstream processing, which include the extraction, purification and concentration of the AMP, are presented and discussed.

4.2.1 Isolation of inclusion bodies

Since the product is present in the cells in the form of inclusion bodies, the cells had to be disrupted, so that the content within the cells could be released. The cell disruption was carried out via high pressure homogenization, since this method is suited for a possible scale up of the downstream processing. Approx. 50 g of frozen cell pellet was resuspended in 1 l Tris-HCl buffer, pH 7.4. The optical density of this suspension as well as the suspension after each passage was measured. As expected, the optical density decreased with every passage. The strongest decrease was obtained after the first passage. The decrease itself got shallower with each subsequent passage. Bradford assay was carried out to track the release of the proteins. The maximum protein amount was released after three passages with the measured protein concentration being 4.1 mg ml^{-1}. After three passages, the protein concentration seemed to slightly decrease with each passage. This may be due to the slight dilution which occured after each passage, since water was filled into the inlet between the passages to prevent the machine to work under dry conditions. Before the first passage, protein were already present in the supernatant obtained from centrifuging unbroken cells. This indicated that some cells were already lysed. The effect of dilution can be minimized by taking the samples directly from the outlet after a bit of homogenate has left the outlet. In figure 25 the behavior of the optical density and the release of protein dependent on the number of passages is depicted.

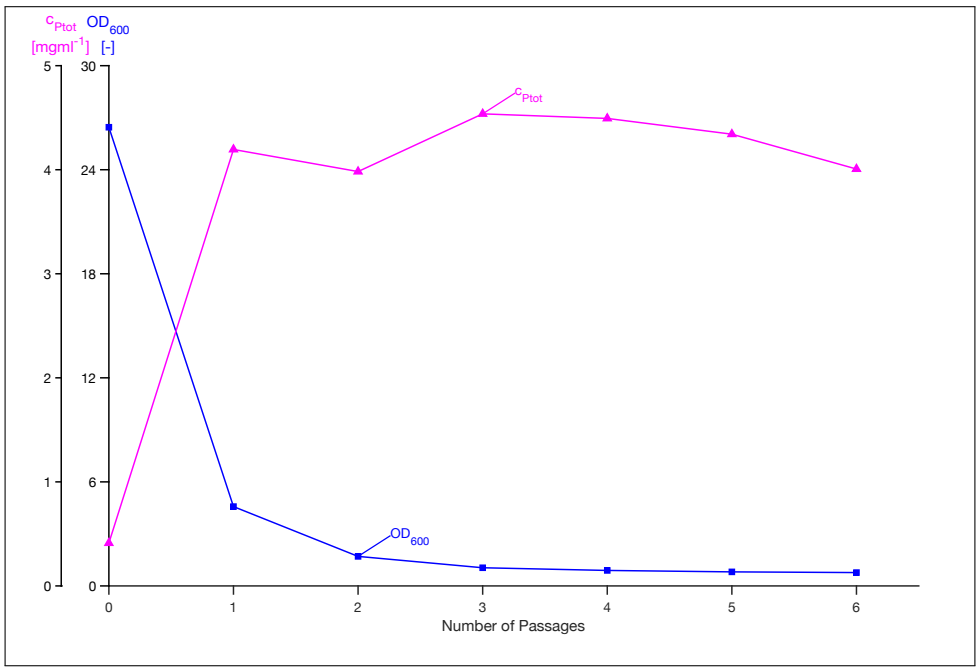

Figure 25: In this figure the optical density (blue) and the total protein concentration (magenta) are plotted against the number of passages.

40 ml and 20 ml of the homogenate were filled into a 50 ml falcon respectively. After that, a centrifugation step was carried in order to seperate the liquid phase from the insoluble particles, which also contains the inclusion bodies. The pellet obtained from centrifugation of 40 ml homogenate was visibly larger then that obtained from 20 ml of homogenate. Solubilization with 20 ml of solubilization buffer (see table 7 for recipe) was sufficient for dissolving both pellets. Only a little amount insoluble fractions remained after centrifugation. For further clarification of the obtained solutions, syringe filters made of cellulose acetate with a pore size of 0.2 µm were used. Two filters were sufficient for 20 ml of solution. The volume of the filtrates were approx. 17 ml. The solution was now ready for purification via IMAC.

4.2.2 Purification of the AMP with IMAC (HisTrap)

15 ml of solution containing solubilized inclusion bodies were applied on the column. Samples originating from 20 ml and 40 ml of homogenate were used in the purification experiments. Proteins, which did not interact with the column, were not retained and therefore were present in the breakthrough. In the first series of the experiments

equilibration buffer 1 (see table 8 for recipe) was used. After sample application was finished, the column was washed with 10 CV of equilibration buffer 1. No peak was detected during the washing step. The washing step was followed by an elution step. The elution was executed in an isocratic manner. The concentration of Imidazole was set to 100 mM.

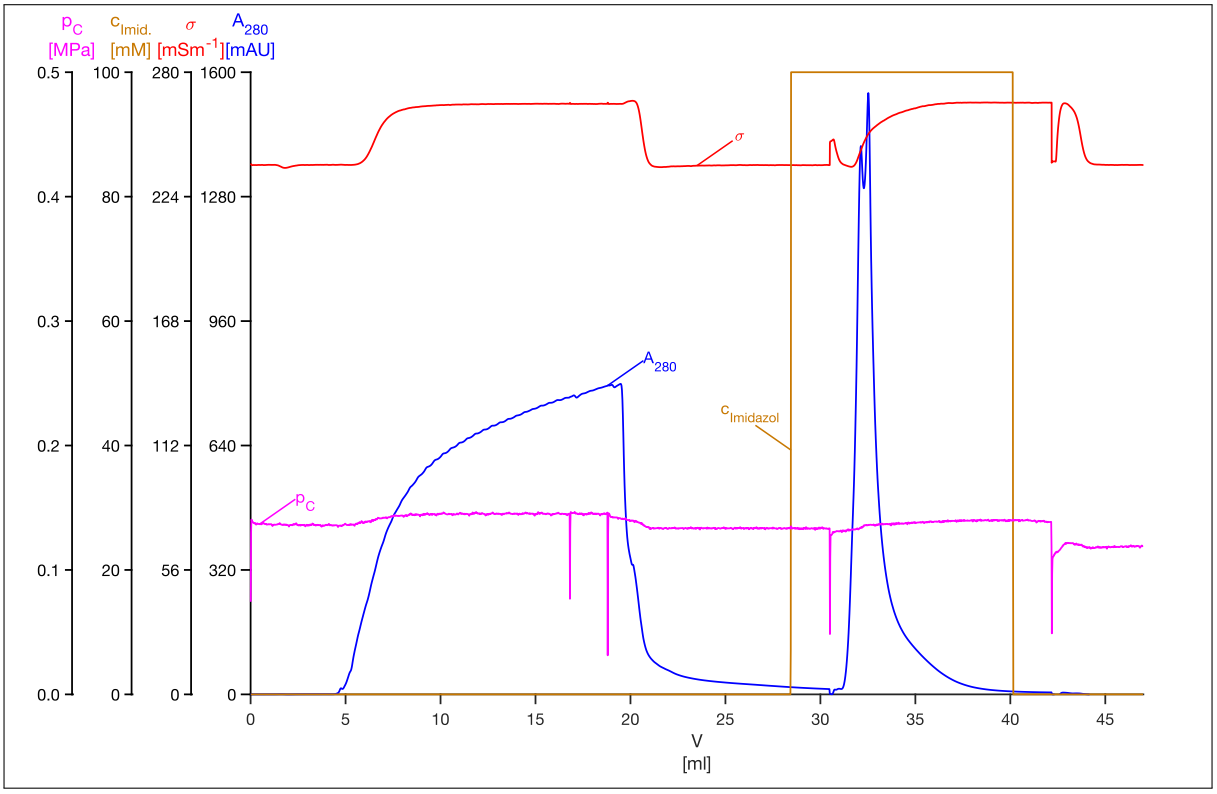

Figure 26: chromatogram obtained from applying 15 ml of sample on HisTrap FF 1 ml. The sample was obtained from 40 ml of homogenate. Depicted on this plot are: the absorption at a wavelength of 280 nm (blue), conductivity(red), pre column pressure (magenta) and concentration of imidazole (brown) within the system flow. Composition of the equilibration buffer: 20 mM Tris-HCl, pH 7.4; 4 M guanidine-HCl. Composition of the elution buffer: 20 mM Tris-HCl, pH 7.4; 6 M guanidine-HCl; 100 mM imidazole. Flow rate was set to 1 ml/ min.

It is important to note that, it was observed that prefilling the inlet for the elution buffer with said buffer prevented the binding of the target protein to the column. The reason for this phenomenon, might be that the mixing chamber, where the inlets of A and B join together, is too large. Thus, a residual amount of imidazole is present and is carried onto the column via the equilibration buffer. The concentration is apparently high enough to prevent the binding of the target protein. To overcome this problem, the

inlet for the elution buffer was filled with equilibration buffer. A method was written, which replaced the equilibration buffer with the elution buffer just before start of the elution step. During the elution a peak is detected, which is probably composed of two overlapping peaks as two seperate spikes are seen at the top. The maximum absoprtion for a sample, which was obtained from 40 ml of homogenate, was approx. 1550 mAU. The peak was significantly smaller for the sample originating from 20 ml of homogenate, since the maximum value of A_{280} is at around 1290 mAU.

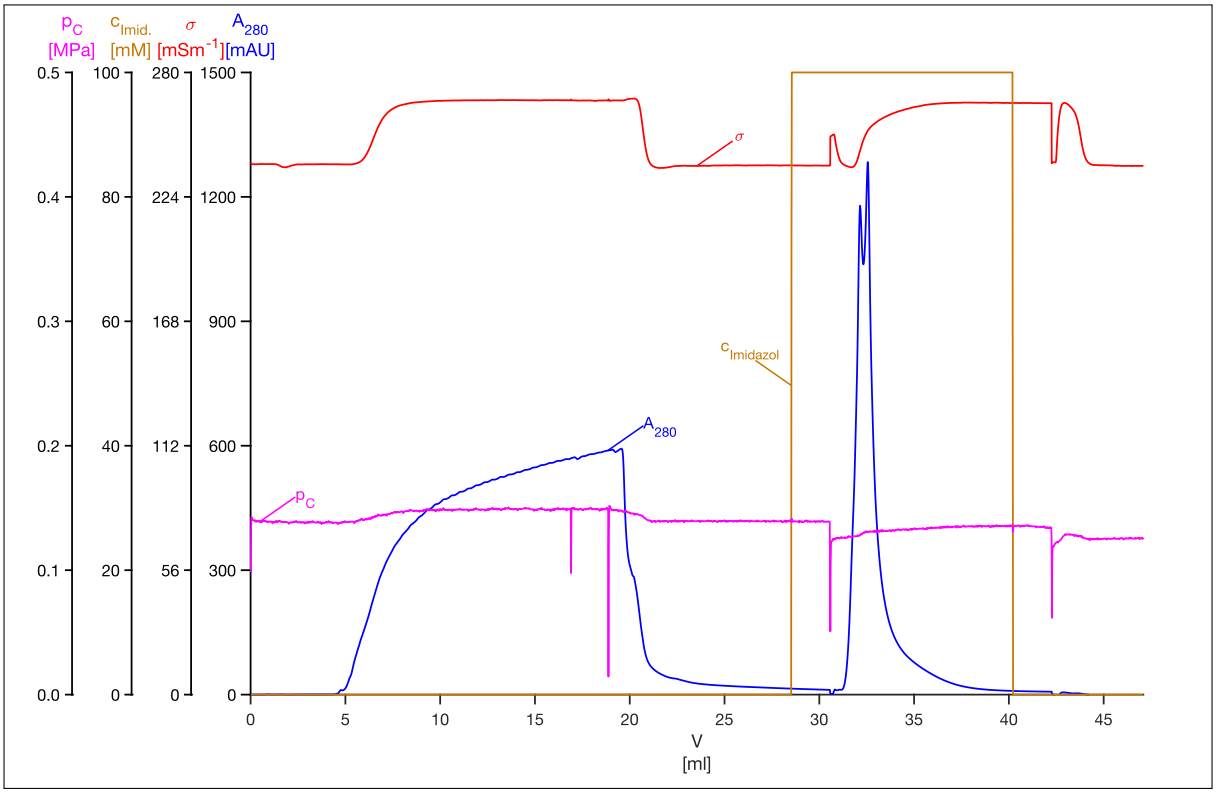

Figure 27: chromatogram obtained from applying 15 ml of sample on HisTrap FF 1 ml. The sample was obtained from 20 ml of homogenate. Depicted on this plot are: the absorption at a wavelength of 280 nm (blue), conductivity(red), pre column pressure (magenta) and concentration of imidazole (brown) within the system flow. Composition of the equilibration buffer: 20 mM Tris-HCl, pH 7.4; 4 M guanidine-HCl. Composition of the elution buffer: 20 mM Tris-HCl, pH 7.4; 6 M guanidine-HCl; 100 mM imidazole. Flow rate was set to 1 ml/ min.

It was possible to reduce the concentration of guanidine-HCl in the equilibration buffer from 6 mM to 4 mM without causing aggregation of the solubilized fusion protein. This is the reason, why the conductivity was lower during equilibration and washing. The concentration of guanidine-HCl within the solubilisation buffer and elution buffer was

not changed. As mentioned above, seemingly overlapping peaks were eluted from the column. Therefore, the stringency of the washing step had to be increased in order to wash away non-his-tagged proteins. Stringency of the washing condition is achieved by increasing the imidazole concentration, so that weakly bond proteins are displaced from the column. In previous works (Lampert, 2019; Steinhart, 2019), a step elution technique with two different imidazole concentration was applied. First the pump rate of system pump B was set to 10 %, meaning that the concentration within the system flow was 10 mM (the elution buffer with same composition as in this work was used).

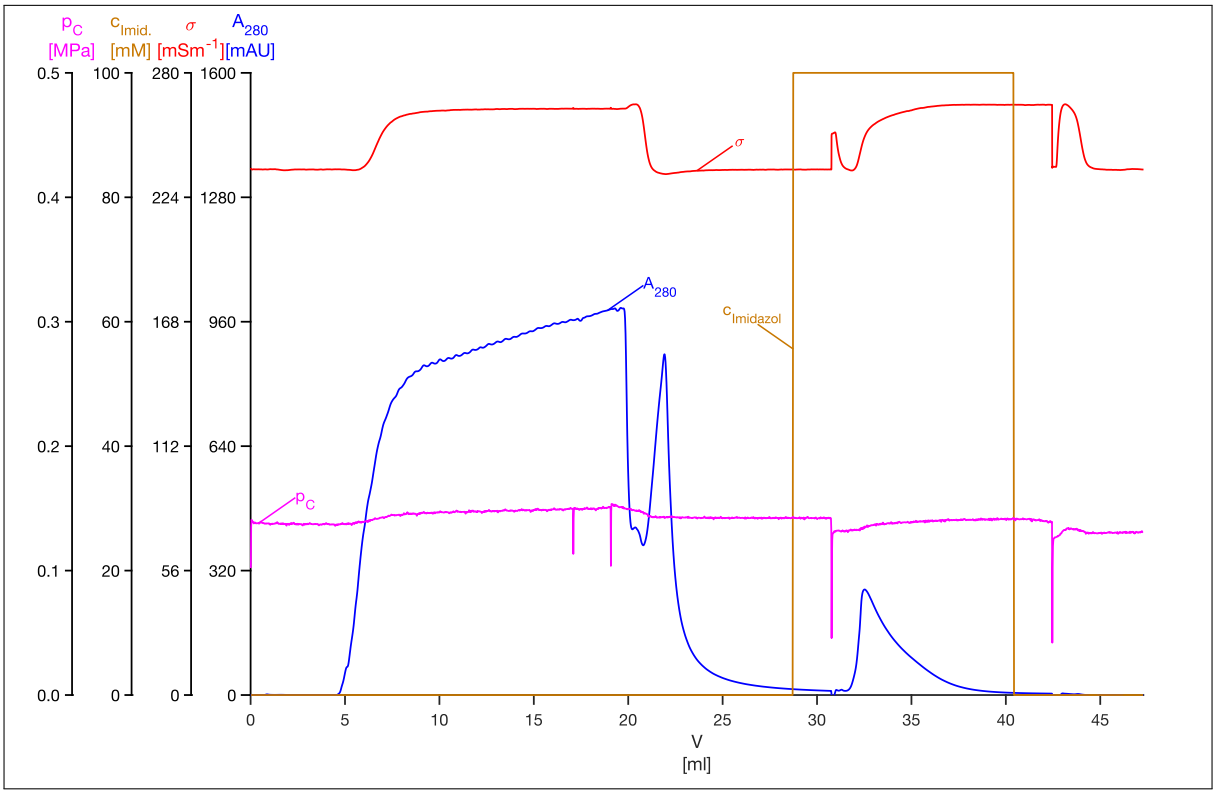

Figure 28: chromatogram obtained from applying 15 ml of sample on HisTrap FF 1 ml. The sample was obtained from 40 ml of homogenate. Depicted on this plot are: the absorption at a wavelength of 280 nm (blue), conductivity(red), pre column pressure (magenta) and concentration of imidazole (brown) within the system flow. Composition of the equilibration buffer: 20 mM Tris-HCl, pH 7.4; 4 M guanidine-HCl; 10 mM imidazole. Composition of the elution buffer: 20 mM Tris-HCl, pH 7.4; 6 M guanidine-HCl; 100 mM imidazole. Flow rate was set to 1 ml/ min.

This led to the displacement of weakly bound proteins. In the second step, the system pump B was increased to 10 %, and thus the concentration of imidazole rose to 100 mM. These elution conditions eluted the his-tagged fusion protein from the column. It has to

be noted, that a different FPLC system was used in the works of Steinhart (2019) and Lampert (2019). The range of flow rate for chromatographic purposes is 0 ml min^{-1} to 150 ml min^{-1}. Since the recommended flow rate of 1 ml min^{-1} were used, the application of the two-step elution technique at this low flow rate would be hard to implement. Rising the system pump B to 10 %, would mean that actual flow rate of system pump B is 0.1 ml min^{-1} and this value is approx. 0.07 % of the maximum operational flow rate of Äkta Avant. Therefore, imidazole was added to the equilibration buffer (see table 9 for recipe) so that a final concentration of 10 mM is achieved.

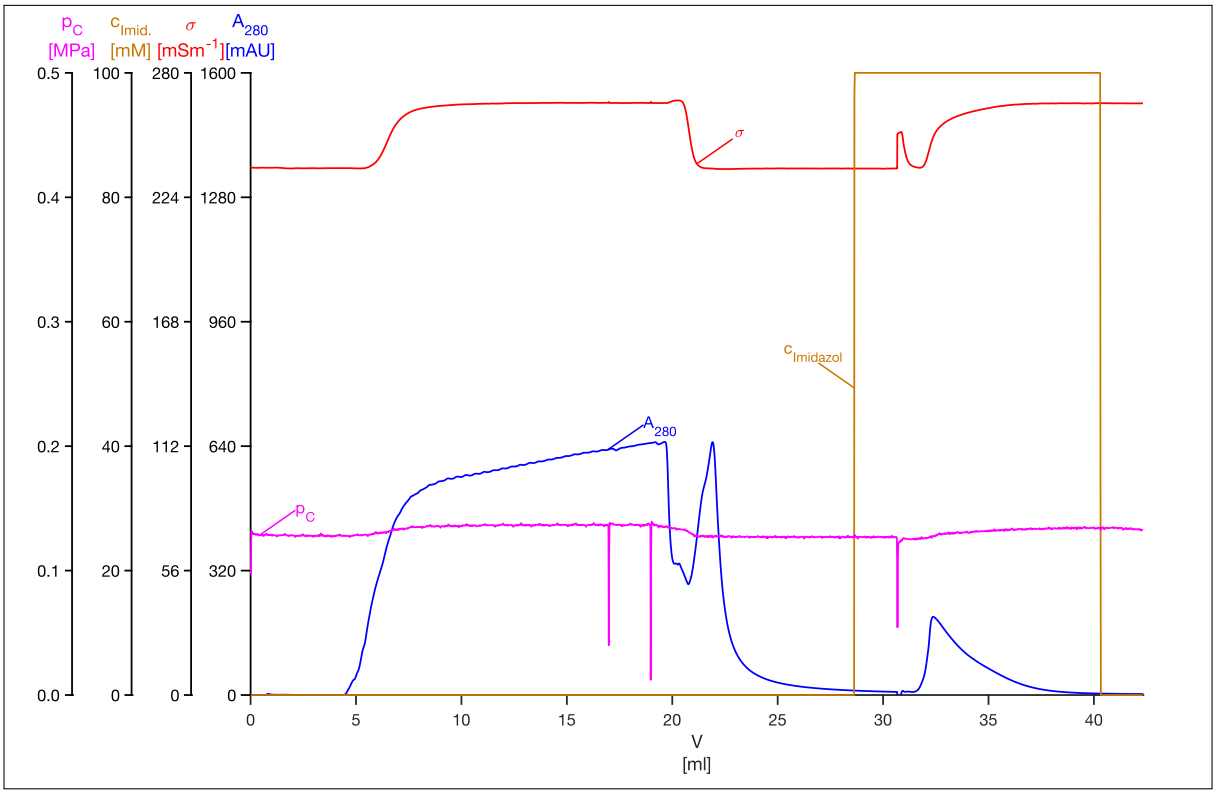

Figure 29: chromatogram obtained from applying 15 ml of sample on HisTrap FF 1 ml. The sample was obtained from 20 ml of homogenate. Depicted on this plot are: the absorption at a wavelength of 280 nm (blue), conductivity(red), pre column pressure (magenta) and concentration of imidazole (brown). Composition of the equilibration buffer: 20 mM Tris-HCl, pH 7.4; 4 M guanidine-HCl; 10 mM imidazole. Composition of the elution buffer: 20 mM Tris-HCl, pH 7.4; 6 M guanidine-HCl; 100 mM imidazole. Flow rate was set to 1 ml/ min.

Washing with equilibration buffer 2 led to the appearance of a peak shortly after the sample application was finished. During elution, a peak with a maximum absoprtion of 270 mAU for 40 ml homogenate was detected. For the sample originating from 20 m of

homogenate, the peak detected during elution had an maximum absoprtion of approx. 200 mAU. The peak exhibited a tailing behaviour. The peak tailing was also observed in a previous work (Lampert, 2019). The fractions, which contained the breakthrough and the eluted peak were stored at 4 °C. The fractions of the eluted peak were pooled together. Dilution was not an issue, since concentration via spin filter/ultrafiltration was the next step.

4.2.3 Purification of the AMP with IMAC (packed column)

A column was packed for the purification of larger volume of solubilized inclusion bodies. The bed height and bed diameter was 12.3 cm and 1.6 cm respectively. 10 IB pellets were solubilized for the purification procedure. Each of the pellet originated from 40 ml of homogenate, meaning that the sample originated from 400 ml of homogenate in total. Since 20 ml of solubilization buffer is used per pellet, the total sample volume applied on the column was approx. 200 ml. The chromatogram of the purification procedure is depicted in figure 30.

Compared to the chromatogram obtained from the small prepacked column, the different peaks are better seperated from each other. This is due the much greater length of the packed column. Also the peak of the target protein was more symmetrical in contrast to the peak of the fusion protein obtained from the chromatogram of HisTrap 1 ml. Additionally, the absorbance of the peaks were much higher than the signals obtained from purification with the HisTrap 1 ml column. This was to expected due to the larger amount of sample applied to the column. The maximum absorbance of the assumed fusion protein peak was approx. 1430 mAU. Elution was carried out with elution buffer 2 (see table 11 for recipe). A two-step elution method was applied for displacing the fusion protein from the column. First, the relative system pump rate for inlet B was set to 20 %. Thus, the concentration of imidazole was 100 mM. A short while after the peak of the assumed fusion protein was detected, the relative pump rate was increased from 20 % to 100 %. Thus, the imidazole concentration rose from 100 mM to 500 mM. The increase was executed in order to see if 100 mM imidazole was enough to elute the total protein. Only a small rise of A_{280} occured after rising the

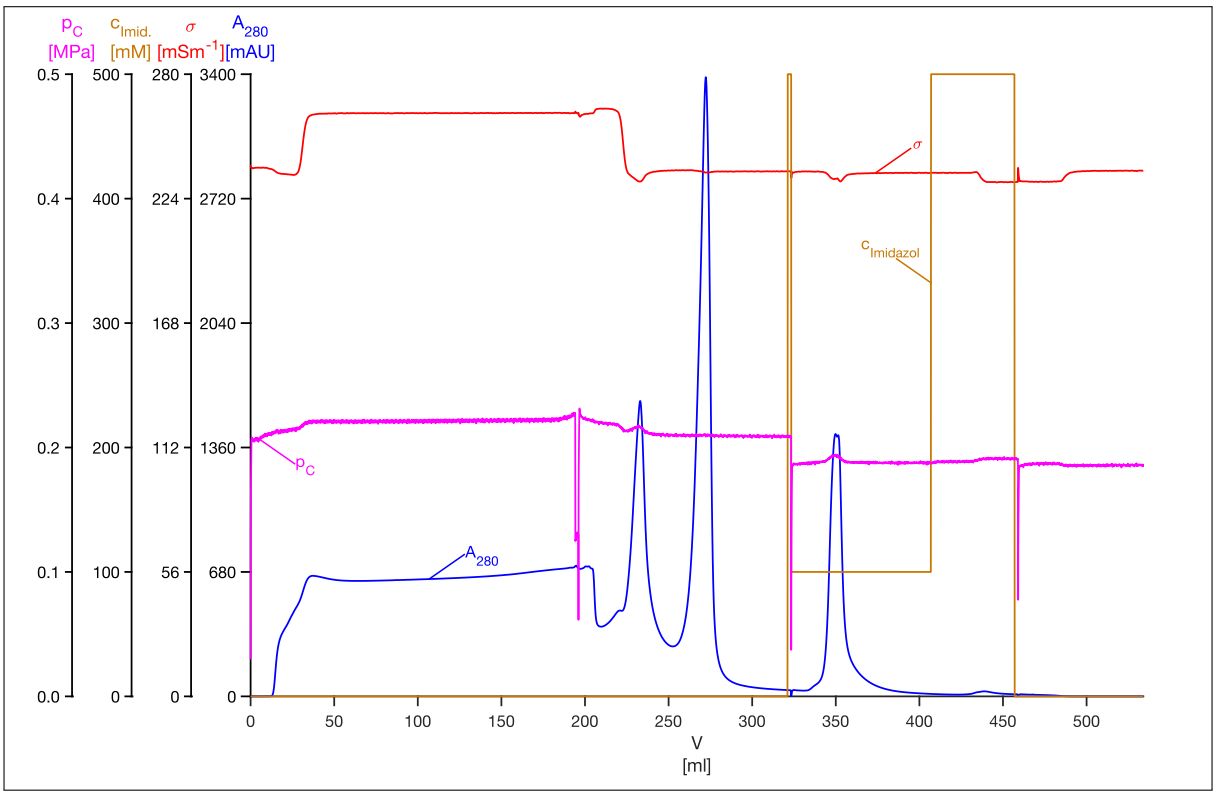

Figure 30: chromatogram obtained from applying 200 ml of sample on a packed column. The bed height and diameter are 12.3 cm and 0.16 cm respectively. The sample was obtained from 400 ml of homogenate. Depicted on this plot are: the absorption at a wavelength of 280 nm (blue), conductivity(red), pre column pressure (magenta) and concentration of imidazole (brown) within the system flow. The rise of $c_{imid.}$ indicates the filling of the flow path with elution buffer. The column is bypassed during the filling. Composition of the equilibration buffer: 20 mM Tris-HCl, pH 7.4; 4 M guanidine-HCl; 10 mM imidazole. Composition of the elution buffer: 20 mM Tris-HCl, pH 7.4; 4 M guanidine-HCl; 500 mM imidazole. Flow rate was set to 5 ml/ min.

imidazole concentration to 500 mM. This may be caused by residual fusion protein, which were not displaced by the previous elution step. But since the absorbance is really low, it can be concluded that 100 mM of imidazole is sufficient for elution of the target protein. In previous works, it could be shown, that the target protein can be eluted with a imidazole concentration of just 40 mM (Steinhart, 2019). Lowering the imidazole concentration may be beneficial for large scale production, since cost would be reduced. Four fractions containing the fusion protein were collected and pooled. The volume of the pool was approx. 60 ml. The breakthrough was also collected for SDS-PAGE analysis.

Another run was performed with the packed column. This time, the column washing

was prolonged in order to see if the purity of the target protein would increase. Column washing as performed with 10 CV of equilibration buffer 2 instead of 5 CV. Also the amount solubilized IBs applied to the column was decreased. 10 IB pellets stemming from 20 ml of homogenate were solubilized. Each pellet was solubilized with 20 ml solubilization buffer. During sample preparation, approx. 10 ml of the sample was lost. Thus, the total volume decreased to roughly 190 ml.

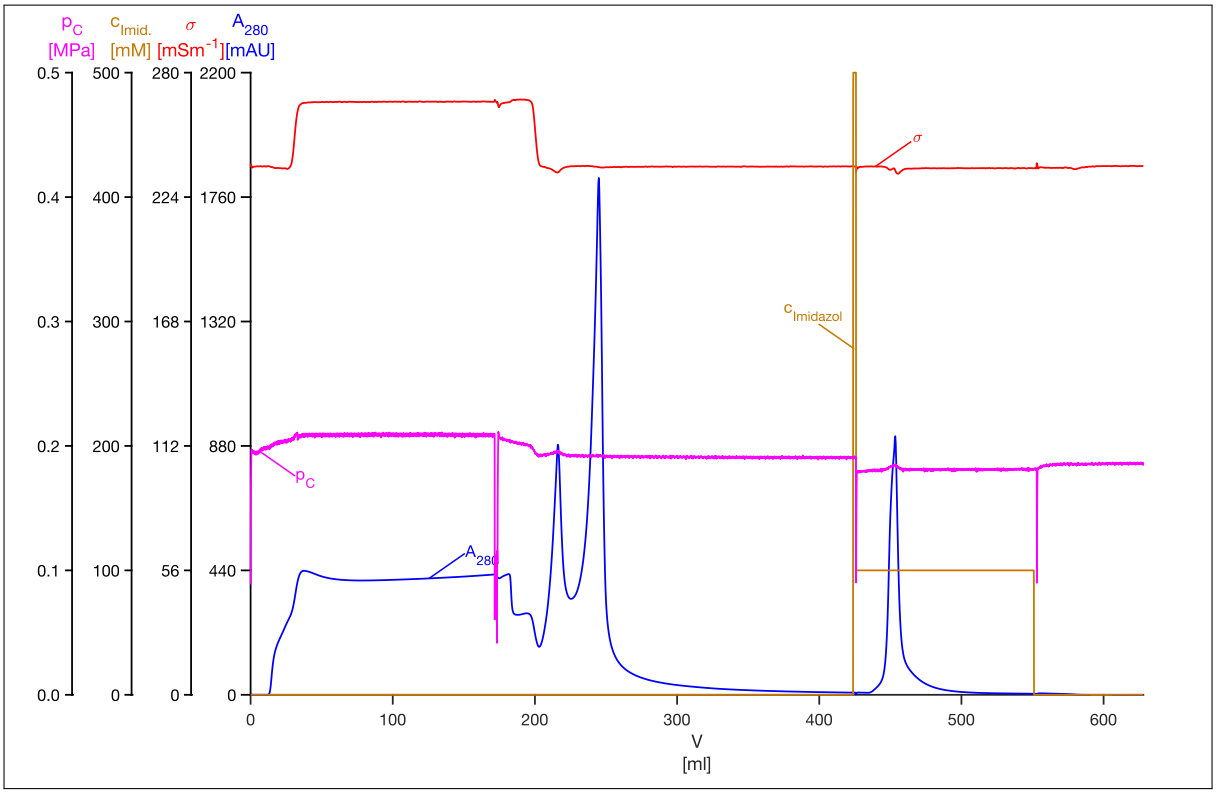

Figure 31: chromatogram obtained from applying 190 ml of sample on a packed column. The bed height and diameter are 12.3 cm and 0.16 cm respectively. The sample was obtained from 200 ml of homogenate. Depicted on this plot are: the absorption at a wavelength of 280 nm (blue), conductivity(red), pre column pressure (magenta) and concentration of imidazole (brown) within the system flow. The rise of $c_{imid.}$ indicates the filling of the flow path with elution buffer. The column is bypassed during the filling. Composition of the equilibration buffer: 20 mM Tris-HCl, pH 7.4; 4 M guanidine-HCl; 10 mM imidazole. Composition of the elution buffer: 20 mM Tris-HCl, pH 7.4; 4 M guanidine-HCl; 500 mM imidazole. Flow rate was set to 5 ml/ min.

Compared to the chromatogram obtained from applying 400 ml of homogenate onto the column, the absorbance signals were much lower. The maximum absorbance of the assumed target protein peak was approx. 950 mAU. The fractions containing the fusion protein were pooled together. The total volume of the pool amounted to roughly 55 ml.

4.3 Analytics

SDS-PAGE was applied to verify the expression of the fusion protein after induction and also for monitoring of the purification process.

4.3.1 Expression of the fusion protein

The samples, which were taken after induction, were chemically lysed in order to see if the target protein was successfully expressed. In figure 32 the lysates from four differents fed-batch cultivations are depicted. In all lanes a band just below the 20 kDa is visible. It can be assumed, that this band is the fusion protein, which has a molecular weight of 16.6 kDa. This assumption is supported by the lanes, which contain lysate of cells before induction. In these lanes no bands are visible. The intensity of the band assumed to be the fusion protein is significantly higher in 7 and 9 compared to lane 3. The lysates in lane 7 and 9 are samples taken 2 h after induction, while the lysate in lane 3 originated from a sample taken 1 h after induction. This may explain why the intensity of the band in lane 3 is significantly lower than the corresponding bands in lane 7 and 9.

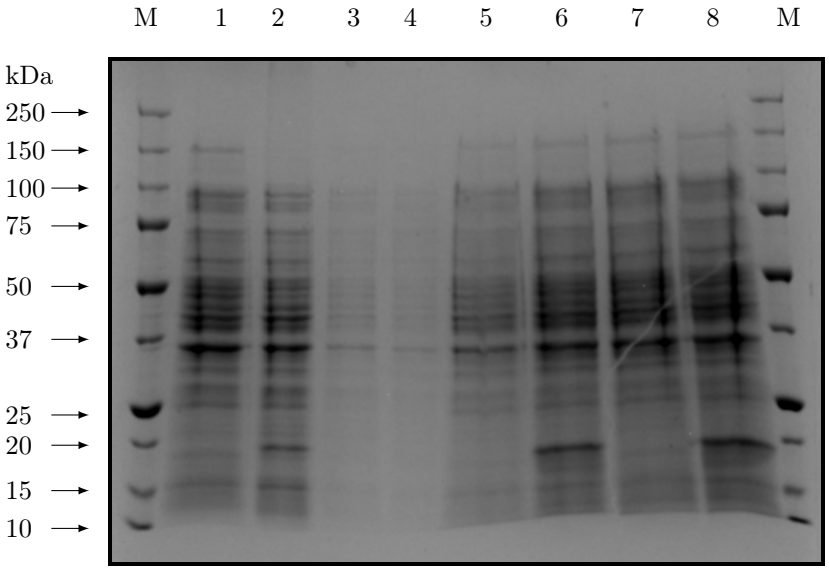

Figure 32: Visualization of chemically lysed cells on a 10 % acrylamide SDS-PAGE gel. The molecular weights of the standards are depicted on the left side of the gel. Lane M represents the marker.Lane 1,3,5 and 7 show the lysate of non-induced cells. in lane 2,4,6 and 8 the total protein content of lysed cells after induction are displayed. Origin of the samples: 1 & 2 from fermentation 3, 3 & 4 from fermentation 4, 5 & 6 from fermentation 8, 7 & 8 from fermentation 9 Voltage during SDS-PAGE: 200 V. Electrophoresis was carried on a 10 % polyacrylamide gel.

In lane 4 and 5 the lysate of cells from fed-batch cultivation 4 were applied. The lysate in lane 4 was obtained from non-induced cells, while the lysate in lane 5 originated from cells 2 h after induction was executed. But due to a calculation error, the amount of cells for the chemical lysis was low and therefore the intensity of these bands were too low for visually determining the succesful expression of the fusion protein.

4.3.2 Validation of purification

The fractions after IMAC were collected and stored at 4 °C. SDS PAGE was used to determine if the peak, which was detected during elution, contained the target protein. Since two different washing conditions were used, the fractions obtained from these conditions were loaded on to a 10 % acrylamide gel. In figure 33 the image of the gel is displayed. Both washing conditions yielded the fusion protein, as a distinctive band is visible in all fractions below the 20 kDa standard of the marker. Apart from that, there is a visible difference in the purity of the fractions obtained from the different washing conditions. Washing with equilibration buffer, which contained no imidazole, a double peak was obtained (see figure 27 and 26). It was assumed, that proteins without his-tag but with exposed histidine residues on the surface could bound to the column due to the absence of imidazole in the equilibration buffer. The assumptions seems to be true, as the fractions, which were obtained from the equilibration buffer without imidazole, had several visible bands apart from band representing the fusion protein. The most prominent band beside that of the fusion protein, was the band at 50 kDa. Interestingly, the band at 50 kDa had the highest intensity in the first fraction (see lane 5 on figure 33). In the following two fractions, there was a visible decrease of the intensity. The intensity of the fusion protein is seemingly at the lowest in the first fraction, while fraction 2 containing the most intense band out of the three fractions. Since the corresponding chromatograms depicted two overlapping fractions, it can be assumed, that the untagged protein was mainly present at the front of the double peak.
When washing was executed with equilibration buffer 2, which contained 10 mM imidazole, the puritiy of the fusion protein was increased, as there is almost no other impurities detected via SDS-PAGE analysis (see lane 1 to 4 on figure 33). Only a very weak band

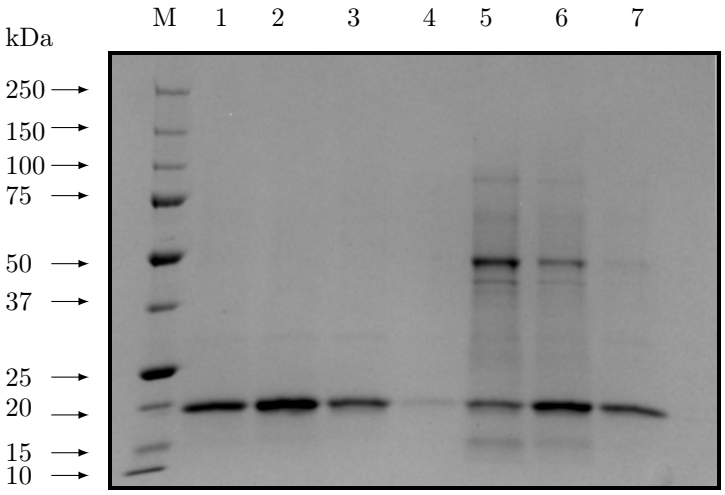

Figure 33: SDS-PAGE showing the purity of the fractions obtained from different washing conditions. Lane M represents the marker. Lane 1 to 4 show the fractions obtained from washing with equilibration buffer 2. The lanes 5 to 7 were obtained from washing with equilibration buffer 1. Voltage during SDS PAGE: 200 V. Electrophoresis was performed with a 10 % polyacrylamide gel.

is visible between 25 kDa and 37 kDa. This band may be a result of dimers formed by two fusion proteins as the theoretical molecular weight would be 33.2 kDa.

The fractions originating from one peak were pooled. Dilution was not an issue, since a concentration step via spin filtration was the subsequent step. The pooled fractions were also analysed via SDS-PAGE. In order to estimate the mass of the fusion proteins, different bovine serum albumine (BSA) masses were looaded on to the same gel. It is interesting to note, that the intensity of the fusion protein band, which were obtained from 40 ml of homogenate, were not much higher than the ones obtained from 20 ml.
For the concentration of the fusion protein, three different durations for the centrifugation of the spin filter were examined. These three durations are: 5 min, 10 min and 15 min. The concentrated samples were then analyzed via SDS-PAGE (see figure 35). BSA standards were loaded on to the same gel in order to estimate the concentrations of the spin filtered samples.
As expected, the concentration is proportional to the centrifugation step, as the intensity of the bands were greater the longer the duration of the centrifugation was.

In order to keep track of the purification success, samples from each crucial step of

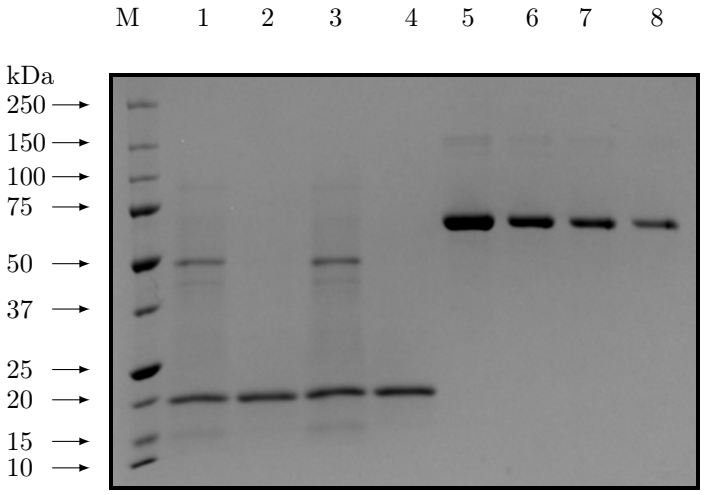

Figure 34: Lane M represents the marker. Lane 1 and 3 show the pooled fractions obtained by washing with equilibration buffer 1 whereas the pooled fraction in lane 1 and lane 3 originated from 20 ml and 40 ml homogenate respectively. The lanes 2 and 4 were obtained by washing with equilibration buffer 2 whereas the pooled fraction in lane 1 and lane 3 originated from 20 ml and 40 ml homogenate respectively. The BSA protein standards were loaded in lanes 5 to 8. Masses of the protein standards in different lanes are: 2 µg in lane 5, 1 µg in lane 6, 0.75 µg in lane 7 and 0.5 µg in lane 8 .Voltage during SDS-PAGE: 200 V. Electrophoresis was performed with a 10 % polyacrylamide gel.

the downstream processing were taken and analyzed via SDS-PAGE. The gel image is depicted in figure 36. As expected, the lysate contains numerous bands including the target protein, since no seperation step had occured at this stage. The pellet, obtained after cell disruption and subsequent centrifugation, is mixed with solubilization buffer. This suspension was also applied on the gel and it is obvious that far less bands were present compared to the lysate. This is due to the soluble proteins being removed by discarding the supernatant after centrifugation of the cell lysate. The band of the fusion protein was present and thereby indicating that it was successfully solubilized. The suspension itself was also centrifuged and filtered, so that it could be applied on an IMAC column. A sample of this preparation was also applied on SDS-PAGE gel (see lane 3 of the gel in figure 36). Compared to the suspension, the bands of the filtered and centrifuged solution were slightly less intensive. That means that a slight loss of sample occured.

The breakthrough after application of the solubilized proteins onto the IMAC column were collected and also visualized via SDS-PAGE. Two pools of the breakthrough were prepared. The first pool contained the majority of the breakthrough minus the distinct

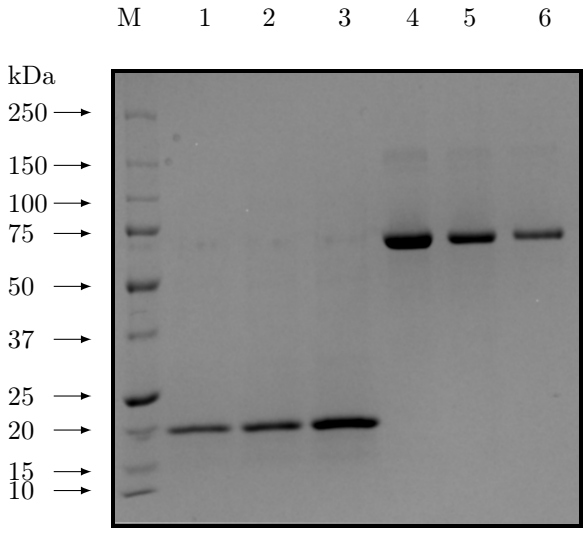

Figure 35: In lanes 1 to 3, concentrated pool fractions were applied. Different durations of the centrifugation steps are represented by the lanes: 5 min in lane 1, 10 min in lane 2 and 10 min in lane 3. The BSA protein standards were loaded in lanes 4 to 6. Masses of the protein standards in the different lanes are: 4 µg in lane 4, 2 µg in lane 5 and 1 µg in lane 6 .Voltage during SDS-PAGE: 200 V. Electrophoresis was performed with a 10 % polyacrylamide gel.

trailing peak (see figure 28 and 29), while the second pool contained the trailing peak. Both pools were also applied on the same SDS-PAGE gel. The first pool of the IMAC breakthrough (see lane 4 in figure 36) contained the same bands as the solution/suspension obtained after solubilization of the inclusion bodies minus the target protein. But the intensity of its bands was lesser than the corresponding bands of lane 2 and 3. The most prominent band of the first breakthrough is just below the 37 kDa protein standard. The the banding pattern of the second part of the breakthrough is seen in lane 5. The most prominent band is at the same height as the 50 kDa standard of the marker. Thus, it can be assumed that this protein was responsible for the trailing peak of the breakthrough. This band was also responsible for the impurity if no imidazole was present in the equilibration buffer as distinct bands were present at 50 kDa (see figure 33, lane 5 and 6). A small amount of the fusion protein was also present in the second breakthrough, since a band is barely visible at 20 kDa. The pool of the purified fusion protein was applied on lane 6. There was only one distinct band visible at 20 kDa and therefore it can be assumed that the purity is very high. In lane 7, the supternatant obtained from the spin filter (3 kDa MWCO) after centrifuging for 10 min was applied. The concentration step seemed to have failed as the intensity was comparable to that of

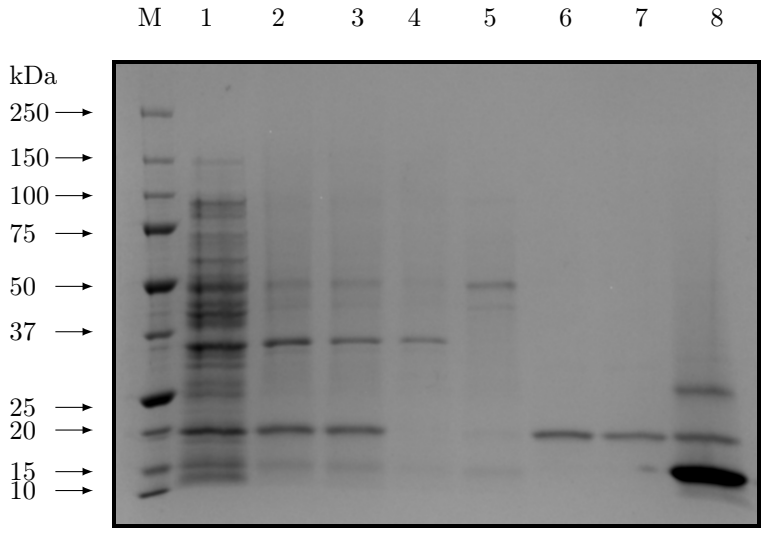

Figure 36: On this gel samples obtained from different steps of the downstream processing were applied. Lane M represents the marker. Lane 1: Lysate; Lane 2: Solubilized pellet containing inclusion bodies of fusion protein; Lane 3: Solubilized pellet containing inclusion bodies of fusion protein after centrifugation and filtration (0.2 µm); Lane 4: Breakthrough 1; Lane 5: Breakthrough 2 (trailing peak); Lane 6: fraction pool of fusion protein; Lane 7: Supernatant after spin filtration (3 kDa MWCO; 10 min); Lane 8: Pellet after acid cleavage and neutralization of fusion protein. Voltage during SDS-PAGE: 200 V. Electrophoresis was performed with a 10 % polyacrylamide gel.

the non spin filtered fusion protein in lane 6. Loss of protein probably occured during ethanol precipitation. The pellet obtained from centrifugation of the acid cleaved and subsequently neutralized fusion construct, was resuspended and applied on lane 8. As expected, the most intense band was visible at the height of the 20 kDa protein standard of the marker and thereby indicating that cleavage occured. This is the onconase, whose molecular weight is 14.3 kDa. Uncleaved fusion protein was also present as band was visible at the height of 20 kDa, but its intensity is far less than the onconase. Then there was a thrid prominent band visible slightly above the height of 25 kDa. These were probably dimers formed by the onconase. Since the SDS-PAGE was performed with a tris-glycine system, the cleaved AMP could not be visualized. Interestingly, in all other lanes except lane 6 and 7, a band was barely visible at the height of 15 kDa. This could be the onconase, which would man, that a small amount of the fusion protein was already cleaved before the acid cleavage. Then again, if it was truly the onconase, it would seem contradictory that no additional band was present in the pool of the purified fusion protein as well as the concentrated fusion protein solution as the poly-histidine

tag should be present at the c-terminus of of the onconase. Either this band is a host protein with a similiar size as the onconase or the His-tag of the cleaved onconase is no longer exposed and accessible making capturing via IMAC impossible. This could be verified by applying the cleaved onconase on an IMAC resin.

The scaled up purification procedure was also visualized via SDS-PAGE. Like with the small prepacked column, the samples from different stages during the downstream process were applied on a 10 % acrylamide gel (see figure 37). The band of the fusion protein in the fraction pool obtained after IMAC purification with the packed column seemed to be significantly more intense than the purified protein obtained from the small IMAC column. A greater concentration occured here, since 200 ml of samples was applied on the column whereas the volume containing the target protein was approx. 60 ml. The concentration factor for the smaller column was lower, since 15 ml samples were applied on the column and the volume of the fraction pool containing the protein was between 6 ml to 8 ml.

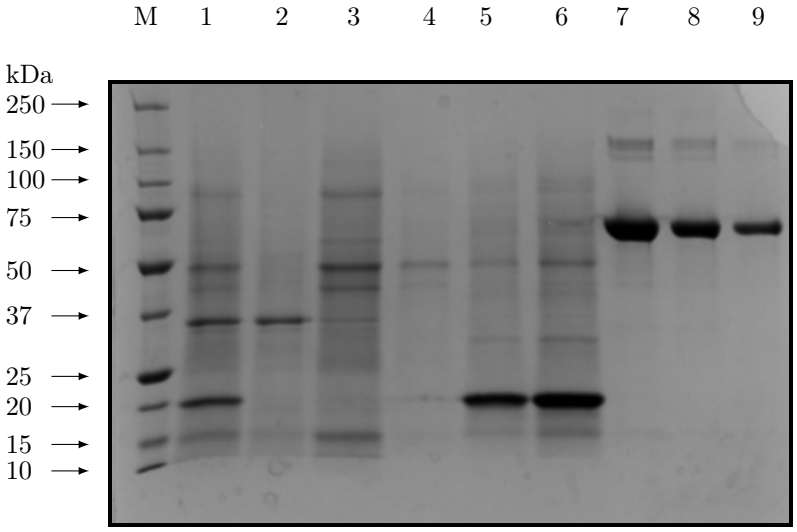

Figure 37: On this gel samples obtained from different steps of the downstream processing were applied. IMAC purification was carried out with a packed column (bed volume approx. 25 ml). Lane M represents the marker. Lane 1: Solubilized pellet incuding inclusion bodies of fusion protein after centrifugation and filtration; Lane 2: Breakthrough 1; Lane 3: Breakthrough 2 (trailing peak); Lane 4: Breakthrough 3; Lane 5: Fraction pool of fusion protein; Lane 6: Supernatant after spin filtration (3 kDa MWCO; 2 h); Lane 7: 4000 ng BSA; Lane 8: 2000 ng BSA; Lane 9: 1000 ng BSA. Voltage during SDS-PAGE: 200 V. Electrophoresis was performed with a 10 % polyacrylamide gel.

But despite the higher concetration effect, impurities seem to be present in the fraction pool containing the target protein due to the presence of various bands. The distinctive band between 25 kDa and 37 kDa may be dimer of the fusion protein as discussed earlier. This claim is supported by the absence of this band in the solution containing the solubilized inclusion (see lane 1 in figure 37) bodies as well as in the breakthrough (lane 2-4 in figure 37). The IMAC purified fusion protein was concentrated by using a spin filter with a MWCO of 3 kDa. The spin filter was centrifuged at $6000 \times g$ for 2 h. The concentration was successful, since the intensity of the fusion protein band is greater than that of the non-concentrated fusion protein band. Since other proteins beside the target protein were present in the fraction pool, these proteins were co-concentrated.

One reason for the presence of other proteins in the fraction pool may be insufficient column washing. This seemed plausible, since the absorbance did not reach the baseline before start of the elution step. Thus, another IMAC purification with a longer column washing step was performed. The chromatogram of this run is depicted in figure 31. The pooled fraction of the target protein was applied on an 10 % acrylamide gel. For comparison, the fraction pool of the preceeding IMAC purification procedure (chromatogram in figure 30) was also applied on the same gel. The fraction pool of the second run appeared to be more pure (see lane 1 and 6 in . But a smear pattern was visible in the same lane, thus a clear statement could not be made. The fraction pool of the preceeding purification procedure lacked the distinct bands of the non-target proteins as seen in figure 37.
Its possible, that these protein were less stable and were therefore degraded rather fast. Apart from increasing the column washing volume, the sample applied onto the column for the second run was lower. Thus, it can be assumed, that the fraction pool of this IMAC purification procedure appeared to be more pure due to the lower total protein amount. A concentration step with a spin filter could determine if at least non-target protein bigger than the MWCO are present due to them being concentrated along with the fusion protein. For the estimation of the yield, the purity is assumed to be at the same level as fraction pool originating from the preceeding IMAC purification (roughly 80 %). The BSA standards applied on the gel produced several bands apart from the

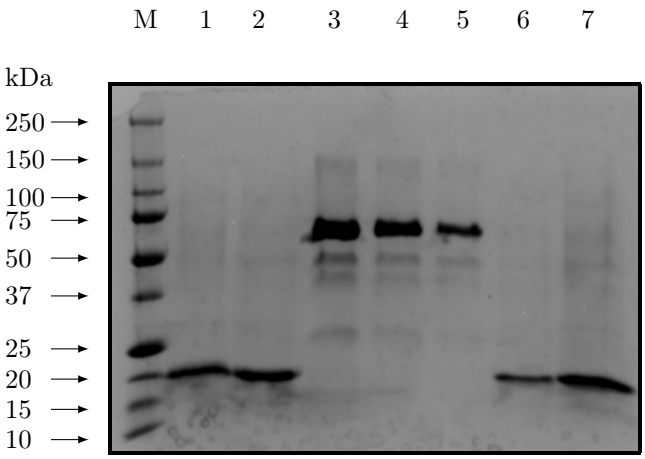

Figure 38: Visualization of IMAC purification of 200 ml homogenate. IMAC purification was carried out with a packed column (bed volume approx. 25 ml). Lane M represents the marker. Lane 1&6: pooled fractions obtained from 200 ml of homogenate; Lane 2&7 : pooled fractions obtained from 400 ml of homogenate. Lane 3: 4000 ng BSA; Lane 4: 2000 ng BSA; Lane 5: 1000 ng BSA; Voltage during SDS-PAGE: 200 V. Electrophoresis was performed with a 10 % polyacrylamide gel.

prominent band at the proper height of approx. 70 kDa. The BSA stock solution was in solution and stored at 4 °C for a few days. It is likely that proteolysis occured, and thus several fragments were produced. Therefore, densitometry would provide less reliable results.

4.3.3 Validation of the acid cleavage via tris-tricin SDS-PAGE

In order to validate the release of the AMP from its fusion partner after acid cleavage, a tris-tricin SDS-PAGE was carried out. A duplicate sample originating from the same solubilized pellet was prepared. Two different storing conditions were compared to each other. For one, the solution containing the AMP after the acid cleavage procedure was aliqouted and stored at −20 °C and for another, the remaining solution was stored at 4 °C. The storage duration was 7 days. Guanidine-HCl was probably present in the solution. Thus, 1:5 dilution of the recombinant AMP was also applied on the same gel. Indeed, guanidine-HCl was present as precipitation occured within the undiluted samples. These samples were still used for the electrophoresis by heating them up to 95 °C again and then quickly loading them onto the gel. The gel image revealed, that only duplicate 2 generated a visible band at the height just below the 6.512 kDa protein standard. The size of the AMP is 3.3 kDa, and therefore it is expected to be just below the 3.496 kDa

protein standard. This phenomenon was also observed by Embruch (2018). The absence of a band for the samples originating from duplicate 1 were in accordance with the observation, that the centrifugation step at the and of the acid cleavage procedure did produce a far smaller pellet compared to duplicate 2. Since it is the onconase, which is precipitated after neutralization with NH_3, it can be assumed, that a visibly very small precipitate indicates inefficient cleaving.

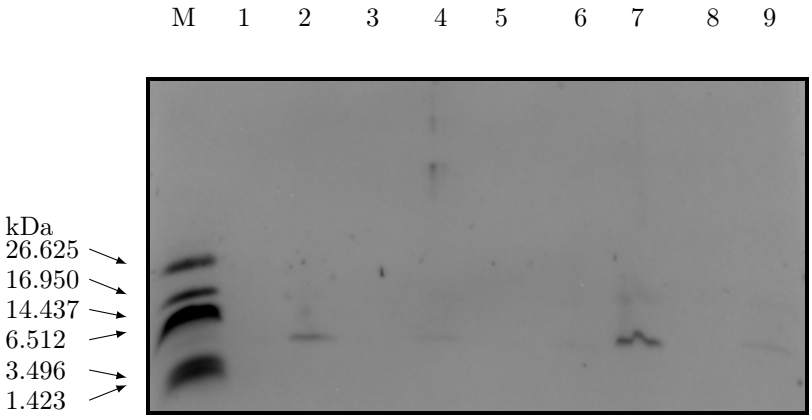

Figure 39: Visualization of recombinant NK2-ALK via tris-tricine SDS-PAGE. Lane M represents the marker. Lane 1: Recombinant NK2-ALK (dulpicate 1), stored at −20 °C; Lane 2: Recombinant NK2-ALK (dulpicate 2), stored at −20 °C; Lane 3: Recombinant NK2-ALK (dulpicate 1) 1:5 dilution, stored at −20 °C; Lane 4: Recombinant NK2-ALK (dulpicate 2) 1:5 dilution, stored at −20 °C; Lane 5: empty; Lane 6: Recombinant NK2-ALK (dulpicate 1), stored at 4 °C; Lane 7: Recombinant NK2-ALK (dulpicate 2), stored at 4 °C; Lane 8: Recombinant NK2-ALK (dulpicate 1) 1:5 dilution, stored at 4 °C; Lane 9: Recombinant NK2-ALK (dulpicate 2) 1:5 dilution, stored at 4 °C. Current during SDS-PAGE: 20 mA.

The diluted samples did not precipitate, but only very weak bands were visible for duplicate 2. The storing did not appear to alter the AMP except for the band appering to be distorted for the undiluted sample of duplicate 2 stored at 4 °C (see figure 39, lane 7). This may not be due to the storing conditions, since the 1:5 dilution of the same sample does not look distorted (see figure 39, lane 9).

4.3.4 Estimation of the fusion protein concentration

Estimation of the protein concentration was performed via SDS-PAGE densitometry and/or bradford assay. For reasons of clarity and comprehensibility, a key is assigned to all samples, whose concentration were estimated (see table 33).

Table 33: Overview of samples, whose concentration were determined via bradford assay and/or SDS-PAGE densitometry. For convennience, a key is assigned to each sample. V_{Hg} refers to the volume of homogenate.

Purification Step	V_{Hg} [ml]	Key
Solubilization of inclusion bodies	20	*Sol. IB 20*
	40	*Sol. IB 40*
IMAC fraction pool of fusion protein	20	*IMAC FP 20*
	40	*IMAC FP 40*
	200	*IMAC FP 200*
	400	*IMAC FP 400*
Concentration of fusion protein via spin filter (5 min)	20	*SF5min 20*
	40	*SF5min 40*
Concentration of fusion protein via spin filter (10 min)	20	*SF10min 20*
	40	*SF10min 40*
Concentration of fusion protein via spin filter (15 min)	20	*SF15min 20*
	40	*SF15min 40*

The total protein concentration of samples taken right after solubilization, IMAC and ultrafiltration (spin filter) were determined via bradford assay. The estimation was carried out for samples obtained from 20 ml and 40 ml of homogenate respectively. Theoretically, the protein concentration of samples originating from 40 ml of homogenate should be two times bigger than the samples obtained from 20 ml of homogenate. But this was not the case as the bar plot in figure 40 indicates. The samples from 40 ml did have higher concentration than their corresponding samples obtained from 20 ml of homogenate. The biggest difference regarding the total protein concentration was present between *Sol. IB 40* and *Sol. IB 20*, with the former having a 1.5 times greater concentration than the latter. The difference between the samples originating from 20 ml and 40 ml decreased after IMAC. The measured total protein concentration of *IMAC FP 20* was 0.35 mg ml^{-1}, while the measured protein concentration of *IMAC FP 40* was just 1.2 times greater. The same ratio was present after concentration of *IMAC FP 20* and *IMAC FP 40* via

spin filter since the protein concentration of *SF10min 40* was 1.2 times greater than the protein concentration of *SF10min 20*. But it should be taken into account, that volume of the pooled fraction differed between *IMAC FP 20* and *IMAC FP 40*. The volume of the former was approx. 6.5 ml while the latter was approx. 8 ml. Thus, the total protein mass of *IMAC FP 40* was 1.5 times greater than that of *IMAC FP 20*. It was expected, that the total protein mass *IMAC FP 40* would be approx. two times higher than that of *IMAC FP 20*. The maximum binding capacity of the column might have been reached if solubilized inclusion bodies obtained from 40 ml of homogenate has been applied on the column. The bradford assay confirmed, that a stronger concentration occured for the fusion protein during IMAC purification with the packed column.

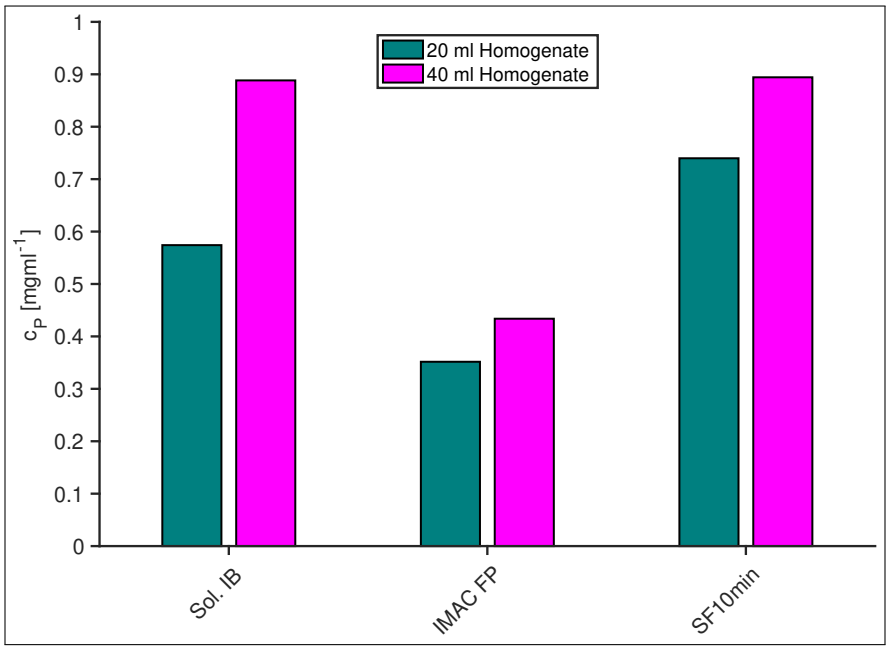

Figure 40: Estimation of the total protein concentration of samples taken at different steps during downstream processing. Concentrations were determined via Bradford assay. These steps include: solubilization of inclusion bodies (Sol. IB), pooled fractions of the fusion protein right after IMAC (IMAC FP) and concentration of purified fusion protein via spin filter (SF10min). The samples originating from 20 ml of homogenate (green) are compared those originating from 40 ml of homogenate (magenta). The homogenates were obtained through high pressure homogenization of the harvested cells from fed-batch fermentation 3.

The concentrations obtained through SDS-PAGE densitometry are listed in table 34. For the spin filter experiment it could be shown, that longer centrifugation times decrease the volume of the supernatant, which leads to the higher final concentration of the

Table 34: In this table the protein concentrions (c_P) determined via SDS-PAGE densitometry are listed. The gel images, which were used for the estimation are also listed. Legend: *IMAC FP 20* and *IMAC 40 FP* are the pooled fraction of the fusion protein originating from 20 ml and 40 ml of homogenate respectively. *IMAC FP 20* was concentrated via spin filter. Three different centrifugation duration were executed: 5 min (*SF5min 20*), 10 min (*SF10min 20*) and 15 min (*SF15min 20*).

Samples	c_P [mg ml^{-1}]	Gel image reference
IMAC FP 20	0.30	Figure 34, lane 2
IMAC FP 40	0.36	Figure 34, lane 4
SF5min 20	0.41	Figure 35, lane 1
SF10min 20	0.71	Figure 35, lane 2
SF15min 20	1.66	Figure 35, lane 3

fusion protein due to it being retained by the ultrafiltration membrane. In some cases, when a centrifugation time of 15 min was chosen, no supernatant was present above the membrane, therefore a suitable buffer had to be used to resuspend the precipitated protein. This may lead to a substantial loss of proteins. Therefore, a centrifugation time of 10 min should not be exceeded for future experiments, as a supernatant was always present above the membrane.

The gel image in figure 34 revealed that, the purity of *IMAC FP 20* (lane 2) and *IMAC FP 40* (lane 4) was apparently very high. Impurities were probably present, but their concentrations were below the limit of detection. Thus it could be assumed, that the fusion protein is mainly responsible for the measured protein concentration. In figure 41 a comparison between the protein concentration determined by bradford assay and SDS-PAGE densitometry was made. The fusion protein purified with the packed IMAC column had lower purity. Therefore, the purity was considered for the estimation of the fusion protein. The purity was estimated via densitometry.

Even though SDS-PAGE densitometry is regarded as a semi-quantitative method while bradford assay is an established protein quantification method, it produced similar results as the bradford assay. In all cases, the concentration determined through densitometry

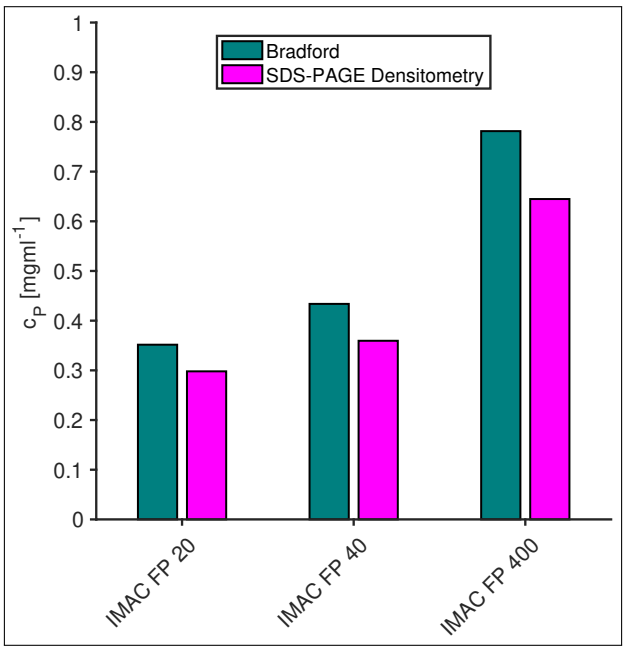

Figure 41: Estimation of the target protein concentration of *IMAC FP 20*, *IMAC FP 40* and *IMAC FP 400* via bradford assay and SDS-PAGE densitometry. The purity of the samples were considered for estimation of the target protein concentration.

were lower than the concetrations determined via bradford assay. Nonetheless, bradford assay should be chosen over SDS-PAGE densitometry if possible. Determination via SDS-densitometry includes more steps, which automatically increases the number of potential pitfalls. For instance, samples after the solubilization step have to be precipitated with ethanol before being subjected to SDS-PAGE. Inappropiate handling may decrease the recovery, and thus the results may not be interpreted properly. Another possible pitfall may be the loading of the samples into the wells of an polyacrylamide gel, since loss of samples will reduce the measured signal.

The wet biomass was used for estimation of the fusion protein yield. For *IMAC FP 40* a yield of 1.7 mg g^{-1} was estimated while 20 ml of homogenate led to a yield of 2.3 mg g^{-1}. The yields of fusion protein obtained from purification with the packed column were 2.6 mg g^{-1} and 2.3 mg g^{-1} for *IMAC FP 200* and *IMAC FP 400* respectively. The yields are in the same order of magnitude as estimated by Steinhart (2019), since 2.746 mg of fusion protein were purified out of 1 g of wet biomass. Assuming that the acidic cleavage results in the total cleavage of the fusion protein, then the yield of NK2-ALK for *IMAC*

Table 35: In this table relevant numbers concerning the calculation of the yields of the fusion protein are listed. Legend: $c_{P,tot}$:= total protein concetrations determined via bradford; m_P := mass of the target protein (purity of the sample is considered); V_{FP} := volume of the pooled fractions obtained after IMAC purification; V_{Hg} := volume of the homogenate; $m_{XL,wet}$:= wet biomass of cells; y_P := yield of target protein per wet biomass; $y_{AMP,max}$:=maximum theoretical yield of AMP per wet biomass. The purity of the samples were determined via SDS-PAGE densitometry. The t The total protein concentrations $c_{P,tot}$ were determined via bradford. The purity of the purified samples were determined through SDS-PAGE densitometry.

Sample	$c_{P,tot}$ [mg ml^{-1}]	Purity [%]	m_P [mg]	V_{FP} [ml]	V_{Hg} [ml]	$m_{XL,wet}$ [mg]	y_P [mg g^{-1}]	$y_{AMP,max}$ [mg g^{-1}]
IMAC FP 20	0.35	100	2.3	6.5	20	1	2.3	0.45
IMAC FP 40	0.43	100	3.5	8	40	2	1.7	0.34
IMAC FP 200	0.56	80	24.5	55	190	9.5	2.6	0.51
IMAC FP 400	0.98	80	46.3	60	400	20	2.3	0.46

FP 200 and *IMAC FP 400* is 0.51 mg g^{-1} and 0.46 mg g^{-1} respectively. But the actual yields of NK2-ALK are lower than these theoretical values since no total cleavage is achieved. All relevant numbers regarding for the calculation of the yields are listed in table 35. The significantly lower yield for *IMAC FP 40* indicates, that a substantial amount of protein was lost during IMAC purification. Thus, it can be concluded that the protein amount within solubilized IB solution originating from 40 ml of homogenate is too high to prevent sample loss, since probably the max binding capacity of the column is being approached.

4.3.5 Verification of AMP activity

To the verifiy the bioactivity of the recombinant produced NK2-ALK, the radial diffusion assay was carried out according to the SOP 'Agardiffusionstest zur Wirksamkeitsprüfung von toxischen Substanzen; speziell antimikrobielle Peptiden'. The assay was carried out by Lisa Michel (unpublished). The assay revealed, that all recombinant AMP exerted an antibacterial effect as clear inhibition zones were visible around the wells (see figure 42) . Melittin with two different concentrations (10 µg ml^{-1} and 50 µg ml^{-1}) was used as positive control. Both concentrations of melittin displayed antimicrobial activity. As expected, the

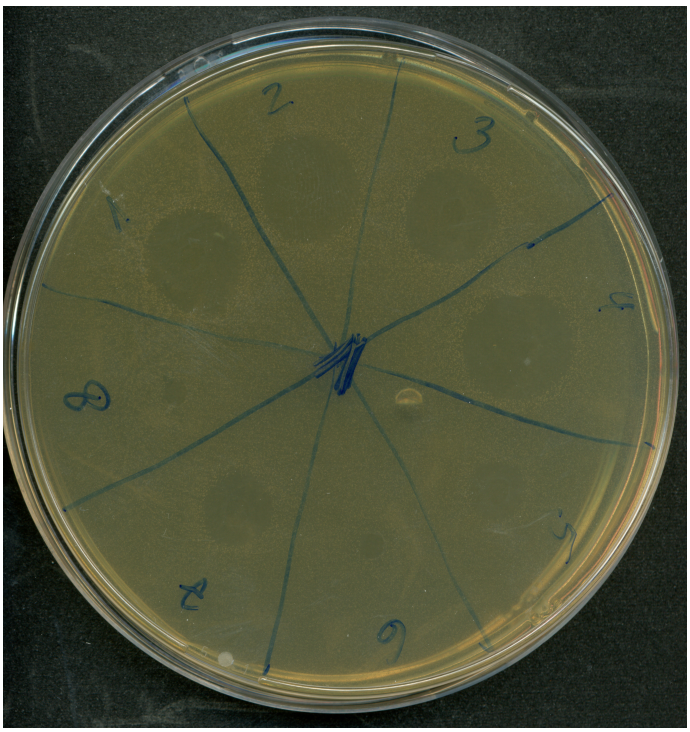

Figure 42: Samples applied for radial diffusion assay: 1. recombinant NK2-ALK (fusion protein spin filtrated for 5 min, purified out of 20 ml homogenate); 2. Recombinant NK2-ALK (fusion protein spin filtrated for 10 min, purified out of 20 ml homogenate); 3. Recombinant NK2-ALK (fusion protein spin filtrated for 15 min, purified out of 20 ml homogenate); 4. Recombinant NK2-ALK (fusion protein spin filtrated for 5 min, purified out of 40 ml homogenate); 5. Melittin (10 µg ml^{-1}); 6. Ampicillin; 7. Melittin (50 µg ml^{-1}); 8) H_2O

inhibtion zone generated by the higher concentrated melittin solution was bigger than the one produced by the lower concentrated melittin solution. But even the inhibition zone produced by 50 µg ml^{-1} of melittin had a smaller surface than the ones produced by the recombinant NK2-ALK. Based off the determined protein concentration via densitometry (see table 34), the final concentration of AMP should all be below 50 µg ml^{-1}. The dilution occuring during the acid cleavage as well as the mass ratio of AMP to fusion protein was regarded for the estimation. The cleaving efficiency was assumed to be 100 %, meaning that the estimation yielded the theoretical maximum concentration of AMP applied for the radial diffusion assay. Thus, the estimated final concentration of *SF5min 20*, *SF10min 20* and *SF15min 20* were in the range of approx. 4 µg ml^{-1} to 33 µg ml^{-1}. The much bigger inhibition zones produced by the recombinant NK2-ALK may indicate, that NK2-ALK is more potent than melittin due to the former having a lower concentration than the letter. This assumption is supported by comparing the minimal inhibitory

concentration (MIC) of both AMP to each other. The MIC of NK2 is 0.15 µM, while that of melittin is 0.60 µM (Andrä and Leippe, 1999). Thus, NK2 is four times more potent than melittin. Synthetic NK2 was also applied on the assay (see figure 44, well no. 4 and 5). Two different concentrations were applied (5 µg ml^{-1} and 25 µg ml^{-1}). The synthetic NK2-ALK also generated larger inhibtion zones than melittin, despite the concentrations being lower. The negative control, which was just demineralized H_2O, did not produce an inhibition zone. In order to rule out the possibility of inhibition induced by acetic acid, a blank solution was prepared, which was created by transferring 100 µl demineralized H_2O on to a spin filter. This sample was then treated like the samples obtained after IMAC, meaning that 1 ml of 0.1 M acetic acid was mixed with the supernatant obtained after centrifugation. Incubation and subsequent neutralisation was also carried out with this blank solution. The blank solution did not produce an inhibition zone (see figure 43, well no. 3) and therefore it could be assumed, that the acetate was not inhibitory for the cells.

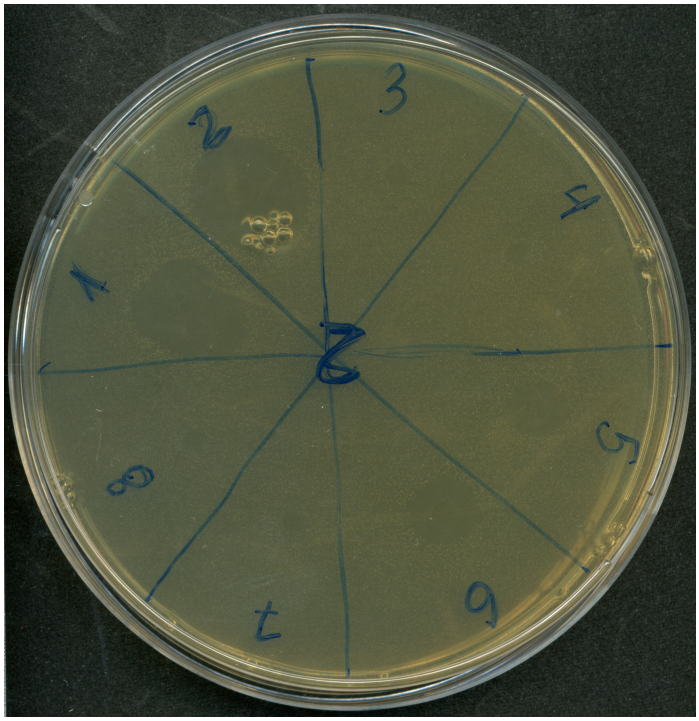

Figure 43: Samples applied for radial diffusion assay: 1. Recombinant NK2-ALK (fusion protein spin filtrated for 10 min, purified out of 40 ml homogenate); 2. Recombinant NK2-ALK (fusion protein spin filtrated for 15 min, purified out of 40 ml homogenate); 3. Blank solution (0.1 M acetic acid + NH_3); 4. H_2O; 5. Melittin (10 µg ml^{-1}); 6. Melittin (50 µg ml^{-1}); 7. Ampicillin; 8. H_2O

Ampicillin was also used as positive control, but the dilution was too high and therefore no inhibition zone was visible. Another blank solution was prepared by mixing different volumes of elution buffer 1 (25 µl, 50 µl and 100 µl) with 1 ml of 0.1 M acetic acid and 75 µl of 2.5 % ammonia solution in order to mimic the matrix composition of the fusion protein after spin filtration. This was done to rule out that guanidine-HCl is involved in the inhibition of the cells, since it is a chaotropic agent and therefore may possess lytic capabilites (Danilevich *et al.*, 2008).

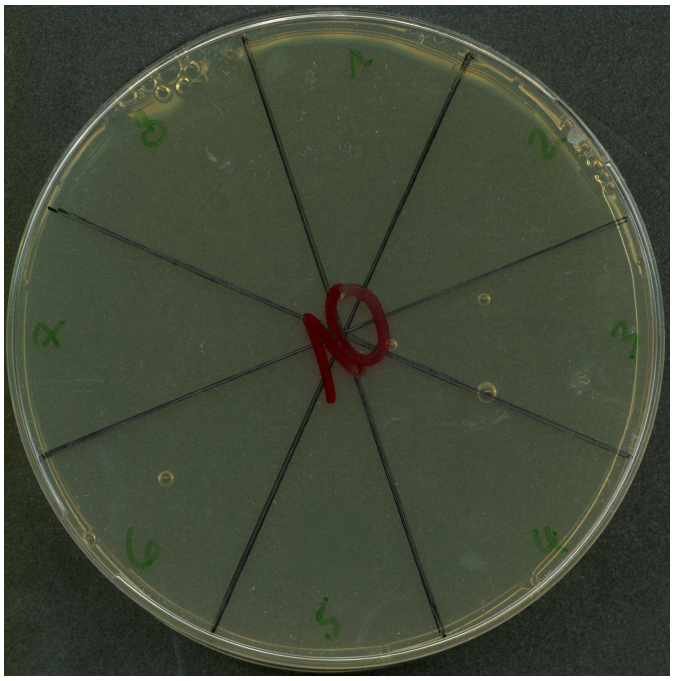

Figure 44: Samples applied for radial diffusion assay: 1. Blank solution 1 (25 µl elution buffer 1); 2. Blank solution 2 (50 µl elution buffer 1); 3. Blank solution 3 (100 µl elution buffer 1); 4. Synthetic NK2-ALK (5 µg ml^{-1}); 5. Synthetic NK2-ALK (25 µg ml^{-1}); 6. Melittin (10 µg ml^{-1}); 7. Melittin (50 µg ml^{-1}); 8. H_2O

A dilution occurs during the acid cleavage. This dilution is dependent on the volume of the supernatant above the spin filter, which in turn is depentent on the duration of centrifugation. The supernatant was between 50 µl and 100 µl, meaning that the dilution was at least 1:10 after addition of 1 ml acetic acid. That was the reason for choosing aforementioned volumes of the elution buffer for the preparation of the blank solutions. These blank solutions did not produce an inhibition zone. Thus, it can be concluded, that the AMP is responsible for the growth inhibition of the cells.

5 Conclusion

The upstream processing revealed, that by aerating with air and oxygen during cultivations, cell density greater than $70\,\mathrm{g\,l^{-1}}$ can be achieved. The disruption of larger volume of cell suspension was easily handled by the use of high pressure homogenization. By measuring the released protein via bradford assay, it could be determined, that 3 passages are sufficient for releasing most of the intracellular contents. A relative high purity (at least 80 %) of the fusion protein is achieved with just one IMAC step. Using a prepacked column, 46.3 mg of fusion protein could be obtained out of a 400 ml cell suspension ($c_{XL,wet}$= $50\,\mathrm{g\,l^{-1}}$). Thus, the maximum amount of NK2-ALK, which can be released from the fusion protein, is 9.2 mg. The applied downstream procedure did not damage the AMP, as antimircobial activity was retained. No refolding step was necessary, which greatly simplified the downstream process and avoided greater substantial loss of the target product.

6 Outlook

Future study could focus on increasing the yield of the AMP. The easiest way would be to just increase the cell density, since the fusion protein concentration is proportional to the cell density. As mentioned in 4.1.2, a higher cell density could be reached by increasing the oxygen transfer rate with the help of pure oxygen. It may be possible to reach a cell density greater than $100\,\mathrm{g\,l^{-1}}$. Although the use of pure oxygen in a large scale production is not desired, since it is expensive. Also, a focused could be set on determining optimal control parameters for the pO_2/agitation controller. This may be beneficial for achieving a higher cell density, since pO_2 would not drop to 0 % and thereby triggering the production of by-products, which can inhibit the growth of the cells. Then there is the possibility of increasing the cleaving efficiency, which would directly increase the amount of AMP released from the fusion protein. This may be enabled by switching from chemical to enzymatic cleavage. But the latter is unlikely to be used in an large scale process due to cost reasons. A more sophisticated approach to increase the expression of the fusion protein, and thus the AMP, may be achieved by improving the expression system via metabolic engineering.

Then there is also the possibility of substituting the fusion partner by a carrier protein, which leads to expression of the fusion protein in a solubles state as opposed to the insoluble expression of the fusion protein due to the rational designed onconase. The advantage of having an agglomeration of the fusion protein with a relative high purity would be lost. But in combination with an expression system, which secretes the protein (e.g. *Bacillus subtilis* and yeast expression systems), downstream processing could be simplified since cell disuption no longer is necessary. This method would also be suited for intensifying the process by developing an integrated process. Capturing of the protein could be carried out directly after end of the cultivation by IMAC using EBA technology. The total yield of AMP may not be enhanced, but process intensification and integration may have an overall advantage due to less time and money being required for the production of the AMP.

Since therapeutic use is intended for AMPs, the removal of impurities including guanidine-HCl and imidazole is an important step after IMAC. This may be a laborous task due

to the small size of the AMP. Buffer exchange could be achieved by application of size exclusion chromatography (SEC). SEC dilutes the sample and therefore a concentration step is eventually needed. Concentration of the AMP could be accomplished via freeze drying/lyophilization and resolving the lyophilized AMP in a smaller volume of an adequate buffer. Alternatively, preparative reversed-phase high performance liquid chromatography (RP-HPLC) with C4, C8 or C18 could be applied for final polishing of the AMP. A further possibility for concentrating and desalting the AMP, would be the application of nanofiltration techniques (Marchetti *et al.*, 2013).

References

Andersson, M., Gunne, H., Agerberth, B., Boman, A., Bergman, T., Sillard, R., Jörnvall, H., Mutt, V., Olsson, B., and Wigzell, H. (1995). "NK-lysin, a novel effector peptide of cytotoxic T and NK cells. Structure and cDNA cloning of the porcine form, induction by interleukin 2, antibacterial and antitumour activity." In: *The EMBO Journal* 14.8, pp. 1615–1625.

Andrä, J. and Leippe, M. (1999). "Candidacidal activity of shortened synthetic analogs of amoebapores and NK-lysin". In: *Medical Microbiology and Immunology* 188.3, pp. 117–124.

Andrä, J., Monreal, D., Tejada, G. M. de, Olak, C., Brezesinski, G., Gomez, S. S., Goldmann, T., Bartels, R., Brandenburg, K., and Moriyon, I. (2007). "Rationale for the Design of Shortened Derivatives of the NK-lysin-derived Antimicrobial Peptide NK-2 with Improved Activity against Gram-negative Pathogens". In: *Journal of Biological Chemistry* 282.20, pp. 14719–14728.

Arnold, F. H. (1991). "Metal-Affinity Separations: A New Dimension in Protein Processing". In: *Nature Biotechnology* 9.2, pp. 151–156.

Bedding, N. D., McIntyre, A. E., Perry, R., and Lester, J. N. (1982). "Organic contaminants in the aquatic environment I. Sources and occurrence". In: *Science of The Total Environment* 25.2, pp. 143–167.

Block, H., Maertens, B., Spriestersbach, A., Brinker, N., Kubicek, J., Fabis, R., Labahn, J., and Schäfer, F. (2009). "Chapter 27 Immobilized-Metal Affinity Chromatography (IMAC)". In: *Methods in Enzymology*. Elsevier, pp. 439–473.

Bradford, M. M. (1976). "A rapid and sensitive method for the quantitation of microgram quantities of protein utilizing the principle of protein-dye binding". In: *Analytical Biochemistry* 72.1-2, pp. 248–254.

Brandenburg, K., Moriyon, I., Arraiza, M. D., Lewark-Yvetot, G., Koch, M. H. J., and Seydel, U. (2002). "Biophysical investigations into the interaction of lipopolysaccharide with polymyxins". In: *Thermochimica Acta* 382.1-2, pp. 189–198.

Braund, R., Peake, B. M., and Shieffelbien, L. (2009). "Disposal practices for unused medications in New Zealand". In: *Environment International* 35.6, pp. 952–955.

Brogan, D. M. and Mossialos, E. (2013). "Incentives for new antibiotics: the Options Market for Antibiotics (OMA) model". In: *Globalization and Health* 9.1, p. 58.

Brogden, K. A. (2005). "Antimicrobial peptides: pore formers or metabolic inhibitors in bacteria?" In: *Nature Reviews Microbiology* 3.3, pp. 238–250.

Brunelle, J. L. and Green, R. (2014). "One-dimensional SDS-Polyacrylamide Gel Electrophoresis (1D SDS-PAGE)". In: *Methods in Enzymology*. Elsevier, pp. 151–159.

Cinar, A. (2003). *Batch fermentation : modeling, monitoring, and control*. New York: Marcel Dekker. ISBN: 0824740343.

Compton, S. J. and Jones, C. G. (1985). "Mechanism of dye response and interference in the Bradford protein assay". In: *Analytical Biochemistry* 151.2, pp. 369–374.

Danilevich, V. N., Petrovskaya, L. E., and Grishin, E. V. (2008). "A Highly Efficient Procedure for the Extraction of Soluble Proteins from Bacterial Cells with Mild Chaotropic Solutions". In: *Chemical Engineering & Technology* 31.6, pp. 904–910.

Deng, T., Ge, H., He, H., Liu, Y., Zhai, C., Feng, L., and Yi, L. (2017). "The heterologous expression strategies of antimicrobial peptides in microbial systems". In: *Protein Expression and Purification* 140, pp. 52–59.

Du, L. and Liu, W. (2011). "Occurrence, fate, and ecotoxicity of antibiotics in agro-ecosystems. A review". In: *Agronomy for Sustainable Development* 32.2, pp. 309–327.

Embruch, J. E. (2018). "Herstellung des antimiktobiellen Peptids NK-2 ALK als Fusionsprotein in Escherichia coli BL21 (DE3)". Bachelor's Thesis. Hochschule für Angewandte Wissenschaften Hamburg.

Floeter, C. (2017). *Arzneimittelbelastung in Gewässern: Projekt PharmCycle erforscht Lösungen*. Ed. by H. für Angewandte Wissenschaften Hamburg. URL: https://www.haw-hamburg.de/forschung/projekte-uebersicht/projekt-news/projekt-news-detail/artikel/arzneimittelbelastung-in-gewaessern-projekt-pharmcycle-erforscht-loesungen.html (visited on 04/26/2020).

Gaberc-Porekar, V. and Menart, V. (2001). "Perspectives of immobilized-metal affinity chromatography". In: *Journal of Biochemical and Biophysical Methods* 49.1-3, pp. 335–360.

Galdiero, E., Maselli, V., Falanga, A., Gesuele, R., Galdiero, S., Fulgione, D., and Guida, M. (2015). "Integrated analysis of the ecotoxicological and genotoxic effects of the antimicrobial peptide melittin on Daphnia magna and Pseudokirchneriella subcapitata". In: *Environmental Pollution* 203, pp. 145–152.

Gaw, S., Thomas, K. V., and Hutchinson, T. H. (2014). "Sources, impacts and trends of pharmaceuticals in the marine and coastal environment". In: *Philosophical Transactions of the Royal Society B: Biological Sciences* 369.1656, pp. 1–11.

Halling-Sørensen, B., Nielsen, S. N., Lanzky, P. F., Ingerslev, F., Lützhøft Holten, H. C., and Jørgensen, S. E. (1998). "Occurrence, fate and effects of pharmaceutical substances in the environment- A review". In: *Chemosphere* 36.2, pp. 357–393.

Harrison, S. T. L. (1991). "Bacterial cell disruption: A key unit operation in the recovery of intracellular products". In: *Biotechnology Advances* 9.2, pp. 217–240.

Hignite, C. and Azarnoff, D. L. (1977). "Drugs and drug metabolites as environmental contaminants: Chlorophenoxyisobutyrate and salicylic acid in sewage water effluent". In: *Life Sciences* 20.2, pp. 337–341.

Hwang, P. M. and Vogel, H. J. (1998). "Structure-function relationships of antimicrobial peptides". In: *Biochemistry and Cell Biology* 76.2-3, pp. 235–246.

internetchemie.info (2017). *Dichtetabelle: Zuckerlösung (Rohrzucker, Saccharose)*. Ed. by internetchemie.info. URL: https://www.internetchemie.info/chemie-lexikon/daten/s/saccharose-dichtetabelle.php (visited on 04/26/2020).

Jacobsen, P. and Berglind, L. (1988). "Persistence of oxytetracycline in sediments from fish farms". In: *Aquaculture* 70.4, pp. 365–370.

Jeong, H., Barbe, V., Lee, C. H., Vallenet, D., Yu, D. S., Choi, S.-H., Couloux, A., Lee, S.-W., Yoon, S. H., Cattolico, L., Hur, C.-G., Park, H.-S., Ségurens, B., Kim, S. C., Oh, T. K., Lenski, R. E., Studier, F. W., Daegelen, P., and Kim, J. F. (2009). "Genome Sequences of Escherichia coli B strains REL606 and BL21(DE3)". In: *Journal of Molecular Biology* 394.4, pp. 644–652.

Kemper, N. (2008). "Veterinary antibiotics in the aquatic and terrestrial environment". In: *Ecological Indicators* 8.1, pp. 1–13.

Khetan, S. K. and Collins, T. J. (2007). "Human Pharmaceuticals in the Aquatic Environment: A Challenge to Green Chemistry". In: *Chemical Reviews* 107.6, pp. 2319–2364.

Knight, M. I. and Chambers, P. J. (2003). "Problems Associated with Determining Protein Concentration: A Comparison of Techniques for Protein Estimations". In: *Molecular Biotechnology* 23.1, pp. 19–28.

Koch, P.-J., Frank, J., Schüler, J., Kahle, C., and Bradaczek, H. (1999). "Thermodynamics and Structural Studies of the Interaction of Polymyxin B with Deep Rough Mutant Lipopolysaccharides". In: *Journal of Colloid and Interface Science* 213.2, pp. 557–564.

Korz, D. J., Rinas, U., Hellmuth, K., Sanders, E. A., and Deckwer, W.-D. (1995). "Simple fed-batch technique for high cell density cultivation of Escherichia coli". In: *Journal of Biotechnology* 39.1, pp. 59–65.

Kümmerer, K. and Henninger, A. (2003). "Promoting resistance by the emission of antibiotics from hospitals and households into effluent". In: *Clinical Microbiology and Infection* 9.12, pp. 1203–1214.

Kümmerer, K. (2009). "Antibiotics in the aquatic environment – A review – Part I". In: *Chemosphere* 75.4, pp. 417–434.

Laemmli, U. K. (1970). "Cleavage of Structural Proteins during the Assembly of the Head of Bacteriophage T4". In: *Nature* 227.5259, pp. 680–685.

Lampert, M. (2019). "Untersuchung der biotechnologischen Herstellung eines Antimikrobiellen Peptids als Fusionsprotein mit Escherichia coli BL21 (DE3)". Master's Thesis. Hochschule für Angewandte Wissenschaften Hamburg.

Larsson, D. G. J., Pedro, C. de, and Paxeus, N. (2007). "Effluent from drug manufactures contains extremely high levels of pharmaceuticals". In: *Journal of Hazardous Materials* 148.3, pp. 751–755.

LaVallie, E. R., Lu, Z., Diblasio-Smith, E. A., Collins-Racie, L. A., and McCoy, J. M. (2000). "[21] Thioredoxin as a fusion partner for production of soluble recombinant proteins in Escherichia coli". In: *Methods in Enzymology*. Elsevier, pp. 322–340.

Lazarev, V. N. and Govorun, V. M. (2010). "Antimicrobial peptides and their use in medicine". In: *Applied Biochemistry and Microbiology* 46.9, pp. 803–814.

Lee, J. H., Kim, J. H., Hwang, S. W., Lee, W. J., Yoon, H. K., Lee, H. S., and Hong, S. S. (2000). "High-Level Expression of Antimicrobial Peptide Mediated by a Fusion Partner Reinforcing Formation of Inclusion Bodies". In: *Biochemical and Biophysical Research Communications* 277.3, pp. 575–580.

Levy, S. B. (1998). "The Challenge of Antibiotic Resistance". In: *Scientific American* 278.3, pp. 46–53.

Levy, S. B. and Marshall, B. (2004). "Antibacterial resistance worldwide: causes, challenges and responses". In: *Nature Medicine* 10.S12, S122–S129.

Li, Y. (2009). "Carrier proteins for fusion expression of antimicrobial peptides in Escherichia coli". In: *Biotechnology and Applied Biochemistry* 54.1, pp. 1–9.

Longobardi, G. P. (1994). "Fed-batch versus batch fermentation". In: *Bioprocess Engineering* 10.5-6, pp. 185–194.

Luli, G. W. and Strohl, W. R. (1990). "Comparison of growth, acetate production, and acetate inhibition of Escherichia coli strains in batch and fed-batch fermentations." In: *Applied and Environmental Microbiology* 56.4, pp. 1004–1011.

Makrides, S. C. (1996). "Strategies for achieving high-level expression of genes in Escherichia coli." In: *Microbiological reviews* 60.3, pp. 512–538.

Marchetti, P., Butté, A., and Livingston, A. G. (2013). "Quality by Design for peptide nanofiltration: Fundamental understanding and process selection". In: *Chemical Engineering Science* 101, pp. 200–212.

Martinez, J. L. (2009). "Environmental pollution by antibiotics and by antibiotic resistance determinants". In: *Environmental Pollution* 157.11, pp. 2893–2902.

Michael, C. A., Dominey-Howes, D., and Labbate, M. (2014). "The Antimicrobial Resistance Crisis: Causes, Consequences, and Management". In: *Frontiers in Public Health* 2, pp. 1–8.

Middelberg, A. P. J. (1995). "Process-scale disruption of microorganisms". In: *Biotechnology Advances* 13.3, pp. 491–551.

Müller, F. (Unpublished). "Model Based Controller Design of a pO2 Controller for Microbial Fermentation Processes". Master's Thesis. Hochschule für Angewandte Wissenschaften Hamburg.

Nguyen, L. T., Haney, E. F., and Vogel, H. J. (2011). "The expanding scope of antimicrobial peptide structures and their modes of action". In: *Trends in Biotechnology* 29.9, pp. 464–472.

Pane, K., Durante, L., Pizzo, E., Varcamonti, M., Zanfardino, A., Sgambati, V., Maro, A. D., Carpentieri, A., Izzo, V., Donato, A. D., Cafaro, V., and Notomista, E. (2016). "Rational Design of a Carrier Protein for the Production of Recombinant Toxic Peptides in Escherichia coli". In: *PLOS ONE* 11.1. Ed. by M. J. van Raaij, pp. 1–23.

Persson, M., Sabelström, E., and Gunnarsson, B. (2009). "Handling of unused prescription drugs — knowledge, behaviour and attitude among Swedish people". In: *Environment International* 35.5, pp. 771–774.

Piers, K. L., Brown, M. H., and Hancock, R. E. W. (1993). "Recombinant DNA procedures for producing small antimicrobial cationic peptides in bacteria". In: *Gene* 134.1, pp. 7–13.

Rai, M., Pandit, R., Gaikwad, S., and Kövics, G. (2016). "Antimicrobial peptides as natural bio-preservative to enhance the shelf-life of food". In: *Journal of Food Science and Technology* 53.9, pp. 3381–3394.

Richardson, M. L. and Bowron, J. M. (1985). "The fate of pharmaceutical chemicals in the aquatic environment". In: *Journal of Pharmacy and Pharmacology* 37.1, pp. 1–12.

Riesenberg, D. (1991). "High-cell-density cultivation of Escherichia coli". In: *Current Opinion in Biotechnology* 2.3, pp. 380–384.

Sahl, H.-G., Pag, U., Bonness, S., Wagner, S., Antcheva, N., and Tossi, A. (2004). "Mammalian defensins: structures and mechanism of antibiotic activity". In: *Journal of Leukocyte Biology* 77.4, pp. 466–475.

Santos, L. H. M. L. M., Araújo, A. N., Fachini, A., Pena, A., Delerue-Matos, C., and Montenegro, M. C. B. S. M. (2010). "Ecotoxicological aspects related to the presence of pharmaceuticals in the aquatic environment". In: *Journal of Hazardous Materials* 175.1-3, pp. 45–95.

Sapkota, A., Sapkota, A. R., Kucharski, M., Burke, J., McKenzie, S., Walker, P., and Lawrence, R. (2008). "Aquaculture practices and potential human health risks: Current knowledge and future priorities". In: *Environment International* 34.8, pp. 1215–1226.

Schägger, H. and Jagow, G. von (1987). "Tricine-sodium dodecyl sulfate-polyacrylamide gel electrophoresis for the separation of proteins in the range from 1 to 100 kDa". In: *Analytical Biochemistry* 166.2, pp. 368–379.

Shai, Y. and Oren, Z. (2001). "From "carpet" mechanism to de-novo designed diastereomeric cell-selective antimicrobial peptides". In: *Peptides* 22.10, pp. 1629–1641.

Sørensen, H. P. and Mortensen, K. K. (2005). "Advanced genetic strategies for recombinant protein expression in Escherichia coli". In: *Journal of Biotechnology* 115.2, pp. 113–128.

Steinhart, J. (2019). "Aufreinigung von rekombinanten Fusionsproteinen und Peptiden aus E. coli." Bachelor's Thesis. Hochschule für Angewandte Wissenschaften Hamburg.

Studier, F. W. and Moffatt, B. A. (1986). "Use of bacteriophage T7 RNA polymerase to direct selective high-level expression of cloned genes". In: *Journal of Molecular Biology* 189.1, pp. 113–130.

Terpe, K. (2006). "Overview of bacterial expression systems for heterologous protein production: from molecular and biochemical fundamentals to commercial systems". In: *Applied Microbiology and Biotechnology* 72.2, pp. 211–222.

Wise, R. (2002). "Antimicrobial resistance: priorities for action". In: *Journal of Antimicrobial Chemotherapy* 49.4, pp. 585–586.

Yamanè, T. and Shimizu, S. (1984). "Fed-batch techniques in microbial processes". In: *Bioprocess Parameter Control*. Springer-Verlag, pp. 147–194.

Yang, L., Harroun, T. A., Weiss, T. M., Ding, L., and Huang, H. W. (2001). "Barrel-Stave Model or Toroidal Model? A Case Study on Melittin Pores". In: *Biophysical Journal* 81.3, pp. 1475–1485.

Yee, L. and Blanch, H. W. (1992). "Recombinant Protein Expression in High Cell Density Fed-Batch Cultures of Escherichia Coli". In: *Nature Biotechnology* 10.12, pp. 1550–1556.

Yoshida, F., Yamane, T., and Nakamoto, K.-I. (1973). "Fed-batch hydrocarbon fermentation with colloidal emulsion feed". In: *Biotechnology and Bioengineering* 15.2, pp. 257–270.

Zasloff, M. (2002). "Antimicrobial peptides of multicellular organisms". In: *Nature* 415.6870, pp. 389–395.

Appendix A Material lists

Table 36: Consumables used

Consumables	Manufacturer	Order number
Aeration filter	Sartorious	17805
Disposable cuvettes	ROTH	XK20
Filter paper	Whatman (now GE Healthcare)	10 311 852
Membrane filter	GE Healthcare	10401712
Petri dish	Carl Roth	TA19.1
Pipette tips (10 µl)	nerbe plus	07-112-000
Pipette tips (1000 µl)	nerbe plus	07-132-0095
Pipette tips (200 µl)	nerbe plus	07-122-0073
Reaction tube (1.5 ml)	nerbe plus	04-212-1000
Reaction tube (15 ml)	neoLabLine	C-8215
Reaction tube (15 ml)	ROTH Selection	N458.1
Reaction tube (50 ml)	ROTH Selection	N463.1
Reaction tube (50 ml)	VWR	21008-242
Silicone tubing	VWR	228-1528
Silicone tubing	VWR	228-0704
Spinfilter (3 kDa, PES,20 ml)	Satorius	VS2091
Spinfilter (3 kDa, PES,500 µl)	VWR	82 031 344
Syringe filter	ROTH	P666.1

Table 37: Chemicals used

Chemical	Manufacturer	Order number
1,4-Dithiothreitol	Carl Roth	6908
10x Tris/Glycine/SDS	Bio-Rad	161-0772
Acetic acid (100 %)	Carl Roth	3738.5
Agarose	Carl Roth	2267.2
Ammonia solution (25 %)	Carl Roth	5460.2
Boric acid	Riedel de Haën	31146
Citric acid	Carl Roth	X863.2
Cobald(II)chlorid Hexahydrate	Riedel de Haën	12914
Copper(II)chloride dihydrate	Riedel de Haën	31286
D(+)Glucose Monohydrate	Carl Roth	6887.3
Diammonium hydrogen phosphate	Carl Roth	0268.2
E. coli BL21 (DE3)	NEB	C2527H
Ethanol	Carl Roth	K928.2
Ethylenediaminetetraacetic acid	Carl Roth	8040.3
Glutardialdehyde (25 %)	MERCK	8.20603.0100
Glycerol ($\geq$ 99.5 %)	Carl Roth	3783.5
Guanidine hydrochloride	Carl Roth	0037.1

Table 37: (continued)

Chemical	Manufacturer	Order number
Hydrochloric acid (37 %)	Carl Roth	4625.1
Imidazol	MERCK	1.04716.1000
Iron(III)citrate	Fluka	44941
Kanamycin sulfate	Boehringer Mannheim	106 801
Magnesium sulfate heptahydrate	Carl Roth	T888.3
Manganese(II)dihydrate	Riedel de Haën	925A422017
Marker (Polypeptide SDS-PAGE Molecular Weight Standards)	Bio-Rad	161-0326
Marker (Precision Plus Protein™Unstained Standards)	Bio-Rad	1610363
Nickel(II)sulfate hexahydrate	MERCK	1.06727.10000
Peptone ex casein (tryptone)	Carl Roth	8986.1
Potassium dihydrogenphosphate	Carl Roth	3904.3
Roti®Blue (5x)	Carl Roth	A152.1
Roti®Load 2	Carl Roth	K930.1
Rotiphorese®Gel 40 (40 %)	Carl Roth	T802.1
Roti®Quant	Carl Roth	K015.3
Sodium azide	Sigma-Aldrich	S2002-25g

Table 37: (continued)

Chemical	Manufacturer	Order number
Sodium chloride	Carl Roth	9265.1
Sodium deoxycholate	Carl Roth	3484.2
Sodium dihydrogen phosphate dihydrate	Carl Roth	T879.3
Sodium dodecylsulfate (SDS)	Sigma-Aldrich	L-3771
Sodium hydrogen phosphate	Carl Roth	P030.1
Sodium hydroxide	Carl Roth	6771.2
Sodium molybdate dihydrate	Riedel de Haën	31439
Tricine	Roth	6977.2
TRIS	Carl Roth	4855.1
Tryptone/Peptone ex casein	Carl Roth	8952.2
Tween 20	Carl Roth	9127.1
Zinc acetate dihydrate	MERCK	1.08802.0250

Table 38: Equipment used

Equipment	Manufacturer	Model name/ Serial
Analytcial balance	Sartorius	BA110S
Balance	Sartorius	FB12CCE-S
Balance	Sartorius	CP2202S
Balance(acid)	Sartorius	LP2200
Balance(base)	Sartorius	LP6200
Balance(bioreactor)	Sartorius	-
Balance(feed)	Sartorius	LP6200
Benchtop centrifuge	Eppendorf	5417R
Bioreactor	B. Braun Biotech International (now Sartorius)	-
Centrifuge	Sigma	94709
Drying cabinet	Köttermann	2711
FPLC system	GE Healthcare	ÄKTA avant 150
HiScale 16/20	GE Healthcare	28964441
Imager	Bio-Rad	GelDoc™EZ Imager
Magnetic stirrer	IKA	RCO 28240
Magnetic stirrer	IKA	REO 1121
Magnetic stirrer	IKA	RET 5203

Table 38: (continued)

Equipment	Manufacturer	Model name/ Serial
Peristaltic pump	Watson Marlow	101 UIR
pH meter	Sartorius	11443020
Photometer	ThermoScientific	Genesys 20
Shaking incubator	GFL	3032
Steam generator	ZIRBUS technology	Steamboy 9
Sterile workbench	HERA safe	161700008839
Thermal Shaker	Eppendorf	Thermomixer compact
Ultrasonic bath	Bandelin	SONOREX RK514BIT
Ultrasonic homogenizer	B. Braun Biotech International (now Sartorius)	83397213

Table 39: Special materials and kits used]

Special material/kit	Manufacturer	Order number
HisTrap IMAC FF crude 1 ml	GE Healthcare	11-0004-58
IMAC Sepharose 6 Fast Flow	GE Healthcare	17092108
TGX™FastCast™ Acrylamide Kit, 10 %	Bio-Rad	1610173

Appendix B Sugar density table

Table 40: Density of sugar solution on the concentration (internetchemie.info, 2017).

Concentration $[\mathrm{g\,l^{-1}}]$	Density $[\mathrm{g\,ml^{-1}}]$
200	1.0810
250	1.1036
300	1.1270
350	1.1513
400	1.1764
450	1.2025
500	1.2296
550	1.2575
600	1.2865
650	1.3163

Appendix C Two pump feeding strategy

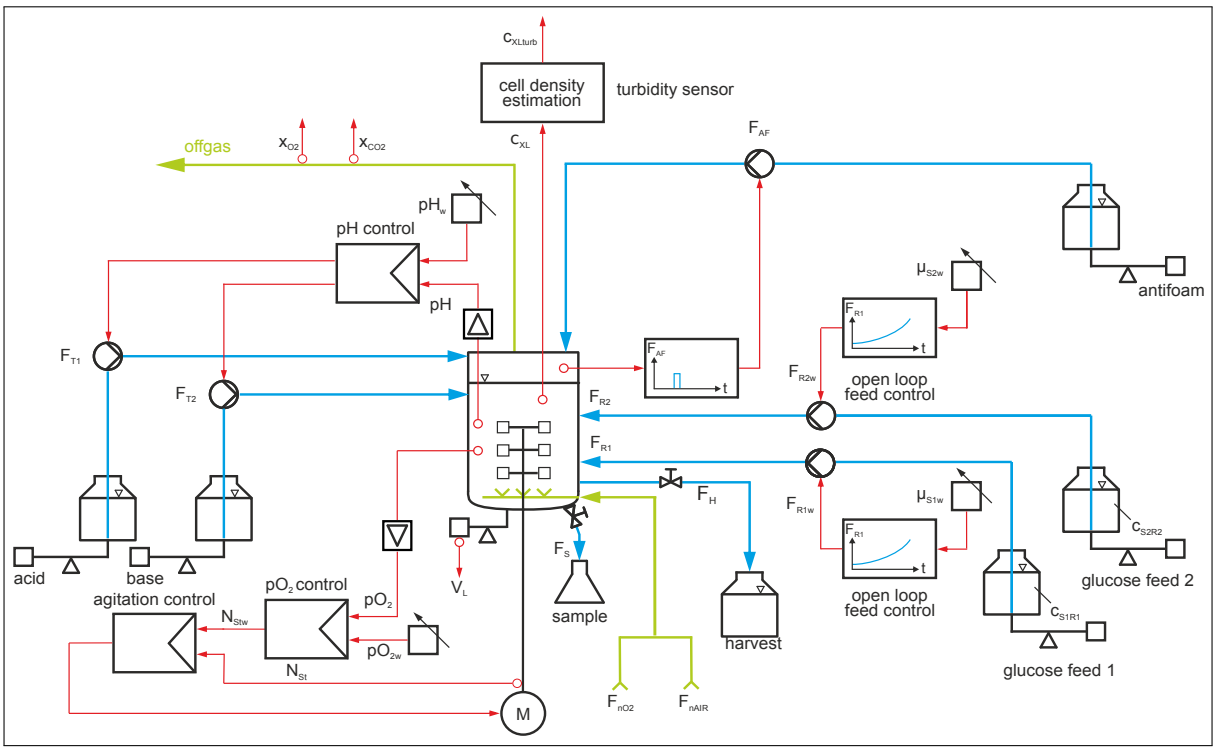

Figure 45: P&I diagram of the ED5 bioreactor system with two pumps. It should be noted, that the temperature control loop was not displayed here for reasons of clarity.

These fermentation were carried out with two pumps. But due to unkown reasons, the growth of the cell density was inhibited everytime during fed-batch phase 2, which prevented the c_{XL} to grow beyond $40\,\mathrm{g\,l^{-1}}$. In fed-batch fermentation 5 (see figure 46) , $MgSO_4$ stock solution, trace metal solution and glucose stock solution were added directly into the medium to see if a limitation occured. Only the addition of $MgSO_4$ triggered a response as x_{CO2} rapidly increased.

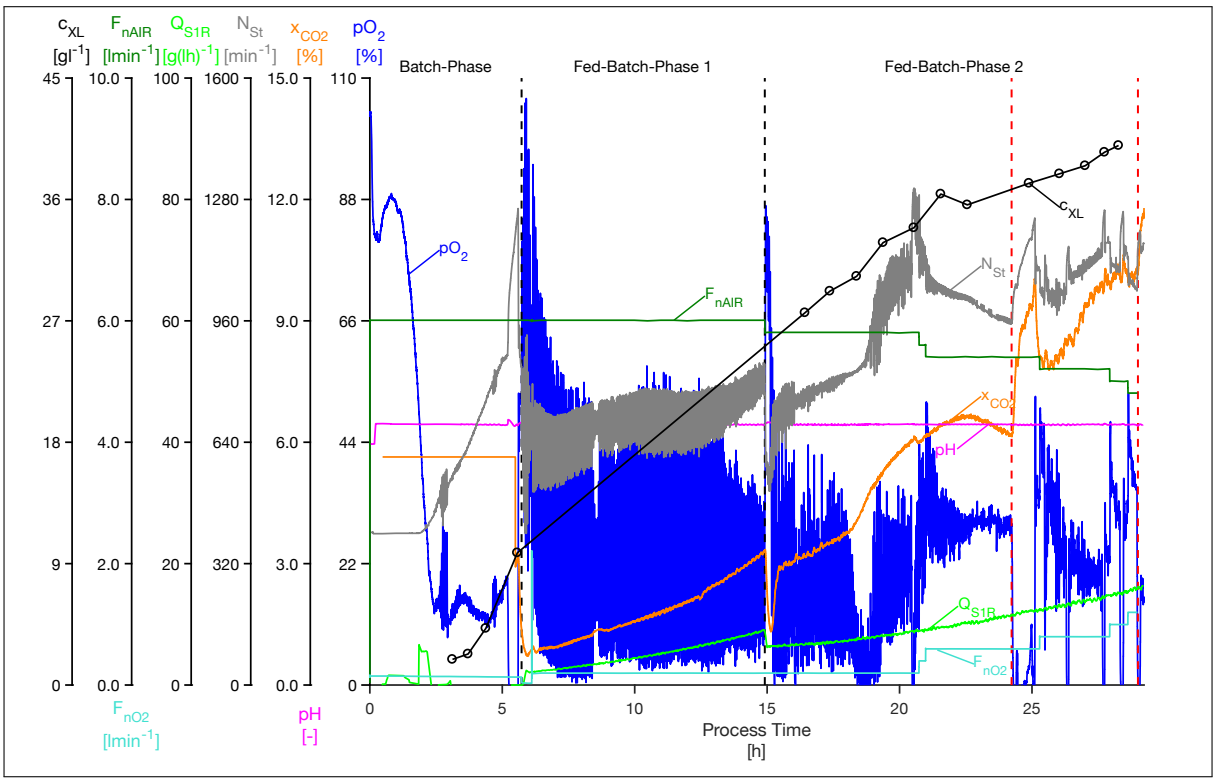

Figure 46: The course of fed-batch fermentation no. 5 is depicted in this figure. The online values, which are shown here, include N_{St}, pO_2, pH, F_{nO2}, F_{nAIR} and x_{CO2}. The offline value c_{XL} was determined gravimetrically. Q_{S1R} was determined via the online measured weight signals of the feeding reservoirs. Two pumps where used for pumping feeding solution into the reactor, so that each reservoir was connected to one pump. Red dotted lines mark the time where $MgSO_4$ stock solution (11.8 % w/v) was injected into the bioreactor.

The rise of x_{CO2} indicates that substrate (glucose) is being metabolized by the cells. But the composition of feeding solution 2 was not altered and therefore identical to the previous fed-batch fermentations as well as the last two fed-batch fermentation (8 and 9). So it is possible that a metabolical shift occured and thus the demand for $MgSO_4$ increased. It should be noted, that apart from two pumps being used, one for each reservoir, a different μ_{set} for fed-batch phase 1 was used compared to the other fed-batch fermentations. μ_{set1} was set to $0.15\,h^{-1}$ instead of $0.2\,h^{-1}$. But this was unlikely the reason for the abnormal beahvior of the cells, since the cells density rose without any disturbance. In fed-batch fermentation 6 (see figure 47) , $MgSO_4$ stock solution was also injected after the c_{XL} remained at approx. $36\,g\,l^{-1}$. Like in fed-batch fermentation 5, the cells immediately responded to the addition of $MgSO_4$, since a steep increase of N_{St} was triggered. The communication between the Off-gas sensors and MFCS broke off in

the middle fed-batch phase 1 and thus no new values for x_{CO2} were registered. c_{XL} also began to rise after supplementation with $MgSO_4$. It should be noted, that the pO_2 probe was not adequately polarized, which led to a value of just under 250 % during the transition from batch phase to fed-batch phase 1.

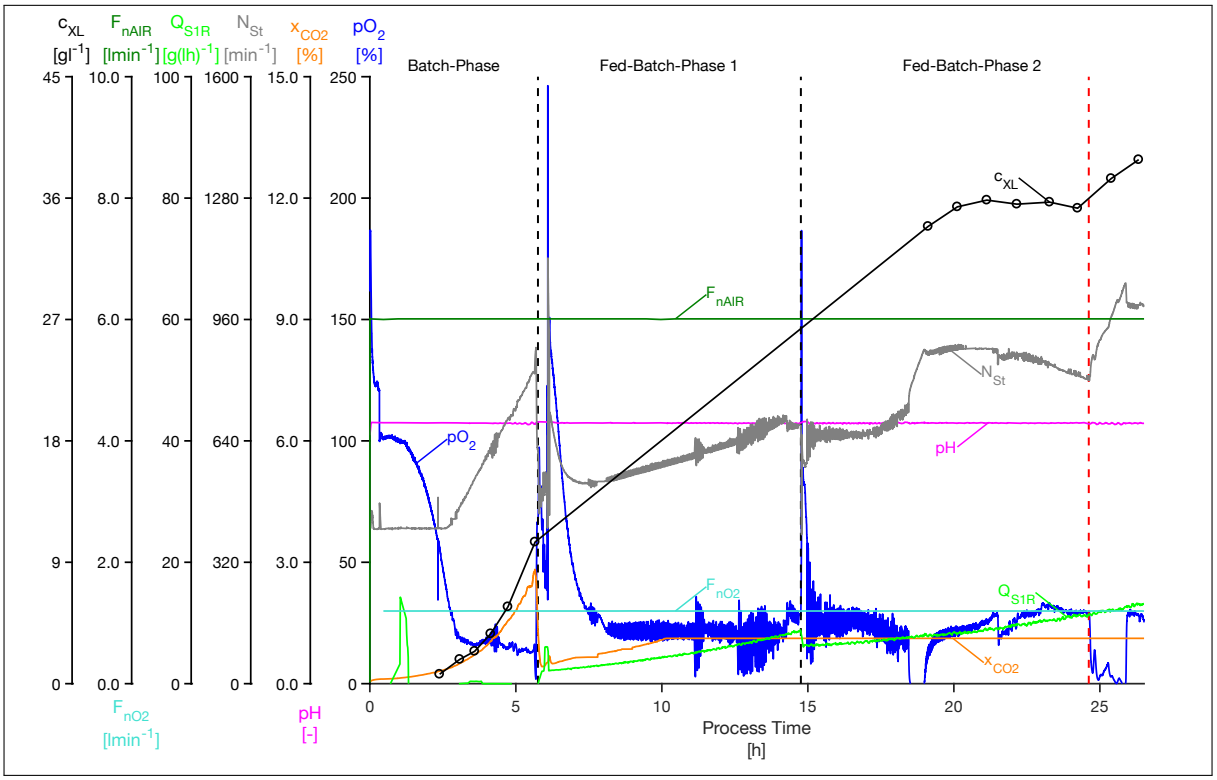

Figure 47: The course of fed-batch fermentation no. 6 is depicted in this figure. The online values, which are shown here, include N_{St}, pO_2, pH, F_{nO2}, F_{nAIR} and x_{CO2}. The offline value c_{XL} was determined gravimetrically. Q_{S1R} was determined via the online measured weight signals of the feeding reservoirs. Two pumps where used for pumping feeding solution into the reactor, so that each reservoir was connected to one pump. Red dotted line mark the time where $MgSO_4$ stock solution (11.8 % w/v) was injected into the bioreactor. Communication between off-gas sensors and MFCS broke off after around 10 h.

Interestingly, as soon as the valve of reservoir 2 was closed, x_{CO2} began to rise. Reservoir 2 was switched back to reservoir 1in order too see how the cells would react to feeding solution 1. Reservoir 1 was filled with unsterile feeding solution 1 and then fed into the reactor. This also led to rise of x_{CO2} . The valve of the two reservoirs differed from each other, since the one connceted to reservoir 1 is a male connector and the one connected to reservoir 2 is a female connector. This prevented the valves to switch there position on the port with each other. So it can not be excluded, that the valve of the

second reservoir 2 somehow led to inhibition of the cells. There may have been some inhibiting residues present within the valve of reservoir 2, which were gradually transported into the cell broth.

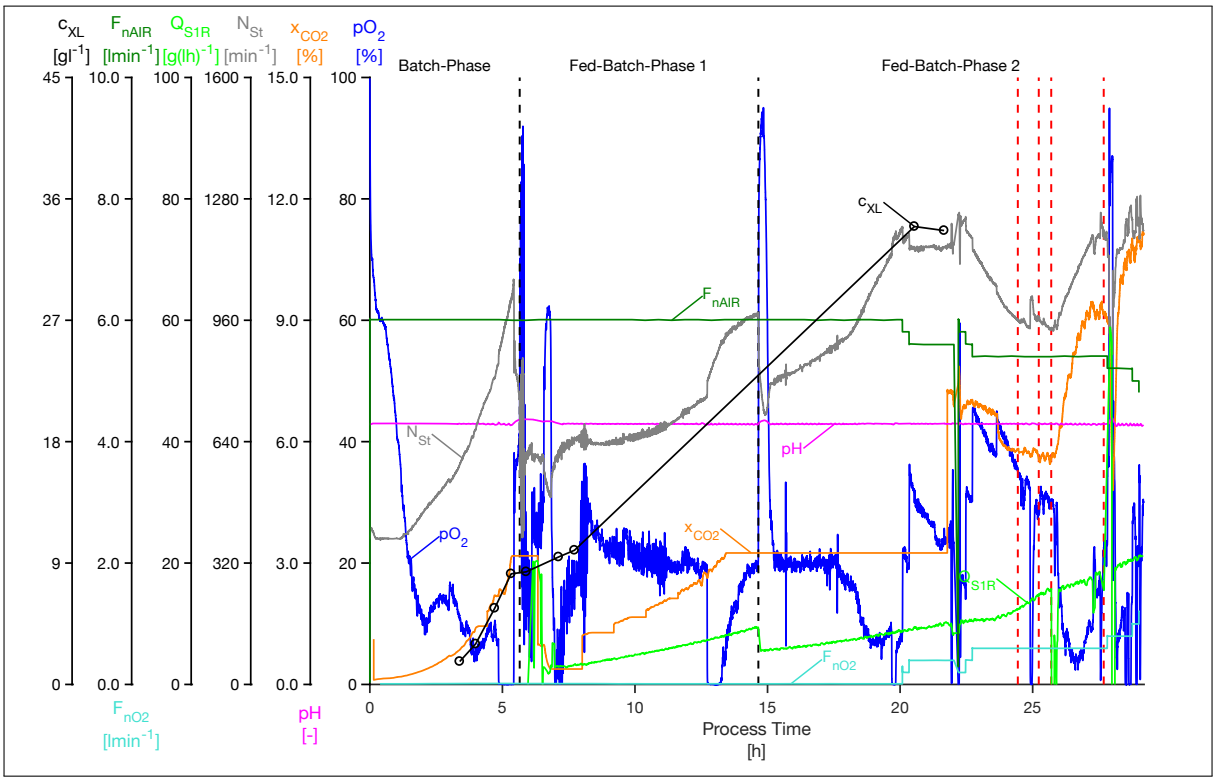

Figure 48: The course of fed-batch fermentation no. 7 is depicted in this figure. The online values, which are shown here, include N_{St}, pO_2, pH, F_{nO2}, F_{nAIR} and x_{CO2}. The offline value c_{XL} was determined gravimetrically. Q_{S1R} was determined via the online weight signals of the feeding reservoirs. Two pumps where used for pumping feeding solution into the reactor, so that each reservoir was connected to one pump. The first (24.44 h) and second (25.23 h) red dotted line mark the time where 7 ml of trace metal stock solution and 10 ml of $(NH_4)_2HPO_4$(20 g l^{-1} were injected into the bioreactor respectively. The third red dotted line (25.70 h) indicate the time, where the switch from reservoir 2 to reservoir 1 occured. At 27.68 h (fourth red dotted line), reservoir 1 was refilled with unsterile feeding solution 1. Communication between off-gas sensors and MFCS broke off after 13.9 h and was restored at 21.8 h.

Appendix D MATLAB scripts

Master file for plotting the course of a bioprocess with MATLAB

```
clear all
clc

M1  = dlmread('20200122 FB9 FAIR.txt','',1,0);                  %FnAIR
M2  = dlmread('20200122 FB9 mB.txt','',1,0);                    %mB
M3  = dlmread('20200122 FB9 NSt.txt','',1,0);                   %Nst
M4  = dlmread('20200122 FB9 pH.txt','',1,0);                    %pH
M5  = dlmread('20200122 FB9 pO2.txt','',1,0);                   %pO2
M6  = dlmread('20200122 FB9 sTurb.txt','',1,0);                 %
   Turbidity
M7  = dlmread('20200122 FB9 TL.txt','',1,0);                    %TL
M8  = dlmread('20200122 FB9 xCO2.txt','',1,0);                  %xCO2
M9  = dlmread('20200122 FB9 xO2.txt','',1,0);                   %xO2
M10= dlmread('20200122 FB9 FR1.txt','',1,0);                    %FR1
M11= xlsread('Fermentation GS KW04.xlsx','Off ML','C2:D20');    %Off OD
M12= xlsread('Fermentation GS KW04.xlsx','Off ML','A3:B20');    %cxl
M13 = dlmread('20200122 FB9 FO2.txt','',1,0);                   %FnO2
M14 = dlmread('20200122 FB9 mR1.txt','',1,0);                   %mR1
%M15 = dlmread('20190828 FB4 FR2.txt','',1,0);                  %FR2

t FAIR          = M1(:,1);          %Process Time [h]
FAIR            = M1(:,2);          %FAIR value [l/min]
t mB            = M2(:,1);          %Process Time [h]
mB              = M2(:,2);          %mB value [kg]
t NSt           = M3(:,1);          %Process Time [h]
NSt             = M3(:,2);          %Nst value [rpm]
t pH            = M4(:,1);          %Process Time [h]
```

```
pH              = M4(:,2);          %pH value [-]
t pO2           = M5(:,1);          %Process Time [h]
pO2             = M5(:,2);          %pO2 value [%]
t Turb          = M6(:,1);          %Process Time [h]
Turb            = M6(:,2);          %Turbidity value [CU]
t TL            = M7(:,1);          %Process Time [h]
TL              = M7(:,2);          %TL value [^{\circ}C]
t xCO2          = M8(:,1);          %Process Time [h]
xCO2            = M8(:,2);          %xCO2 value [%]
t xO2           = M9(:,1);          %Process Time [h]
xO2             = M9(:,2);          %xO2 value [%]
t FR1           = M10(:,1);         %Process Time [h]
FR1r            = M10(:,2);         %FR1 value [%]
t OD            = M11(:,1);         %Time points OD [h]
OD              = M11(:,2);         %OD value [-]
t cxl           = M12(:,1);         %Time points cxl [g/l]
cxl             = M12(:,2);         %cxl value [g/l]
t FO2           = M13(:,1);         %Time points c xl [g/l]
FO2             = M13(:,2);         %FO2 value [l/min]

%%Splitting of mR1 and t mR1 vector
%%(Transition Fed-Batch 1 to Fed-Batch 2)
t mR1           = M14(:,1);                                     %Process
   Time [h]
mR1             = M14(:,2);                                     %mR1 [g]
t mR1 1         = t mR1(1:5274);                                %Process
   Time [h] for Fed-Batch 1
t mR1 2         = t mR1(5273:end);                              %Process
   Time [h] for Fed-Batch 2
mR1 1           = mR1(1:5274);                                  %mR1 [g]
```

```
   for Fed-Batch 1
mR1 2           = mR1(5274:end);                                %mR1 [g]
   for Fed-Batch 2

%%Calculation of FR1 and mass flow of substrate
%set values
FRmax           = 0.647;                                        %Maximum
   Pumprate [l/h]
cSR1            = 300;                                          %
   Concentration of glucose R1 [g/l]
rho glc300      = 1.1270;                                       %Density
   of glucose solution with c = 300 g/l [g/l]
cSR2            = 600;                                          %
   Concentration of glucose R2 [g/l]
rho glc600      = 1.2865;                                       %Density
   of glucose solution with c = 600 g/l [g/l]

%Noise filtering of mB
WS mB           = 500;                                          %
   Windowsize for moving average method (for mB smoothing)
WS QS           = 5;                                            %
   Windowsize for moving average method (for QS smoothing)
mB S            = movmean(mB, [WS mB 0]);                       %
   Smoothing of mB

%Calculation of pumprate FR1 and
%volumetric substrate transfer rate QS1 using theoretical rel. FR1 values
%calculated by MFCS
FR1p            = (FR1r*FRmax)./100;                            %
   Theoretical pumprate [l/h]
```

```
ms300p          = FR1p(1:4676)*cSR1;                                %Mass
   flow glucose for R1 [g/h]
ms600p          = FR1p(4677:end)*cSR2;                              %Mass
   flow glucose for R2 [g/l]
mstotp          = [ms300p; ms600p];
[QS1p]          = cal Q(t FR1, mstotp, t mB, mB S);                 %
   Calculation of theoretical volume specific feeding rate QS1 [g/(lh)]

%Indirect method for calculation of pumprate FR1 and
%volumetric substrate transfer rate QS1 using scale signals (mR1)
[M cal]         = mS calc(mR1 1,t mR1 1,rho glc300,cSR1);           %
   Calculation of FR1 and substrate mass flow mS1 for R1, Matrix with 3
   columns returned
[M cal2]        = mS calc(mR1 2,t mR1 2,rho glc600,cSR2);           %
   Calculation of FR1 and substrate mass flow mS1 for R2, Matrix with 3
   columns returned
t FRt1          = M cal(:,1);                                       %Time
   vector belonging to calculated FR [h]
FRt1            = M cal(:,2);                                       %Pumprate
    FR calculated out of mR1 [l/h]
t FRt2          = M cal2(:,1);                                      %Time
   vector belonging to calculated FR1 [h]
FRt2            = M cal2(:,2);                                      %Pumprate
    calculated out of mR1 [l/h]
t FRt           = [t FRt1;t FRt2];                                  %
   Concatenated time vector [h]
FRt             = [FRt1;FRt2];                                      %Indirect
    caclulated FR1 for R1+R2 [l/h]
ms300           = M cal(:,3);                                       %Mass
   flow glucose for R1 [g/h]
```

```
ms600           = M cal2(:,3);                                  %Mass
   flow glucose for R2 [g/h]
mstot           = [ms300; ms600];                               %Mass
   flow glucose for R1+R2 [g/h]
t QS1           = t FRt;                                        %Time
   vector for QS1
[QS1]           = cal Q(t QS1, mstot, t mB, mB S);              %
   Calculation of volume specific feeding rate QS1 [g/(lh)]
QS1 S           = movmean(QS1, [WS QS 0]);                      %
   Smoothing of QS1


axn             = [1,2,3,4,5,6];                                %Axes
   Index
f length        = 0.04;                                         %Length
   of Flag handle
figureheight    = 750;                                          %Height
   of figure
figurelength0   = 1500;                                         %Length
   of figure
flagangle       = 0.04;                                         %Angle
   flag
fontsize flag   = 16;                                           %Font
   Size of Flag
fontsize plot   = 12;                                           %Fontsize
    plots
fontsize title  = 18;                                           %Font
   Size of Title
lw ax           = 1.75;                                         %
   Linewidth Axes
lw flag         = 1.5;                                          %
```

```
    Linewidth Flag handle
lw plot         = 1.75;                                          %
    Linewidth plots
lw vline        = 2.0;                                           %
    Linewidth vertical lines
markersize      = 8;                                             %Size of
    Marker
naxes           = 6;                                             %Number
    of axes
tpaxis          = 5;                                             %Number
    of Ticks
x flag          = t pO2;                                         %Time for
     Flag positioning, Time with greatest time Point used (sample time
    points for pO2)
Yoffset = 0.05;                                                  %Offset Y
    -axis
ylaboff         = 0.02;                                          %Y label
    offset above
ylab2off        = 0.1;                                           %Y label
    offset below
yntitle         = 0;                                             %Switch
    variable for title, 0 = not displayed, 1 = displayed
vline           = 1;                                             %Switch
    variable for vertical Lines seperating Process Phases, 0 = not
    displayed, 1 = displayed
vlinetext       = 1;                                             %Switch
    variable for text between vlines, 0 = not displayed, 1 = displayed
savename        = 'Kulti Plot KW0420';                           %Name of
    the saved data
titlename       = 'Fed-Batch Fermentation';                      %Title
```

```
    name

%Time events of the bioprocess
tstart          = 0;                                                %Time
    Batch Start [h]
tfbstart        = 5.822;                                            %Time Fed
    -Batch1 Start [h]
tfbstart2       = 13.243;                                           %Time Fed
    -Batch2 Start [h]
tprod           = 22.14;                                            %Time
    Production Start [h]
tend            = 24.35;                                            %End of
    process [h]

%%color scheme                  key           Y-axis minimum  Y-axis
    maximum    Number of decimals  Linesytel       Markerstyle     Y-axis
     label
c1=[0 128/255 0];               k FAIR = 1;   ymin(1)=0;      ymax(1)=10;
          ytickform1='%.1f';  linestyle(1)=0;  mark(1)='o';   ylab1={'F
    {nAIR}';'[lmin^{-1}]'};    %FAIR
c2='green';                     k mB = 2;     ymin(2)=0;      ymax(2)=10;
          ytickform2='%.1f';  linestyle(2)=0;  mark(2)='^';   ylab2={'V
    {L}';'[l]'}; %mB
c3=[128/255 128/255 128/255];   k NSt = 3;    ymin(3)=0;      ymax(3)
    =1600;     ytickform3='%.0f';  linestyle(1)=0;  mark(1)='o';   ylab3
    ={'N {St}';'[min^{-1}]'}; %NSt
c4='magenta';                   k pH = 4;     ymin(4)=6;      ymax(4)=8;
          ytickform4='%.1f';  linestyle(4)=0;  mark(4)='*';   ylab4={'pH
    ';'[-]'}; %pH
c5='blue';                      k pO2 = 5;    ymin(5)=0;      ymax(5)
```

```
   =120;      ytickform5='%.0f';  linestyle(5)=0;  mark(5)='+';   ylab5
   ={'pO {2}';'[%]'}; %pO2
c6='black';                      k Turb = 6;   ymin(6)=0;      ymax(6)
   =1.6;      ytickform6='%.1f';  linestyle(6)=0;  mark(6)='s';   ylab6
   ={'sTurb';'[CU]'}; %Sturb
c7='black';                     k TL = 7;     ymin(7)=34;     ymax(7)=40;
         ytickform7='%.1f';  linestyle(7)=0;  mark(7)='d';   ylab7={'T {
   L}';'[^{\circ}C]'}; %TL
c8=[255/255 128/255 0];          k xCO2 = 8;   ymin(8)=0;      ymax(8)=20;
          ytickform8='%.1f';  linestyle(8)=0;  mark(8)='v';   ylab8={'x
   {CO2}';'[%]'}; %xcO2
c9=[0 0 160/255];                k xO2 = 9;    ymin(9)=12.5;   ymax(9)=40;
          ytickform9='%.1f';  linestyle(9)=0;  mark(9)='h';   ylab9={'x
   {O2}';'[%]'}; %xO2
c10='green';                     k FR1 = 10;   ymin(10)=0;     ymax(10)=1;
          ytickform10='%.2f'; linestyle(10)=0; mark(10)='o';  ylab10={'
   F {R1}';'[lh^{-1}]'}; %FR1
c11=[128/255 0 255/255];         k OD = 11;    ymin(11)=0;     ymax(11)
   =90;      ytickform11='%.0f';linestyle(11)=2;  mark(11)='o';  ylab11
   ={'OD {600}';'[-]'}; %OD offline
c12='black';                     k cXL = 12;   ymin(12)=0;     ymax(12)
   =75;      ytickform12='%.0f'; linestyle(12)=2; mark(12)='o';  ylab12
   ={'c {XL}';'[gl^{-1}]'}; %BTM
c13=[64/255 224/255 208/255];    k FO2 = 13;   ymin(13)=0;     ymax(13)=2;
          ytickform13='%.1f'; linestyle(13)=0; mark(13)='o';  ylab13={'
   F {nO2}';'[lmin^{-1}]'}; %FO2
c14='green';                     k mR1 = 14;   ymin(14)=0;     ymax(14)=0;
          ytickform14='%.0f'; linestyle(14)=0; mark(14)='o';  ylab14={'
   m {R1}';'[g]'}; %mR1
c15=[128/255 224/255 0/255];     k FR2 = 15;   ymin(15)=0;     ymax(15)
```

```
   =100;     ytickform15='%.0f'; linestyle(15)=0; mark(15)='o';  ylab15
   ={'F {R2}';'[lh^{-1}]'}; %QS1
c16='green';                    k QS1 = 16;   ymin(16)=0;     ymax(16)
   =100;     ytickform16='%.0f'; linestyle(16)=0; mark(16)='o';  ylab16
   ={'Q {S1R}';'[g(lh)^{-1}]'}; %QS1
c17=[128/255 224/255 0/255];    k QS1p= 17;   ymin(17)=0;     ymax(17)
   =100;     ytickform17='%.0f'; linestyle(17)=0; mark(17)='o';  ylab17
   ={'Q {S1}';'[g(lh)^{-1}]'}; %QS1p

% Color          red,green,blue
% koenigsblau =    0,   0, 160
% orange      =  255, 128,   0
% magenta     =  255,   0, 255
% gruen       =    0, 255,   0
% grau        =  128, 128, 128
% blau        =    0,   0, 255
% blau2       =   00,  69, 134
% schwarz     =    0,   0,   0
% dunkelgelb  =  128, 128,   0
% gelb2       =  255, 211,  32
% violett     =  128,   0, 255
% lila        =  128,   0, 128
% rot         =  255,   0,   0
% rot2        =  255,  66,  14
% oliv        =    0, 128,   0
% weiss       =  255, 255, 255

%%flag parameters
x diff      = diff(x flag);
avg x diff  = mean(x diff);
```

```
%fpoint rel:                fori: flag orientation      fname: Name
    flag
%relative flag position     1: upper right 2:lower right
%enter value from 1 to 100  3: lower left  4: upper left
fpoint rel(1)=5;               fori(1)=2;      fname(1)={'F {nAIR}'};
fpoint rel(2)=1;               fori(2)=1;      fname(2)={'m {B}'};
fpoint rel(3)=50;              fori(3)=4;      fname(3)={'N {St}'};
fpoint rel(4)=40;              fori(4)=4;      fname(4)={'pH'};
fpoint rel(5)=8;               fori(5)=4;      fname(5)={'pO {2}'};
fpoint rel(6)=50;              fori(6)=2;      fname(6)={'sTurb'};
fpoint rel(7)=1;               fori(7)=1;      fname(7)={'T {L}'};
fpoint rel(8)=65;              fori(8)=4;      fname(8)={'x {CO2}'};
fpoint rel(9)=1;               fori(9)=1;      fname(9)={'x {O2}'};
fpoint rel(10)=1;              fori(10)=1;     fname(10)={'F {R1}'};
fpoint rel(11)=80;             fori(11)=1;     fname(11)={'OD {600}'};
fpoint rel(12)=90;             fori(12)=4;     fname(12)={'c {XL}'};
fpoint rel(13)=85;             fori(13)=3;     fname(13)={'F {nO2}'};
fpoint rel(14)=75;             fori(14)=1;     fname(14)={'m {R1}'};
fpoint rel(15)=70;             fori(15)=1;     fname(15)={'F {R2}'};
fpoint rel(16)=70;             fori(16)=4;     fname(16)={'Q {S1R}'};
fpoint rel(17)=40;             fori(17)=2;     fname(17)={'Q {S1p}'};

%%Plotting
xlab={'Process Time';'[h]'};
[Ypos, figurelength] = layout plot(naxes, Yoffset, figurelength0);
hold on

set(gcf,'Position',[10 10 figurelength0 figureheight])
```

```
%%                  plot1
```

```
axh1=gca;
kax1 = k pO2; %key for parameter e.g. k pO2 = 5 -> 5 is key for pO2;
   label, color and ytickformat have to be changed manually
plotgen(t pO2,pO2,axh1,mark(kax1),c5,lw plot,markersize,Ypos,ymin(kax1),
   ymax(kax1),tstart,tend,tpaxis,fontsize plot,ylab5,xlab,ytickform5,
   lw ax,linestyle(kax1),ylaboff,axn(1));
flagomat3(t pO2,pO2,fpoint rel(kax1),fori(kax1),ymax(kax1),ymin(kax1),
   lw flag,c5,fontsize flag,fname(kax1),axh1,flagangle,f length,tend,
   tstart);
```

```
%%                    plot2
if naxes >= axn(2)
kax21 = k xCO2; %key for parameter e.g. k pO2 = 5 -> 5 is key for pO2;
   label, color and ytickformat have to be changed manually
Ypos2 = [Ypos(1)-Yoffset Ypos(2) Ypos(3) Ypos(4)];
axh2=axes('position',Ypos,'YAxisLocation','left');
plotgen(t xCO2,xCO2,axh2,mark(kax21),c8,lw plot,markersize,Ypos2,ymin(
   kax21),ymax(kax21),tstart,tend,tpaxis,fontsize plot,ylab8,xlab,
   ytickform8,lw ax,linestyle(kax21),ylaboff,axn(2));
flagomat3(t xCO2,xCO2,fpoint rel(kax21),fori(kax21),ymax(kax21),ymin(
   kax21),lw flag,c8,fontsize flag,fname(kax21),axh2,flagangle,f length,
   tend,tstart);

kax22 = k pH; %key for parameter e.g. k pO2 = 5 -> 5 is key for pO2;
   label, color and ytickformat have to be changed manually
axh2=axes('position',Ypos,'YAxisLocation','left');
plotgen2(t pH,pH,axh2,mark(kax22),c4,lw plot,markersize,Ypos2,ymin(kax21)
   ,ymax(kax21),tstart,tend,tpaxis,fontsize plot,ylab4,xlab,ytickform4,
   lw ax,linestyle(4),ylab2off,axn(2));
flagomat3(t pH,pH,fpoint rel(kax22),fori(kax22),ymax(kax21),ymin(kax21),
   lw flag,c4,fontsize flag,fname(kax22),axh2,flagangle,f length,tend,
```

```
    tstart);
end
%%                  plot3
if naxes >= axn(3)
kax3 = k NSt; %key for parameter e.g. k pO2 = 5 -> 5 is key for pO2;
    label, color and ytickformat have to be changed manually
Ypos3 = [Ypos(1)-Yoffset*2 Ypos(2) Ypos(3) Ypos(4)];
axh3=axes('position',Ypos,'YAxisLocation','left');
plotgen(t NSt,NSt,axh3,mark(kax3),c3,lw plot,markersize,Ypos3,ymin(kax3),
    ymax(kax3),tstart,tend,tpaxis,fontsize plot,ylab3,xlab,ytickform3,
    lw ax,linestyle(kax3),ylaboff,axn(3));
flagomat3(t NSt,NSt,fpoint rel(kax3),fori(kax3),ymax(kax3),ymin(kax3),
    lw flag,c3,fontsize flag,fname(kax3),axh3,flagangle,f length,tend,
    tstart);
end
%%                  plot4
if naxes >= axn(4)
kax41 = k QS1; %key for parameter e.g. k pO2 = 5 -> 5 is key for pO2;
    label, color and ytickformat have to be changed manually
Ypos4 = [Ypos(1)-Yoffset*3 Ypos(2) Ypos(3) Ypos(4)];
axh4=axes('position',Ypos,'YAxisLocation','left');
plotgen(t FRt,QS1 S,axh4,mark(kax41),c16,lw plot,markersize,Ypos4,ymin(
    kax41),ymax(kax41),tstart,tend,tpaxis,fontsize plot,ylab16,xlab,
    ytickform16,lw ax,linestyle(kax41),ylaboff,axn(4));
flagomat3(t FRt,QS1 S,fpoint rel(kax41),fori(kax41),ymax(kax41),ymin(
    kax41),lw flag,c16,fontsize flag,fname(kax41),axh4,flagangle,f length
    ,tend,tstart);
end
%%                  plot5
if naxes >= axn(5)
```

```
kax51 = k FAIR; %key for parameter e.g. k pO2 = 5 -> 5 is key for pO2;
    label, color and ytickformat have to be changed manually
Ypos5 = [Ypos(1)-Yoffset*4 Ypos(2) Ypos(3) Ypos(4)];
axh5=axes('position',Ypos,'YAxisLocation','left');
plotgen(t FAIR,FAIR,axh5,mark(kax51),c1,lw plot,markersize,Ypos5,ymin(
    kax51),ymax(kax51),tstart,tend,tpaxis,fontsize plot,ylab1,xlab,
    ytickform1,lw ax,linestyle(kax51),ylaboff,axn(5));
flagomat3(t FAIR,FAIR,fpoint rel(kax51),fori(kax51),ymax(kax51),ymin(
    kax51),lw flag,c1,fontsize flag,fname(kax51),axh5,flagangle,f length,
    tend,tstart);

kax52 = k FO2; %key for parameter e.g. k pO2 = 5 -> 5 is key for pO2;
    label, color and ytickformat have to be changed manually
Ypos5 = [Ypos(1)-Yoffset*4 Ypos(2) Ypos(3) Ypos(4)];
axh5=axes('position',Ypos,'YAxisLocation','left');
plotgen2(t FO2,FO2,axh5,mark(kax52),c13,lw plot,markersize,Ypos5,ymin(
    kax51),ymax(kax51),tstart,tend,tpaxis,fontsize plot,ylab13,xlab,
    ytickform13,lw ax,linestyle(kax52),ylab2off,axn(5));
flagomat3(t FO2,FO2,fpoint rel(kax52),fori(kax52),ymax(kax52),ymin(kax52)
    ,lw flag,c13,fontsize flag,fname(kax52),axh5,flagangle,f length,tend,
    tstart);
end
%%                  plot6
if naxes >= axn(6)
kax6 = k cXL; %key for parameter e.g. k pO2 = 5 -> 5 is key for pO2;
    label, color and ytickformat have to be changed manually
Ypos6 = [Ypos(1)-Yoffset*5 Ypos(2) Ypos(3) Ypos(4)];
axh6=axes('position',Ypos,'YAxisLocation','left');
plotgen(t cxl,cxl,axh6,mark(kax6),c12,lw plot,markersize,Ypos6,ymin(kax6)
    ,ymax(kax6),tstart,tend,tpaxis,fontsize plot,ylab12,xlab,ytickform12,
```

```
    lw ax,linestyle(kax6),ylaboff,axn(6));
flagomat3(t cxl,cxl,fpoint rel(kax6),fori(kax6),ymax(kax6),ymin(kax6),
    lw flag,c12,fontsize flag,fname(kax6),axh6,flagangle,f length,tend,
    tstart);
end
%% Figure Title

if yntitle == 1
    title(titlename,'fontsize',fontsize title,'fontweight','bold')
    set(get(gca,'title')','Position',[500 (ymax(12)-ymin(12))*0.00+ymax
        (12) 1])
end
%% Vertical Lines for Phase seperation

if vline == 1
    plot(axh1,[tfbstart,tfbstart],[ymin(5),ymax(5)],'k--','LineWidth',
        lw vline)

        % Plotting of Batch/Fed-Batch Process line
    plot([tfbstart2,tfbstart2],[ymin(5),ymax(5)],'k--','LineWidth',
        lw vline,'parent',axh1)
                                                                    %
        Plotting of Fed-Batch1/Fed-Batch2 Process line
    plot([tprod,tprod],[ymin(5),ymax(5)],'k--','LineWidth',lw vline,'
        parent',axh1)

        % Plotting of Fed-Batch2/Production Process line
    if vlinetext ==1
        text((tfbstart-tstart)/2,ymax(5)*1.02,'Batch-Phase','color','k','
            HorizontalAlignment','center','fontsize',16,'parent',axh1)
```

```
                                % Text Process Phase batch
        text((tfbstart2-tfbstart)/2+tfbstart,ymax(5)*1.02,'Fed-Batch-
            Phase 1','color','k','HorizontalAlignment','center','fontsize
            ',16,'parent',axh1)   % Text Process Phase fed-batch1
        text((tprod-tfbstart2)/2+tfbstart2,ymax(5)*1.02,'Fed-Batch-Phase
            2','color','k','HorizontalAlignment','center','fontsize',16,'
            parent',axh1)     % Text Process Phase fed-batch2
        text((tend-tprod)/2+tprod,ymax(5)*1.02,'Prod.','color','k','
            HorizontalAlignment','center','fontsize',16,'parent',axh1)
                                    % Text Process Phase production
    end
end

hold off
print(savename,'-depsc')
print(savename,'-dsvg')
```

Function enabling mulit Y-axes plotting

```
%Function enabling the actual plotting and handling the formatting of the
%plots
%To be used in conjunction with master file 'MA Evaluation Master' for
%plotting of cultivation course
%Version 1.0   27.12.2019
%Derived from 'plottomat' script by Jan Niklas Pauk & Markus Stoffel
%Garry Schulze
function []=plotgen(Tdat,Ydat,axh,mark,color,linewidth,markersize,
   Yposition,Ymin,Ymax,Tmin,Tend,tpaxis,fontsize,Y label,X label,
   Ytickform,linewidth ax,linestyle,Ylaboff,Axn)

if  linestyle == 0
        plot(axh,Tdat,Ydat,'Color',color,'LineWidth',linewidth);
end
if  linestyle == 1
        plot(axh,Tdat,Ydat,mark,'Color',color,'MarkerSize',markersize,'
           LineWidth',linewidth);
end
if  linestyle == 2
    line1=cat(2,'-',mark);
    plot(axh,Tdat,Ydat,line1,'color',color,'Markersize',markersize,'
       linewidth',linewidth)
end


if Axn == 1

    set(axh,'Position',Yposition, 'YAxisLocation','left','YLim',[Ymin
       Ymax], 'XLim',[Tmin Tend],'Visible','on');
```

```
    set(axh,'TickDir','out','LineWidth',linewidth ax);
    ytickformat(gca,Ytickform)
    tick=Ymin:((Ymax-Ymin)/tpaxis):Ymax;
    set(axh,'Ytick',tick,'Ylim',[Ymin Ymax],'FontSize',fontsize,'Ycolor',
        'black','Visible','on');
    ylabel(Y label,'Position',[0 (Ymax-Ymin)*Ylaboff+Ymax -1],'Rotation'
        ,0,'HorizontalAlignment','center','Color',color);
    xlabel(X label);

elseif Axn == 2 || Axn == 3 || Axn == 4 ||Axn == 5 || Axn == 6



    set(axh,'YAxisLocation','left','YLim',[Ymin Ymax],'XLim',[Tmin Tend],
        'Visible','off');
    ytickformat(gca,Ytickform)



    axh off=axes('Position',Yposition,'YAxisLocation','left');
    set(axh off,'Position',[Yposition(1) Yposition(2) 0.001 Yposition(4)
        ], 'YAxisLocation','left','YLim',[Ymin Ymax],'Visible','on');
    set(axh off,'TickDir','out','LineWidth',linewidth ax);
    tick=Ymin:((Ymax-Ymin)/tpaxis):Ymax;
    set(axh off,'Ytick',tick,'Ylim',[Ymin Ymax],'FontSize',12,'Ycolor','
        black');
    ylabel(Y label,'Position',[0 (Ymax-Ymin)*Ylaboff+Ymax -1 ],'Rotation'
        ,0,'HorizontalAlignment','center','Color',color);
    ytickformat(gca,Ytickform)
end
end
```

Function enabling multi Y-axes plotting with Y-axis label beneath axis

```
%Like Plotgen, but label is plotted below Y-axis
%To be used in conjunction with master file 'MA Evaluation Master' for
%plotting of cultivation course
%Garry Schulze
function []=plotgen2(Tdat,Ydat,axh,mark,color,linewidth,markersize,
   Yposition,Ymin,Ymax,Tmin,Tend,tpaxis,fontsize,Y label,X label,
   Ytickform,linewidth ax,linestyle,Ylab2off,Axn)

if  linestyle == 0
        plot(axh,Tdat,Ydat,'Color',color,'LineWidth',linewidth);
end
if  linestyle == 1
        plot(axh,Tdat,Ydat,mark,'Color',color,'MarkerSize',markersize,'
           LineWidth',linewidth);
end
if  linestyle == 2
    line1=cat(2,'-',mark);
    plot(axh,Tdat,Ydat,line1,'color',color,'Markersize',markersize,'
       linewidth',linewidth)
end


if Axn == 1

    set(axh,'Position',Yposition, 'YAxisLocation','left','YLim',[Ymin
       Ymax], 'XLim',[Tmin Tend]);
    set(axh,'TickDir','out','LineWidth',linewidth ax);
    ytickformat(gca,Ytickform)
    tick=Ymin:((Ymax-Ymin)/tpaxis):Ymax;
```

```
    set(axh,'Ytick',tick,'Ylim',[Ymin Ymax],'FontSize',fontsize,'Ycolor',
        'black','Visible','off');
    ylabel(Y label,'Position',[0 -(Ymax-Ymin)*Ylab2off -1 ],'Rotation',0,
        'HorizontalAlignment','center','Color',color,'Visible','on')
    xlabel(X label);

elseif Axn == 2 || Axn == 3 || Axn == 4 ||Axn == 5 || Axn == 6



    set(axh,'YAxisLocation','left','YLim',[Ymin Ymax],'XLim',[Tmin Tend],
        'Visible','off');
    ytickformat(gca,Ytickform)



    axh off=axes('Position',Yposition,'YAxisLocation','left');
    set(axh off,'Position',[Yposition(1) Yposition(2) 0.001 Yposition(4)
        ], 'YAxisLocation','left','YLim',[Ymin Ymax],'Visible','on');
    set(axh off,'TickDir','out','LineWidth',linewidth ax);
    tick=Ymin:((Ymax-Ymin)/tpaxis):Ymax;
    set(axh off,'Ytick',tick,'Ylim',[Ymin Ymax],'FontSize',12,'Ycolor','
        black','Visible','off');
    ylabel(Y label,'Position',[0 -(Ymax-Ymin)*Ylab2off -1 ],'Rotation',0,
        'HorizontalAlignment','center','Color',color,'Visible','on');
    ytickformat(gca,Ytickform)
end
end
```

Function for calculating the position of the Y-axes and figurelength

```
%Function for calculating positions of the Y-axes and figurelength
%To be used in conjunction with master file 'MA Evaluation Master' for
%plotting of cultivation course
%Version 1.0
%Garry Schulze
function [Ypos, figurelength] = layout plot(naxes,Yoffset, figurelength0)

switch naxes
    case 1
        figurelength = figurelength0*0.75;
        Ypos = [Yoffset 0.1100 0.90 0.8150];
    case 2
        figurelength = figurelength0*0.8;
        Ypos = [Yoffset*2 0.1100 0.85 0.8150];
    case 3
        figurelength = figurelength0*0.85;
        Ypos = [Yoffset*3 0.1100 0.80 0.8150];
    case 4
        figurelength = figurelength0*0.90;
        Ypos = [Yoffset*4 0.1100 0.75 0.8150];
    case 5
        figurelength = figurelength0*0.95;
        Ypos = [Yoffset*5 0.1100 0.70 0.8150];
    case 6
        figurelength = figurelength0;
        Ypos = [Yoffset*6 0.1100 0.65 0.8150];
end
```

Function for attachement of flags

```
%Function for attaching flags to the plotted curves
%To be used in conjunction with master file 'MA Evaluation Master' for
%plotting of cultivation course
%Version 2.0   27.12.2019
%Original script by Jan Niklas Pauk & Markus Stoffel
%modified by Garry Schulze 27.12.2019
function [] = flagomat3(x,y,fpoint,fori,ymax,ymin,linewidth flag,color,
   fontsize flag,fname,ax,angle,flag length,xmax,xmin)

% Calculation of flag position
x point=(fpoint/100)*max(x);
v=x point*ones(size(x));
[mindiff, position1]=min(abs(v-x));
switch fori
    case 1

       % Position upper right
        text(x(position1(1),1)+(xmax-xmin)*flag length,y(position1(1),1)
           +(ymax-ymin)*angle,fname,'color',color,'fontsize',
           fontsize flag,'HorizontalAlignment','left','parent',ax)  %
           Plotting of flag text
        line([x(position1(1),1) x(position1(1),1)+(xmax-xmin)*flag length
           ],[y(position1(1),1) y(position1(1),1)+(ymax-ymin)*angle],'
           Linewidth',linewidth flag,'color',color,'parent',ax)  %
           Plotting of flag handle
    case 2

       % Position lower right
        text(x(position1(1),1)+(xmax-xmin)*flag length,y(position1(1),1)
```

```
            -(ymax-ymin)*angle,fname,'color',color,'fontsize',
               fontsize flag,'HorizontalAlignment','left','parent',ax)  %
               Plotting of flag text
            line([x(position1(1),1) x(position1(1),1)+(xmax-xmin)*flag length
               ],[y(position1(1),1) y(position1(1),1)-(ymax-ymin)*angle],'
               Linewidth',linewidth flag,'color',color,'parent',ax) %
               Plotting of flag handle
        case 3

            % Position lower left
            text(x(position1(1),1)-(xmax-xmin)*flag length,y(position1(1),1)
               -(ymax-ymin)*angle,fname,'color',color,'fontsize',
               fontsize flag,'HorizontalAlignment','right','parent',ax) %
               Plotting of flag text
            line([x(position1(1),1) x(position1(1),1)-(xmax-xmin)*flag length
               ],[y(position1(1),1) y(position1(1),1)-(ymax-ymin)*angle],'
               Linewidth',linewidth flag,'color',color,'parent',ax) %
               Plotting of flag handle
        case 4

            % Position upper left
            text(x(position1(1),1)-(xmax-xmin)*flag length,y(position1(1),1)
               +(ymax-ymin)*angle,fname,'color',color,'fontsize',
               fontsize flag,'HorizontalAlignment','right','parent',ax) %
               Plotting of flag text
            line([x(position1(1),1) x(position1(1),1)-(xmax-xmin)*flag length
               ],[y(position1(1),1) y(position1(1),1)+(ymax-ymin)*angle],'
               Linewidth',linewidth flag,'color',color,'parent',ax) %
               Plotting of flag handle
    end
```

Function for numerical determination of F_R and m_{S1}

```
%Function for indirect calculation of FR
%Version 1.0
%Garry Schulze
function [M] =    mS calc(y,t,rho,cSR)


[m,n] = size(y);
FR(1) = 0;
%Numeric calculation of FR1
for k=11:10:(m)                                %Every 10th data point is
   used for calculation
    t k(k) =t(k);
 FR(k)=  (-1*(y(k)-y(k-10))/(t(k)-t(k-10)))*1/(rho*1000);
end


mS1 = (FR*cSR);                                %mass flow substrate

%0 are turned into NaN, so that these points are omitted during plotting
FR(FR==0)=NaN;
mS1(mS1==0)=NaN;
t k(t k==0)=NaN;
M = [t k', FR', mS1'];
M(any(isnan(M),2),:) = [];
end
```

Function for calculation of Q_{S1}

```
%Function for calculation of QS1
%Version 1.0
%Garry Schulze
function [QS1] = cal_Q(t_mS1,mS1,t_mB_S, mB_S)

    [t_mB_S, index] = unique(t_mB_S);

    mB_Sn   = interp1(t_mB_S,mB_S(index),t_mS1); %Interpolation necessary
        since number of data varies between t_mS1/mS1 and t_mB_s/mB_S

    QS1     = mS1./mB_Sn;

end
```